U. S. DEPARTMENT OF THE INTERIOR
U. S. GEOLOGICAL SURVEY

Sample Characterizations and Strength Measurements of Serpentinite Gouges

by

D. E. Moore[1], D. A. Lockner[1], R. Summers[1], J. D. Byerlee[1], and Ma Shengli[2]

Open-File Report 96-702

[1]345 Middlefield Road, Menlo Park, CA 94025

[2]Institute of Geology, State Seismological Bureau, Beijing, China

Abstract

In this report, we present supporting data relevant to our continuing investigations of the frictional strength of serpentinite. We have measured the strength of chrysotile-, lizardite-, and antigorite-rich serpentinite gouges under hydrothermal conditions. Identification of serpentine minerals was based on X-ray powder diffraction analysis, and petrographic, scanning electron microscope, and electron microprobe techniques were used to fully characterize the samples. Experimental methods and the determination of correction factors, particularly for jacket strength, are outlined in detail; the corrected room-temperature data are consistent with previous studies.

The coefficient of friction, μ, of chrysotile gouge is roughly 0.2 at 25 °C, whereas the lizardite- and antigorite-rich gouges are at least twice as strong. The very low room-temperature strength of chrysotile appears to be a consequence of its high adsorbed water content; when the adsorbed water is removed, chrysotile is as strong as pure antigorite gouge at room temperature. Heating to nearly 200 °C leads to slight to substantial increases in the frictional strengths of all three gouges. The strength increases of chrysotile and, to a lesser extent, of lizardite, are probably caused by the partial loss of adsorbed water upon heating. In addition, all of the heated gouges may have become slightly lithified at the highest temperatures tested. Limited data suggest that different polytypes of a given serpentine mineral have similar strengths; thus, deformation-induced changes in polytype should not affect fault strength.

At 25 °C, the chrysotile gouge shows a transition from velocity strengthening at velocities $\leq$0.32 μm/s to velocity weakening at velocities $\geq$1 μm/s. At elevated temperatures, however, chrysotile-gouge strength is essentially independent of velocity at low velocities. Overall, at a given temperature chrysotile may show a restricted range of velocities over which velocity-strengthening behavior occurs, and this range may shift to progressively higher

velocities as temperature increases. Although fewer data are available for the heated lizardite and antigorite gouges, their behavior is consistent with that outlined for chrysotile.

Introduction

We are investigating the strengths, under hydrothermal conditions, of a group of serpentinite gouge samples, to compare the behavior of the serpentine minerals chrysotile, lizardite, and antigorite and to help characterize the properties of serpentinite-bearing fault zones at depth. The experiments conducted to date have principally dealt with the effects of temperature and velocity on gouge strength. Planned investigations include additional friction experiments to determine the influence of fluid pressure and effective normal stress on serpentinite strength, and permeability experiments under hydrothermal conditions to estimate the sealing rates of serpentine-bearing faults.

The principal results of our research on serpentinite will be published elsewhere (Moore et al., 1996, and in review). This Open-File report serves as a repository of supporting data for those papers, with emphasis on four topics: (1) We provide full descriptions of the serpentinite samples used in this and previous studies conducted in our laboratory (Summers and Byerlee, 1977a, b; Morrow et al., 1982), specifying the criteria for identification of the different serpentine minerals. (2) Copper jackets were used for most of the experiments, because it is stable at elevated temperatures. However, copper is relatively strong at low temperatures, whereas chrysotile can be extremely weak at temperatures below ≈200 °C. The strength of the copper jacket therefore makes up a large proportion of the measured strength in many of the chrysotile experiments. Because of this, considerable effort was spent determining the appropriate jacket corrections, which are outlined in detail here. (3) We present the results of all of the strength experiments. (4) Measurement of the change in μ with velocity change can be a subjective process. To minimize this problem, separate sets

of velocity-dependence data were compiled by two of the authors and then averaged (Moore et al., in review). This report contains the individual data sets and a description of the averaging procedure.

Background on Serpentine Minerals

Serpentinite is a metamorphic rock that forms as a replacement of ultramafic igneous rocks at temperatures below 500-600°C (Evans et al., 1976) and in the presence of water. The mineral serpentine — $Mg_3Si_2O_5(OH)_4$ — is a sheet silicate in which a given sheet consists of two sub-layers, an Si-bearing tetrahedral layer that is joined to an Mg-bearing octahedral layer. The lateral dimensions of an ideal Mg-bearing octahedral layer are larger than those of an ideal Si-bearing tetrahedral layer (e.g., Coleman, 1971; Wicks and O'Hanley, 1988). The stresses arising within the crystal structure as a result of this discrepancy lead to the development of three major varieties of serpentine — lizardite, antigorite, and chrysotile, in decreasing order of abundance — that have adopted different solutions to the structural problem. Lizardite maintains a platy form by stretching the tetrahedral layer and compressing the octahedral layer to make the structure lie flat. Because the amount of misfit increases with increasing lateral dimensions of a given crystal, lizardite characteristically is extremely fine-grained (e.g., Deer et al., 1962). The sheet structure of chrysotile curls around to form tubes, with the smaller tetrahedral layer on the inside. Only one layer in a given chrysotile crystal will be at the ideal radius of curvature (about 88 Å, Whittaker, 1957) to alleviate the misfit; layers with smaller radii will be overcompensated and ones with larger radii will be under-compensated. As a result, most chrysotile tubes have hollow centers and are less than 270 Å in outer diameter (Wicks and O'Hanley, 1988), although they may reach several millimeters in length. Antigorite has an alternating curved structure that produces a corrugated or wavy pattern; a given tetrahedral sheet is tied to the octahedral sheet above it for one half a

wavelength and tied to the one below it along the other half. Unlike chrysotile, each layer in the antigorite structure can attain a degree of curvature most efficient for misfit relief, making antigorite ideally the most stable structure (Wicks and O'Hanley, 1988). It also generally forms the largest crystals. A detailed review of serpentine crystallography is presented by Wicks and O'Hanley (1988).

Chemically, serpentine minerals tend to reflect the bulk chemistry of the ultramafic rocks that they replace, although the different crystal structures may impose different limits on the amount of substitution. The principal exchanges involve replacement of Si by Al, and Mg by Al, Fe^{2+}, and Fe^{3+}. Coupled substitution of Al into the tetrahedral and octahedral sites of lizardite makes its flat-lying structure more stable, because the Al^{3+} ion is larger than the Si^{4+} ion and smaller than the Mg^{2+} ion, thus increasing the lateral dimensions of the tetrahedral sheet and decreasing those of the octahedral sheet. Chrysotile and to a lesser extent antigorite cannot tolerate as much departure from their ideal formulae, because the misfit between the tetrahedral and octahedral layers must be maintained for their curved structures to form. Consequently, lizardite tends to show the greatest deviation from the Mg end-member composition and chrysotile the least (O'Hanley, 1996).

Polymorphism is defined as the ability of a mineral to exist in more than one form, and one polymorph can convert to another by a simple structural inversion in response to changing physical conditions. The periodic reversals of the antigorite structure lead to slight deficiencies in Mg and OH compared to the ideal serpentine formula, such that its end-member formula is approximately $Mg_{5.626}Si_4O_{10}(OH)_{7.353}$ (e.g., Dungan, 1979). Accordingly, antigorite is not a polymorph of lizardite or chrysotile, because chemical as well as structural modifications are required to convert antigorite into another serpentine mineral. Chrysotile and low-Al lizardite are commonly considered to be polymorphs, but once the Al-content of lizardite exceeds some critical value, chrysotile cannot replace lizardite by a simple structural inversion (O'Hanley et al., 1989). In addition, O'Hanley (1996) recently proposed that low-Al lizardite and

chrysotile may be stable under different chemical conditions at a given temperature and pressure, which would mean that these two serpentine minerals are also not polymorphs. Polytypism is a special case of polymorphism in sheet silicates, representing different stacking arrangements of the layers. Chrysotile can form a limited number of polytypes (Whittaker and Zussman, 1956), and the planar configuration of lizardite allows for the possible formation of numerous regular (Bailey, 1988) and non-standard (Bailey and Banfield, 1995) polytypes.

Evans et al. (1976) worked out the pressure-temperature stability fields of chrysotile and antigorite. Antigorite is the higher-temperature form, consistent with its occurrence in nature. The upper thermal stability limit of chrysotile relative to antigorite is about 300°C at ≈0.1 MPa, dropping to 275 °C at 500 MPa. The relative stability of lizardite with respect to antigorite and chrysotile has not been determined experimentally, and not all of its thermodynamic properties have as yet been measured. Most field occurrences suggest that lizardite and chrysotile are both low-temperature minerals (Coleman, 1971, among many others); oxygen-isotope fractionation studies of lizardite-chrysotile serpentinites suggest that they are stable at temperatures below 250-300°C (e.g., Wenner and Taylor, 1971; O'Hanley and Wicks, 1995). Because of the possible compositional differences between lizardite and chrysotile, these two varieties of serpentine potentially could coexist stably (O'Hanley, 1996). In many occurrences, however, lizardite directly replaces the olivine and pyroxenes of ultramafic rocks, with chrysotile forming later as a replacement of the lizardite (e.g., O'Hanley et al., 1989). Of particular interest to our research, the chrysotile content of sheared serpentinites characteristically is higher than that of nearby unsheared serpentinites (Page, 1968; Coleman and Keith, 1971; Mumpton and Thompson, 1975), probably due to the flow of silica-bearing waters through the shear zones (O'Hanley, 1996).

Sample Descriptions

The serpentinite samples from our current series of experiments have been characterized by various combinations of petrographic and scanning electron microscopy, X-ray diffraction, and electron microprobe techniques. In compiling the results of previous friction experiments on serpentinites, we also found that the mineral contents of many of the samples tested were not specified, making it difficult to evaluate the data. Fortunately, we were able to retrieve the serpentinite samples used in previous studies in this laboratory, and we also describe those samples in this section. Mineral proportions of rock samples are presented in Table 1, and representative compositions of serpentine and other important minerals in those samples are contained in Tables 2 and 3, respectively.

The serpentine-mineral identifications were based on X-ray powder diffraction analysis, with reference to the crystallographic data of Whittaker and Zussman (1956) and Wicks and O'Hanley (1988). The diffraction data compiled by Wicks and O'Hanley (1988) were useful for distinguishing different polytypes of lizardite and chrysotile. Additional X-ray analyses of chrysotile and lizardite from the New Idria area, California are presented by Page and Coleman (1967) and Mumpton and Thompson (1975). Natural serpentinites commonly contain more than one serpentine mineral, but the near-coincidence of many of the principal X-ray peaks makes it almost impossible to identify a minor serpentine constituent by bulk X-ray techniques if it comprises less than 10% of a sample (Faust and Fahey, 1962).

Samples from Current Studies

Chrysotile — The chrysotile sample that we used in our recent experiments comes from New Idria, California, and was provided by R. G. Coleman. It is a relatively soft, layered rock ranging in color from a light to medium, pearly, grayish green. The rock is essentially all serpentine (Table 1), and the X-ray diffraction pattern (Fig. 1) corresponds to

Table 1. Mineral Proportions* of Serpentinite Samples

	Chrysotile (New Idria, CA)	Antigorite (New Idria, CA)	Lizardite (Oregon)	DP-2	Alm-1
serpentine	100.0	76.0	93.0	69.3	84.4
calcite		7.8		0.4	
chlorite		2.9	0.3		Tr
olivine				19.5	
diopside				3.1	
magnetite		12.5	5.4	7.5	13.2
chromite		0.5		0.2	
spinel			1.3		2.4
ilmenite			Tr		Tr
pyrite				Tr	
Cu-sulfide**				Tr	
Ni-sulfide**		0.3			
Mn-Oxide**			Tr		

* Volume percent; ** Elements identified in SEM; Tr = trace amount.

Table 2. Representative Serpentine-Mineral Compositions

	Chrysotile (New Idria, CA)		Antigorite (New Idria, CA)		Lizardite (Oregon, #33-68)				Lizardite (NI,CA)
	grainy crystals	color-less	coarse-grained	finer-grained	mesh cores	mesh rims	bastites	bastites porphs	average
SiO_2	42.77	39.13	40.30	40.55	41.27	41.43	38.13	36.31	41.38
TiO_2	0.01	0.01	0.03	0.02	0.01	0.01	0.05	0.08	0.02
Al_2O_3	0.34	0.36	2.54	2.13	2.17	0.63	3.65	5.04	0.46
Cr_2O_3	0.05	0.07	0.60	0.54	0.07	0.01	1.12	0.93	0.04
FeO*	3.28	3.20	4.25	4.51	7.80	4.13	7.27	7.94	2.01
NiO	0.01	0.01	0.07	0.05	0.53	0.33	0.11	0.21	0.15
MgO	39.92	35.98	37.32	36.73	33.89	38.46	34.68	32.04	40.39
MnO	0.05	0.05	0.10	0.12	0.08	0.04	0.08	0.15	0.10
CaO	0.02	0.03	0.03	0.02	0.06	0.03	0.03	0.05	0.03
Total	86.45	78.84	85.24	84.67	85.88	85.07	85.12	82.75	84.58
Si	4.03	4.05	3.78	3.83	4.01	4.00	3.76	3.70	3.98
Al^{IV}	--	--	0.22	0.17	--	--	0.24	0.30	0.02
Al^{VI}	0.04	0.04	0.07	0.07	0.25	0.07	0.19	0.30	0.03
Ti	--	--	--	--	--	--	--	0.01	--
Cr	--	0.01	0.04	0.04	--	--	0.09	0.08	--
Fe^{2+}*	0.26	0.27	0.33	0.36	0.63	0.33	0.60	0.67	0.16
Ni	--	--	0.01	--	0.04	0.03	0.01	0.02	0.01
Mg	5.61	5.55	5.22	5.17	4.91	5.53	5.09	4.86	5.79
Mn	0.01	0.01	0.01	0.01	0.01	--	0.01	0.01	0.01
Ca	--	--	--	--	0.01	--	--	--	--
O anhydrous†	14	14	13.626	13.626	14	14	14	14	14

* total Fe as FeO; † antigorite formulae based on end-member composition $Mg_{5.626}Si_4O_{10}(OH)_{7.353}$.

Table 2, continued.

	DP-2	Alm-1				Antigorite (Vermont)	
	average	mesh	bastite core	bastite rim	older vein	coarse-grained	finer-grained
SiO_2	40.11	41.32	39.42	40.38	42.40	40.37	42.18
TiO_2	--	0.03	0.07	0.06	0.02	0.02	0.01
Al_2O_3	0.14	0.56	4.04	2.75	1.42	4.66	1.48
Cr_2O_3	--	0.05	1.10	0.32	0.02	0.31	0.20
FeO*	6.90	3.36	5.47	6.31	5.64	4.56	3.58
NiO	0.01	0.39	0.38	0.09	0.11	0.39	0.17
MgO	37.67	38.25	35.46	35.25	37.03	37.79	38.49
MnO	0.09	0.05	0.09	0.17	0.11	0.01	0.03
CaO	0.13	0.03	0.07	0.03	0.02	0.03	--
Total	85.05	84.04	86.10	85.36	86.77	88.14	86.14
Si	3.94	4.02	3.80	3.92	4.02	3.67	3.89
Al^{IV}	0.02	--	0.20	0.08	--	0.33	0.11
Al^{VI}	--	0.07	0.26	0.24	0.16	0.17	0.05
Ti	--	--	0.01	--	--	--	--
Cr	--	--	0.08	0.03	--	0.02	0.02
Fe^{2+}*	0.57	0.27	0.44	0.51	0.45	0.36	0.28
Ni	--	0.03	0.03	0.01	0.01	0.03	0.01
Mg	5.51	5.55	5.09	5.10	5.25	5.12	5.29
Mn	0.01	--	0.01	0.01	0.01	--	--
Ca	0.01	--	0.01	--	--	--	--
O anhydrous†	14	14	14	14	14	13.626	13.626

* total Fe as FeO; † antigorite formulae based on end-member composition $Mg_{5.626}Si_4O_{10}(OH)_{7.353}$.

Table 3. Compositions of Other Minerals in Serpentinites

	Antig. S. (NI, CA)	Lizardite Serp. (Oregon)		DP-2			Alm-1	
	Chlorite	Chlorite	Spinel	Olivine	Diopside	Chromite	Chlorite	Spinel
SiO_2	31.07	28.96	0.02	39.98	53.99	0.02	27.63	0.25
TiO_2	0.05	0.04	0.06	--	0.04	0.33	--	0.06
Al_2O_3	16.87	19.62	54.09	--	0.63	12.90	21.63	52.63
Cr_2O_3	1.87	1.08	14.40	--	0.31	49.85	0.87	15.57
FeO*	4.06	7.92	12.21	12.77	2.53	30.60	9.83	13.87
NiO	0.16	0.04	0.32	0.17	0.02	0.04	0.07	0.27
MgO	32.22	27.70	19.43	47.08	17.93	5.55	26.13	18.58
MnO	0.01	0.16	0.14	0.20	0.10	0.53	0.19	0.18
CaO	0.02	0.08	--	0.02	24.38	--	0.07	--
Total	86.33	85.60	100.67	100.22	99.93	99.82	86.42	101.41
Si	5.97	5.70	--	1.00	1.97	--	5.45	--
Al^{IV}	2.03	2.30	1.67	--	0.03	--	2.55	--
Al^{VI}	1.79	2.26	--	--	--	0.52	2.48	1.64
Ti	0.01	0.01	--	--	--	0.01	--	--
Cr	0.28	0.18	0.30	--	0.01	1.35	0.14	0.33
Fe^{2+*}	0.65	1.26	0.27	0.26	0.08	0.88	1.62	0.31
Ni	0.02	0.01	0.01	--	--	--	0.01	0.01
Mg	9.22	8.18	0.76	1.74	0.97	0.28	7.68	0.73
Mn	--	0.02	--	--	--	0.02	0.03	--
Ca	--	0.02	--	--	0.95	--	0.01	--
O anhydrous	28	28	4	4	6	4	28	4

* Total Fe as FeO.

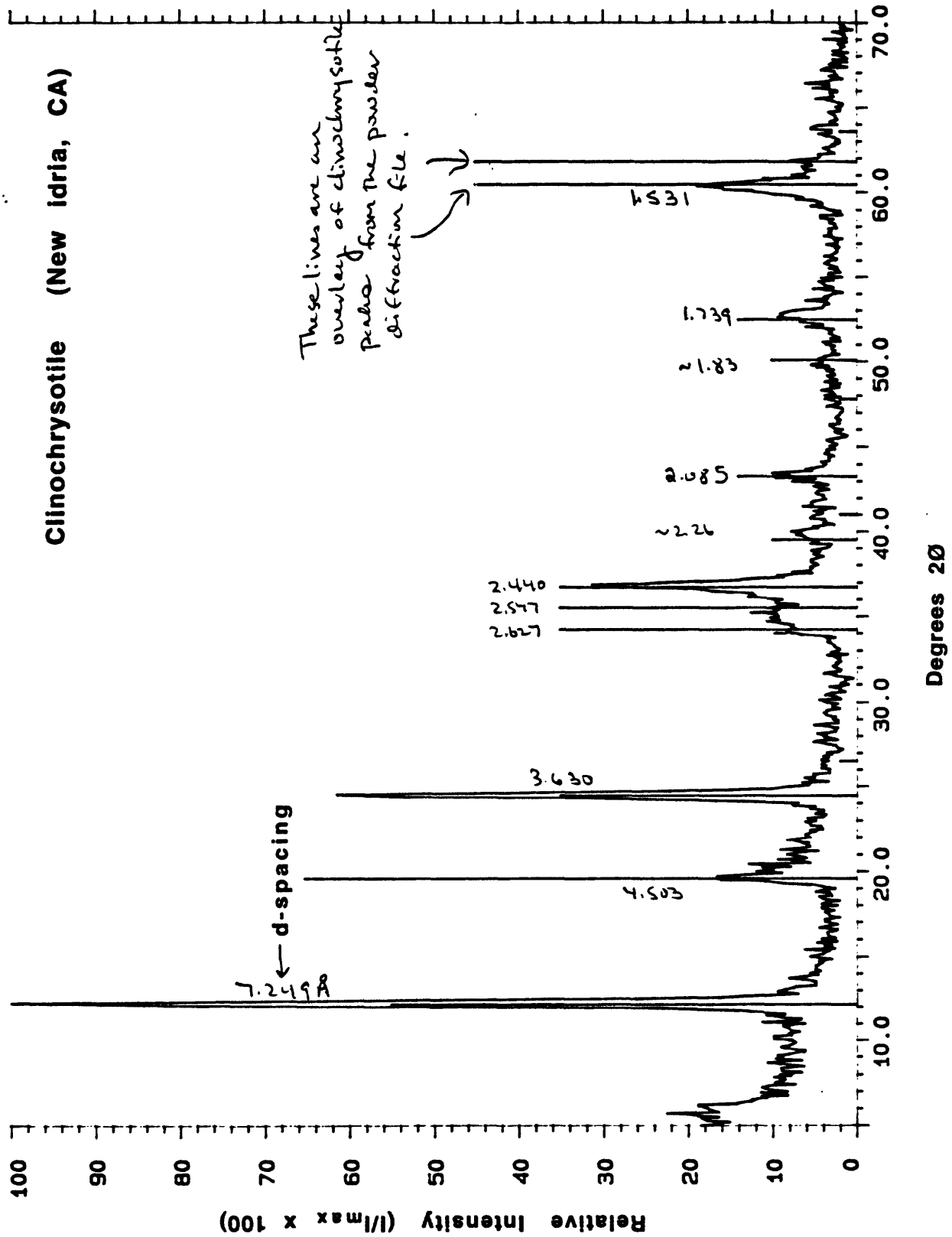

Figure 1. X-ray diffraction pattern of clinochrysotile from New Idria, California. The strong (00l) reflections at ≈7.25 and ≈3.60 Å are common to all serpentine minerals, and identification is based on the d-spacings and relative intensities of some of the less intense peaks. Characteristic of clinochrysotile is that the largest peak in the range 2.4–2.6 Å is at 2.44 Å; other peaks are at 2.09, 1.83, and 1.74 Å.

clinochrysotile, the most abundant polytype of chrysotile. Characteristic X-ray peaks of clinochrysotile include a major peak at 2.44 Å and somewhat less intense ones at 2.09, 1.83, and 1.74 Å (Fig. 1). The chrysotile contains moderate amounts of iron and very little aluminum (Table 2), consistent with the crystallographic restrictions on chemical substitutions described previously. Nearly all of the electron microprobe analyses of this sample yielded very low anhydrous totals, commonly below 80 weight % (Table 2), whereas the ideal serpentine composition contains about 13 weight percent H_2O. Mineral formulae calculated from analyses with low and good totals are similar, indicating that no important cations were missed in the analyses. Chrysotile characteristically adsorbs relatively large amounts of water, which causes swelling of fiber bundles (Deer et al., 1962), and this adsorbed water could be the cause of the low anhydrous totals. Sample preparation involved the removal of narrow veinlets and the shiny coatings found on some layer surfaces, although subsequent analysis suggests that the minerals removed were also chrysotile.

T91NI6 — To allow us to conduct an interlaboratory comparison of reported strengths, L. Reinen and T. Tullis generously provided some of their sample T91NI6 (Reinen et al., 1994), which was collected by T. Tullis at New Idria, California. The material was sent to us as a prepared, simulated gouge that had been passed through a 90-μm sieve. Although the dominant serpentine mineral in the sample was originally identified by Reinen et al. (1994) as lizardite, its X-ray diffraction pattern (Fig. 2) has only clinochrysotile peaks, essentially identical to our chrysotile sample (Fig. 1). Reinen et al. (1994) apparently based their identification on the diffraction data for lizardite from New Idria, California, presented in Table 2 of Page and Coleman (1967). R. G. Coleman provided us with the lizardite separate used for that analysis, and a diffraction pattern from that sample is presented in Figure 3. As Page and Coleman noted in their paper, their sample contains some chrysotile, indicated by the minor peaks at 2.43, 2.09, and 1.73 Å. The lizardite in this sample is the polytype 1*T*, which is the most abundant polytype of lizardite; its distinguishing peaks are at 2.49, 2.14, 1.78, and 1.70 Å. The

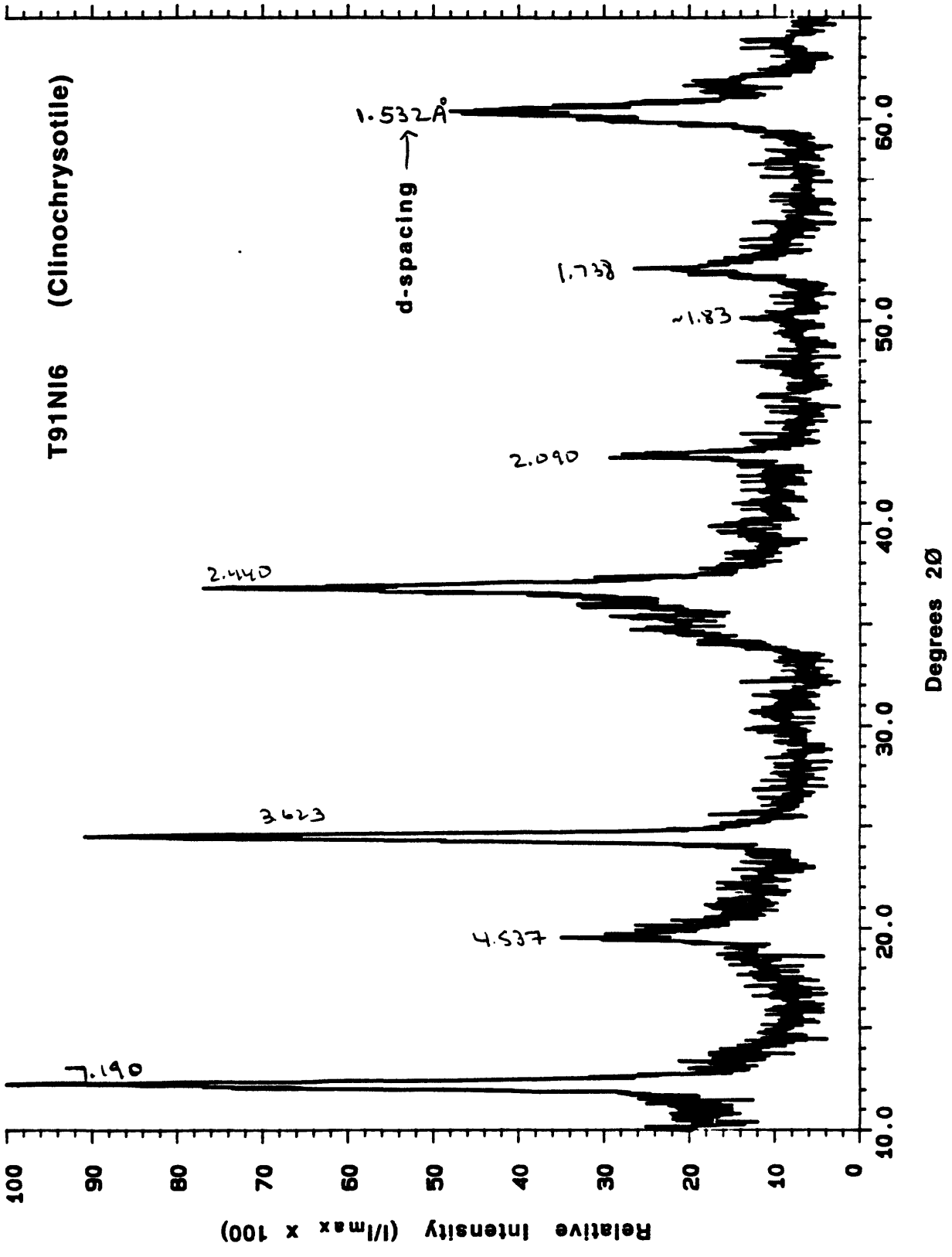

Figure 2. X-ray pattern of gouge sample T91NI6, furnished by L. Reinen and T. Tullis. This sample was identified by Reinen et al. (1994) as lizardite, but the diffraction pattern matches the clinochrysotile peaks in Figure 1.

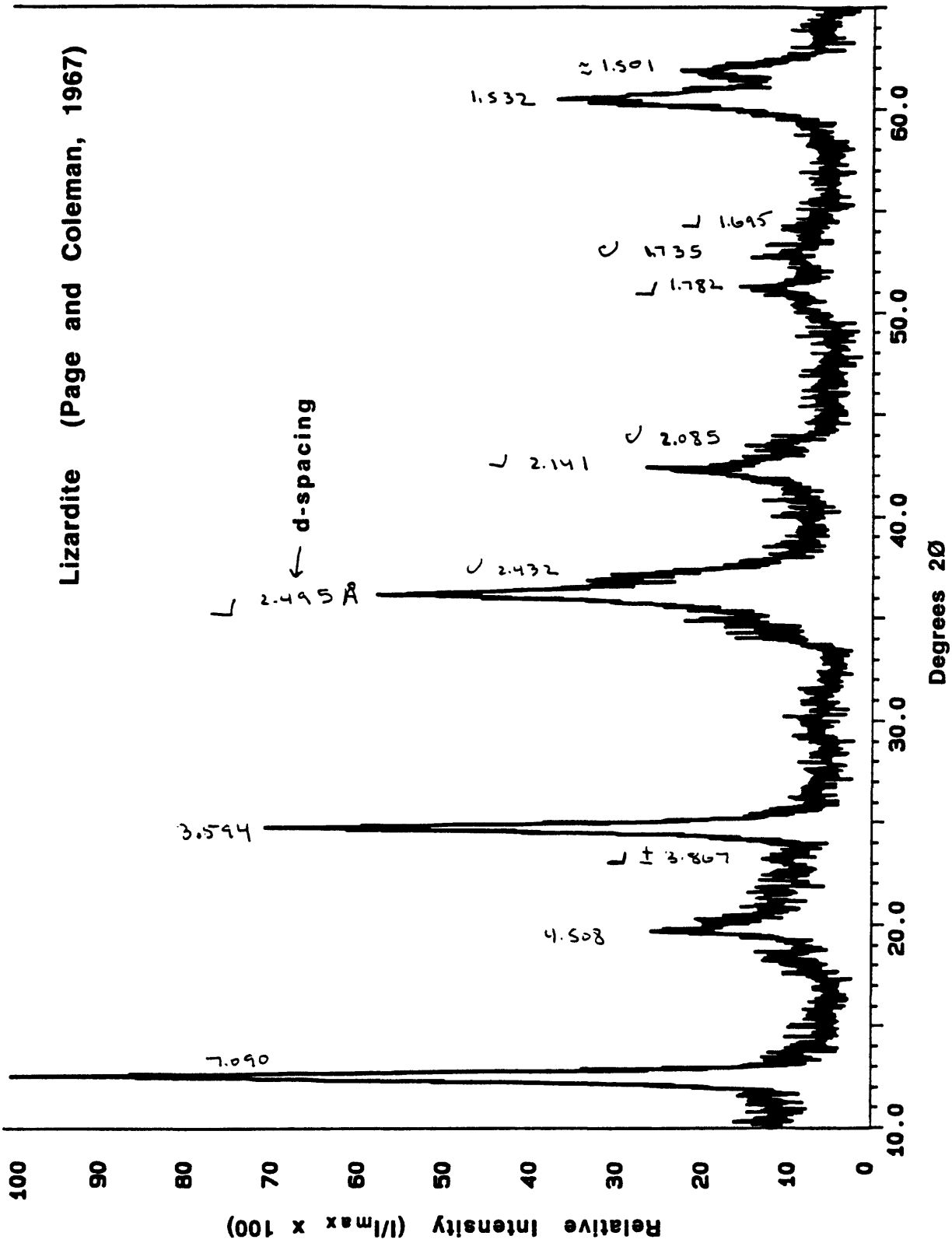

Figure 3. Diffraction pattern of the lizardite separate that was analyzed by Page and Coleman (1967). Characteristic of lizardite 1*T* is that the largest peak in the range 2.4–2.6 Å is at ≈2.50 Å; other peaks are at about 2.15, 1.79 and 1.70 Å. L = lizardite 1*T*; C = clinochrysotile.

lizardite data in Table 2 of Page and Coleman (1967) omits the 2.14 Å lizardite peak and reverses the relative intensities of the peaks at 2.49 and 2.44 Å, which probably misled Reinen in her identification of the serpentine mineral.

Lizardite-Rich Serpentinite (Oregon) — R. G. Coleman collected this sample of thoroughly serpentinized peridotite (#33-68) near Hunter Creek just south of Gold Beach, Oregon. The rock is dark greenish brown in color and fine-grained overall, but it also contains scattered large, platy crystals of serpentine up to 5 mm in diameter. The rock has a bulk specific gravity of 2.51 (Coleman, unpublished data), consistent with thorough serpentinization of the original peridotite, and in thin section it is seen to consist principally of serpentine minerals with minor magnetite and scattered crystals of spinel rimmed by chlorite (Tables 1, 3). The serpentine forms both the mesh and bastite textures that are considered to represent the replacement of olivine and pyroxenes, respectively. The differences in Si and Al contents between serpentine minerals with the mesh and bastite textures (Table 2) are consistent with the compositional differences found by Rutter and Brodie (1988) for lizardite replacing olivine and pyroxene. Sample preparation involved the removal of pale bluish-green veins that were suspected to be chrysotile. An x-ray pattern of the resulting separate (Fig. 4) is essentially all lizardite 1*T*, but very minor, questionable peaks at 2.44 and 2.09 Å suggest the possible presence of a few percent clinochrysotile.

Lizardite-Rich Serpentinite (New Idria, CA) — This sample, also provided by R. G. Coleman, is a relatively soft, fine-grained, mottled yellow rock that contains scattered opaque minerals, probably pyrite and magnetite. Rocks very similar in appearance to this sample partly replace blocks of antigorite-rich serpentinite at the open pit mine run by the Calidria Asbestos Company (KCAC) at New Idria, California. In thin section, the serpentinite has an apparent mesh texture that has been overprinted by multiple generations of veins, some fibrous, others apparently platy. The X-ray pattern of the bulk sample, NI-2 (Fig. 5), is dominated by lizardite 1*T* peaks, but clinochrysotile is also relatively abundant. An attempt was

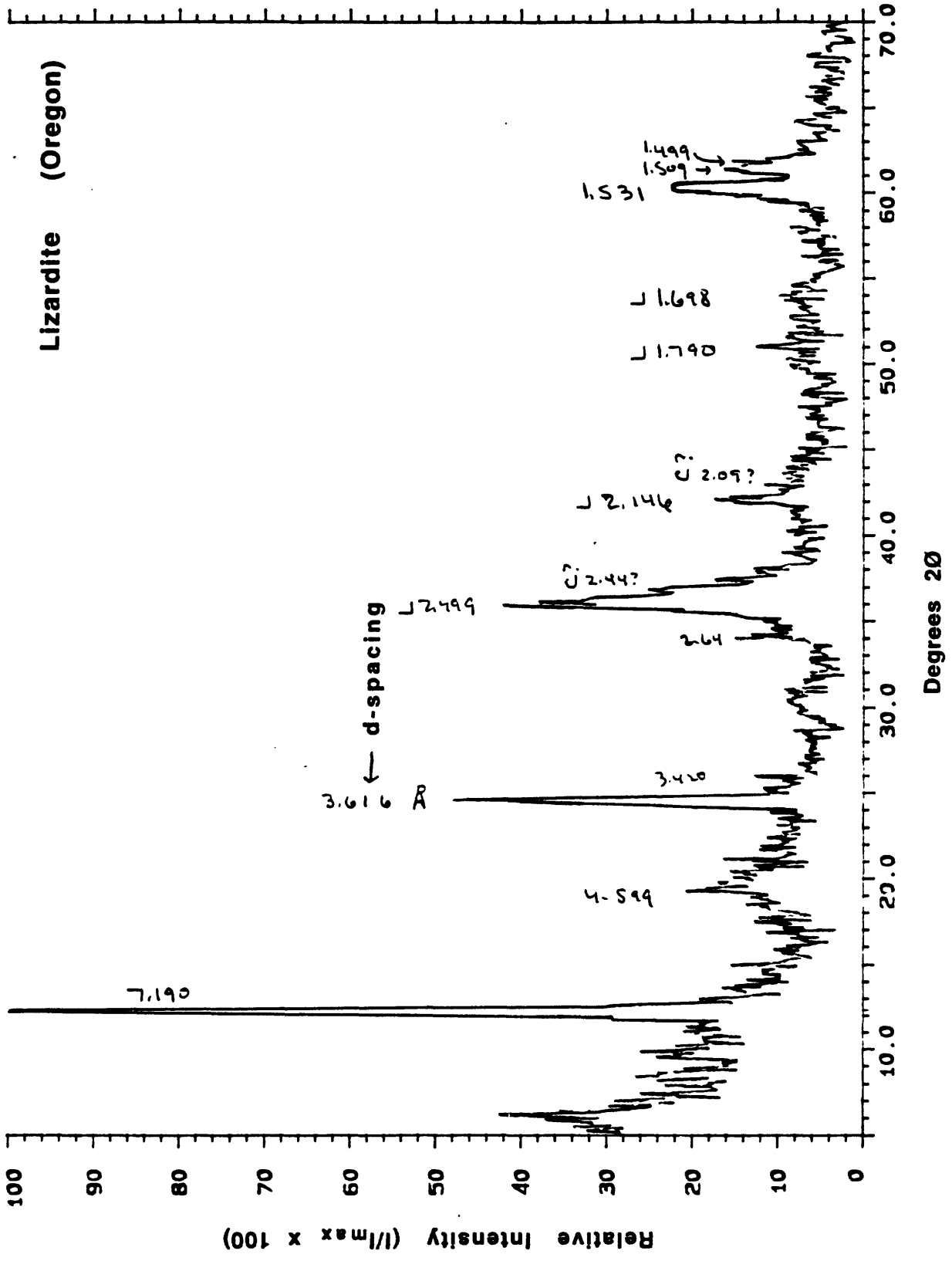

Figure 4. X-ray pattern of the lizardite-rich serpentinite collected near Gold Beach, Oregon. The presence of small amounts of clinochrysotile (C) is suggested by possible low-intensity peaks at 2.44 and 2.09 Å. L = lizardite 1*T*.

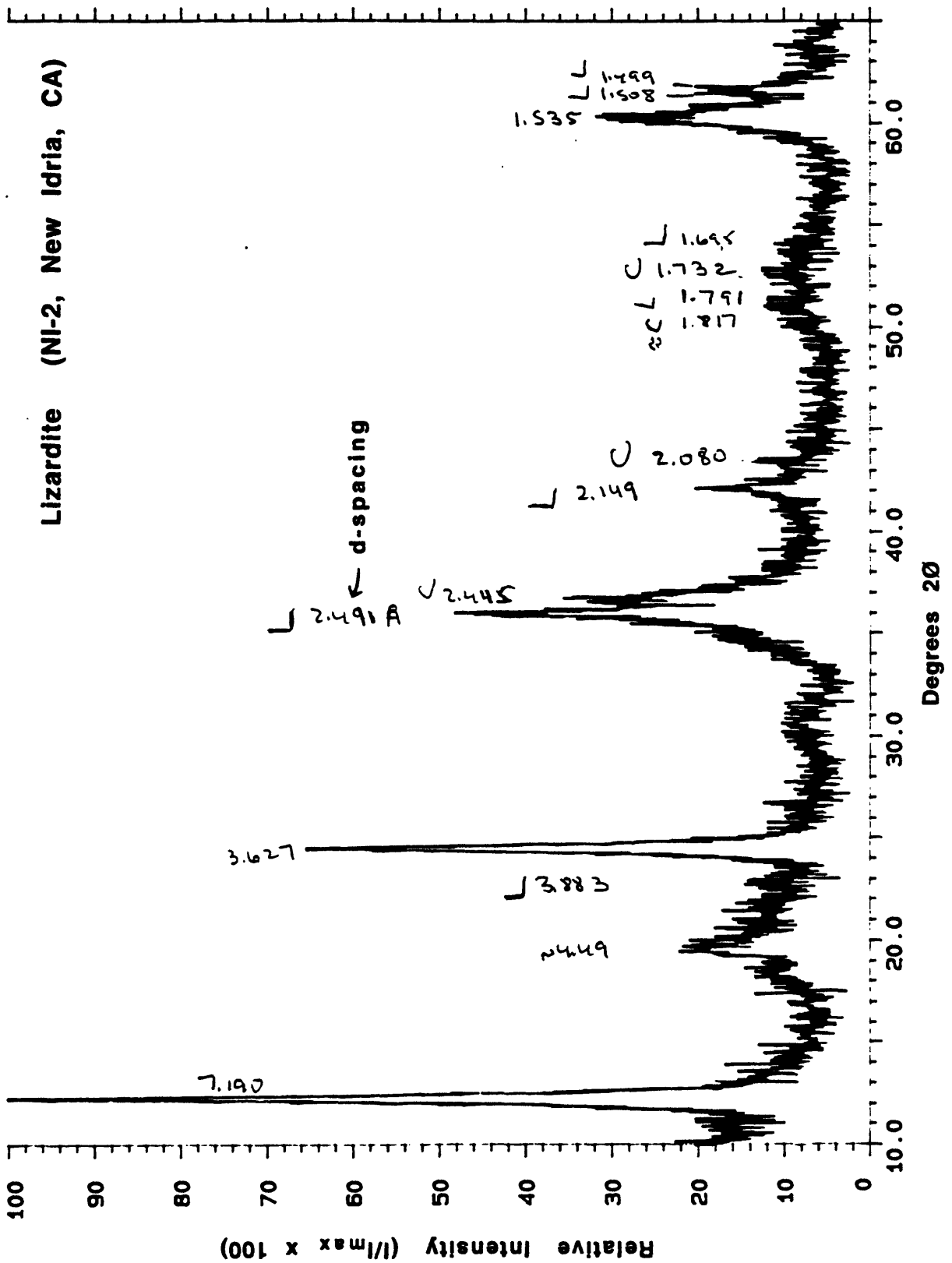

Figure 5. X-ray diffraction pattern of the bulk lizardite sample from New Idria, California (NI-2). Lizardite 1*T* (L) is the dominant serpentine mineral, but relatively prominent peaks at 2.44 and 2.08 Å and minor peaks at 1.83 and 1.73 Å indicate the presence of clinochrysotile (C) in larger amounts than in Figure 3. A separate from this sample (NI-1) has slightly more intense clinochrysotile peaks than the bulk material.

made to remove some of the chrysotile from the sample, but the separate, NI-1, turned out to be slightly enriched in chrysotile compared to the bulk sample.

Antigorite-Rich Serpentinite (New Idria) — The sample came from a large, weather-resistant block collected from the tailings piles of the KCAC mine. The rock is dark green to brownish black in color, relatively hard, and strongly magnetic. It also contains numerous light green to bluish green veins of probable chrysotile, and sample preparation involved removal of the chrysotile veins and associated altered rock, where possible. Antigorite, magnetite, and calcite peaks all appear on the X-ray pattern of the prepared sample (Fig. 6), and chlorite (Tables 1, 3) is visible in thin section. The diffraction pattern is complicated, but the presence of antigorite is indicated by a strong peak at 2.52 Å, a subsidiary peak at 2.39 Å, and one at 1.55-1.56 Å that is unique to antigorite (representing the 330 reflection, Whittaker and Zussman, 1956). The antigorite contains moderate amounts of Al and Fe (Table 2), consistent with other published analyses of antigorite (e.g., Wicks and Plant, 1979).

Antigorite (Vermont) — We obtained pieces of a blue-green, antigorite-rich serpentinite that is mined as a decorative stone (verde antique) in the vicinity of Roxbury, Vermont. The serpentinites of this area have been described by Jahns (1967); Reinen et al. (1994) used material from the same general area for some of their antigorite experiments. The bulk samples contain magnesite and magnetite in addition to the antigorite, but because the rock is relatively coarse-grained, an essentially pure antigorite separate (Fig. 7) could be picked from crushed pieces of the serpentinite. This separate has not as yet been used in any laboratory experiments; it is included here because it provides a reference X-ray diffraction pattern for antigorite.

Orthochrysotile — The sample was collected near Cape San Martin, along the central California coast, from a reaction zone at the contact between serpentinite and Franciscan metasedimentary rocks (R. G. Coleman, personal communication, 1995). It is a clear yellow rock, with disseminated opaque minerals, and sample preparation involved removal of the

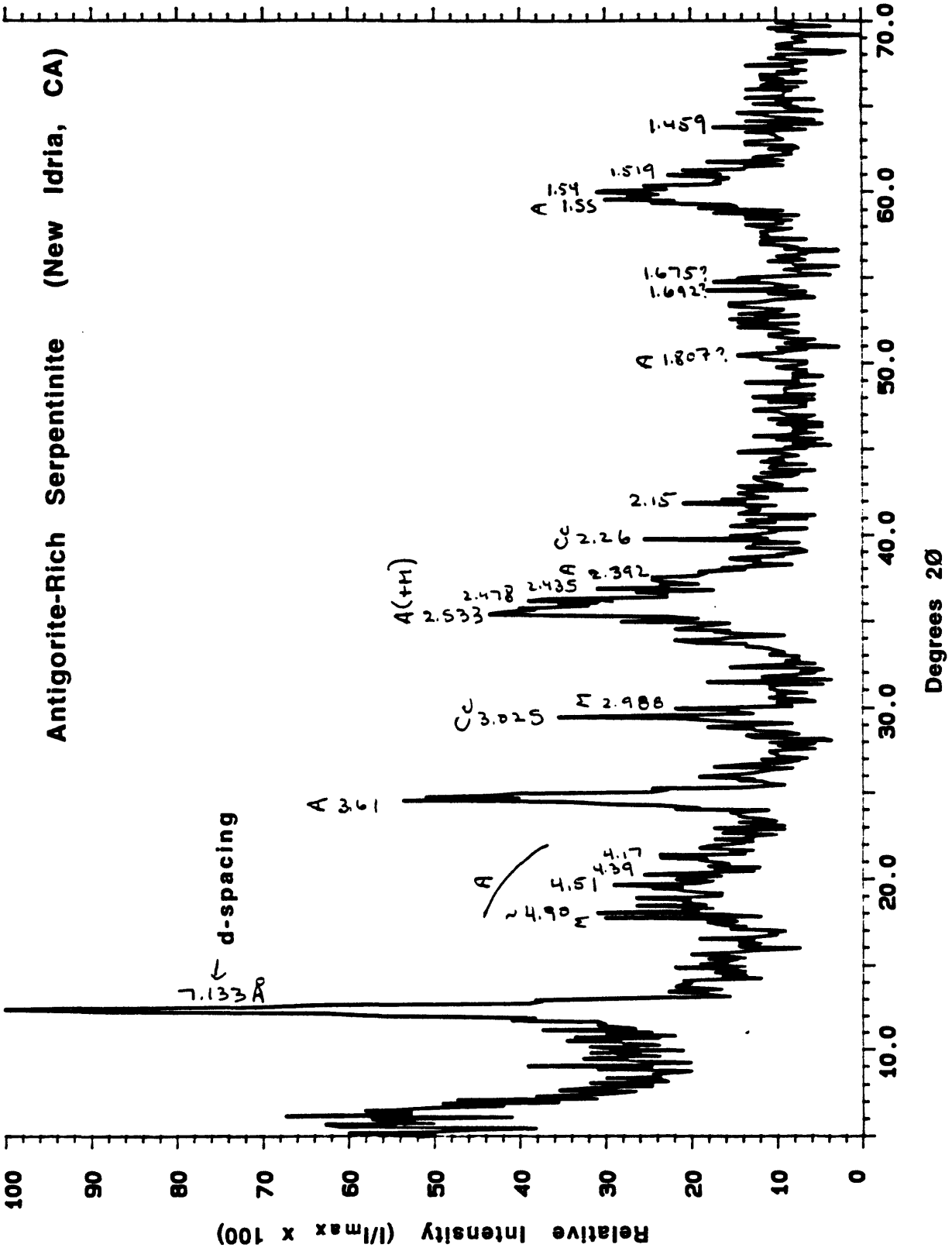

Figure 6. Diffraction pattern of antigorite-rich serpentinite from New Idria, California. Along with antigorite (A), the gouge contains peaks attributable to magnetite (M) and calcite (Cc), consistent with thin-section observations (Table 1).

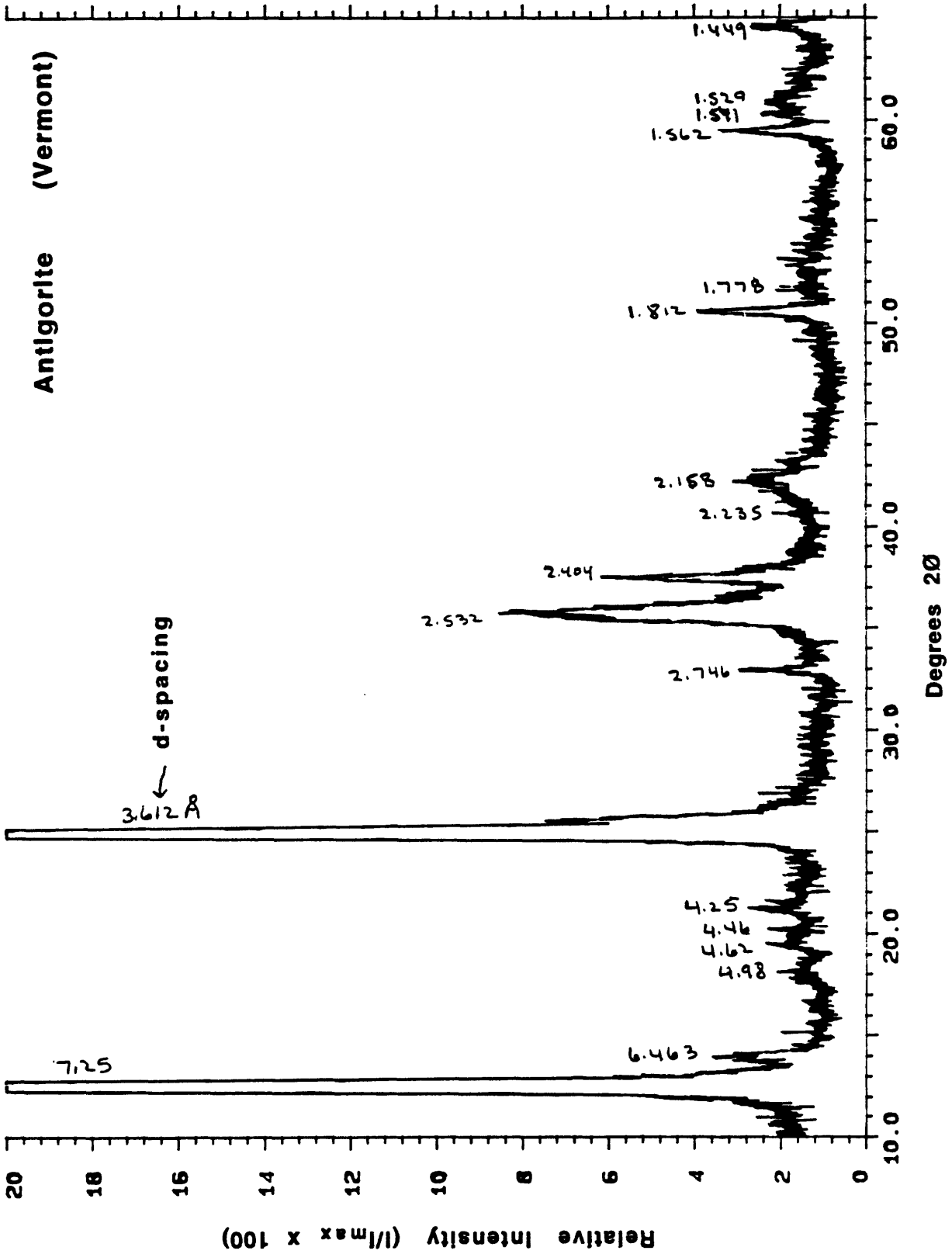

Figure 7. X-ray pattern of antigorite separate from Roxbury, Vermont; only the low-intensity range is shown. Characteristic of antigorite is that in the range 2.4–2.6 Å the major peak is at ≈2.53 Å but, in addition, a relatively prominent peak occurs at ≈2.41 Å. Antigorite also has a peak at 1.55–1.56 Å that other serpentine minerals lack.

opaque grains. The X-ray diffraction pattern (Fig. 8) is consistent with the mineral orthochrysotile, based on the criteria outlined by Wicks and O'Hanley (1988).

Samples from Previous Studies

Summers and Byerlee (1977a, b) measured the strengths of two serpentinite samples, one a serpentinite from New Almaden, California that was identified as antigorite, and the other a "serpentinized harzburgite" from Del Puerto, California, for which serpentine-mineral identification was not provided. Both the original rock samples and the prepared gouges of the two serpentinites were located for thin-section and X-ray diffraction analysis.

DP-2 — In hand specimen, DP-2 is a relatively fine-grained, nearly black rock. The X-ray diffraction pattern of the gouge (Fig. 9) is complex, with peaks attributable to relict olivine and pyroxene as well as lizardite 1*T*, magnetite and possibly clinochrysotile. The olivine is Mg-rich (Fo_{88}), and the pyroxene is diopside (Table 3). Relict olivine comprises nearly 20% by volume of the examined rock sample (Table 1) and serpentine minerals — predominantly lizardite — about 70%. The lizardite is very uniform in composition (Table 2), with relatively high Fe contents but the lowest Al contents of any of the analyzed serpentine minerals.

ALM-1 — The rock is black and mostly fine grained, but with some platy crystals up to 3–4 mm in length. Fractures are lined with a pale green mineral, possibly chrysotile. The principal serpentine mineral in this sample was originally identified as antigorite, and the identification was consistent with the powder diffraction files published before 1980. However, the X-ray pattern of ALM-1 (Fig. 10) does not match the antigorite pattern for the separate from Vermont (Fig. 7). Many serpentine minerals that were initially thought to be antigorite have subsequently been re-identified as polytypes of lizardite, as a result of recent advances in X-ray crystallographic techniques. Based on current powder diffraction data, the serpentine mineral in ALM-1 corresponds most closely to the multilayered lizardite 6*H* , whose

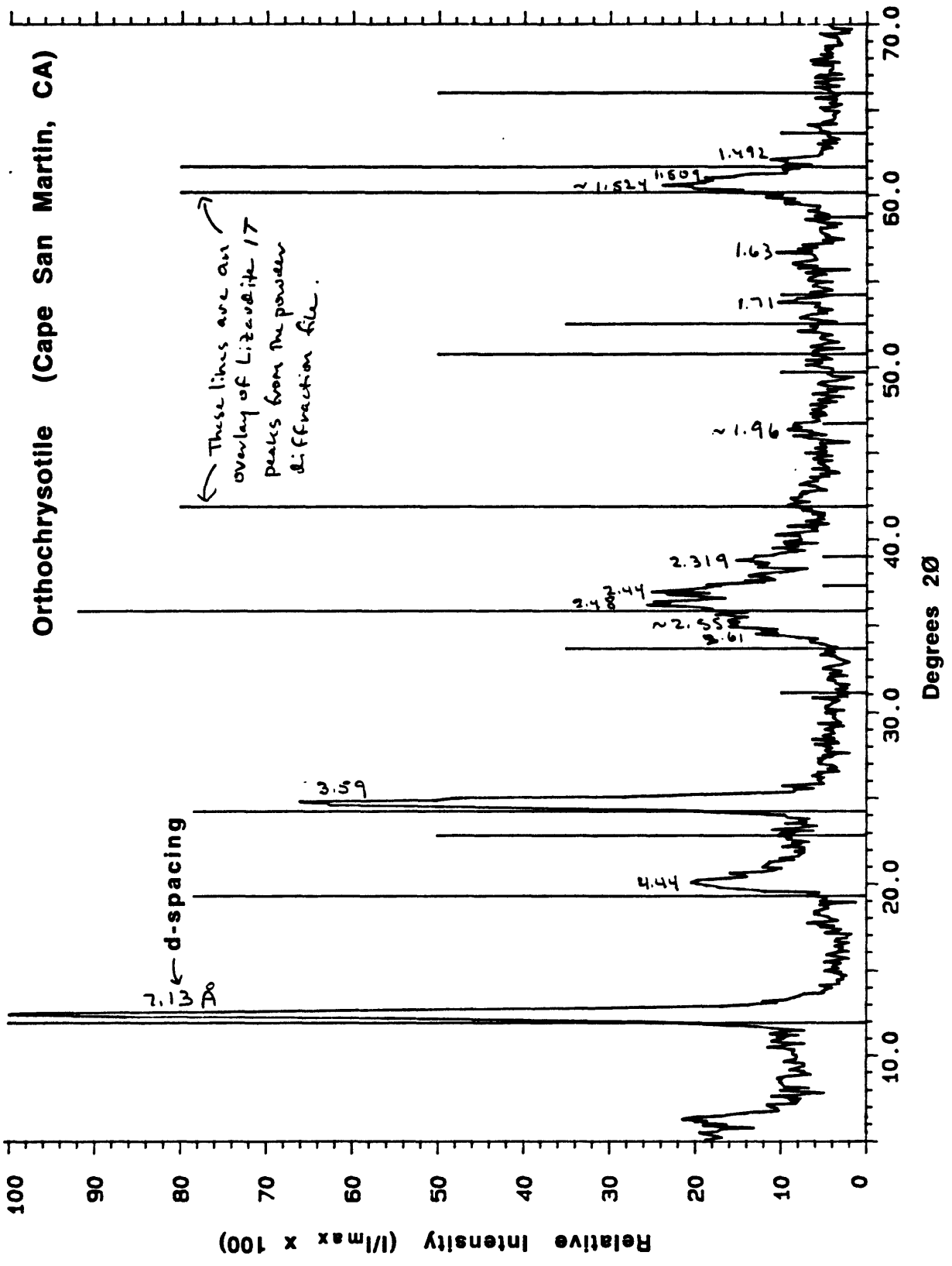

Figure 8. Diffraction pattern of clear yellow serpentinite from Cape San Martin, California, which corresponds most closely to orthochrysotile (see Wicks and O'Hanley, 1988).

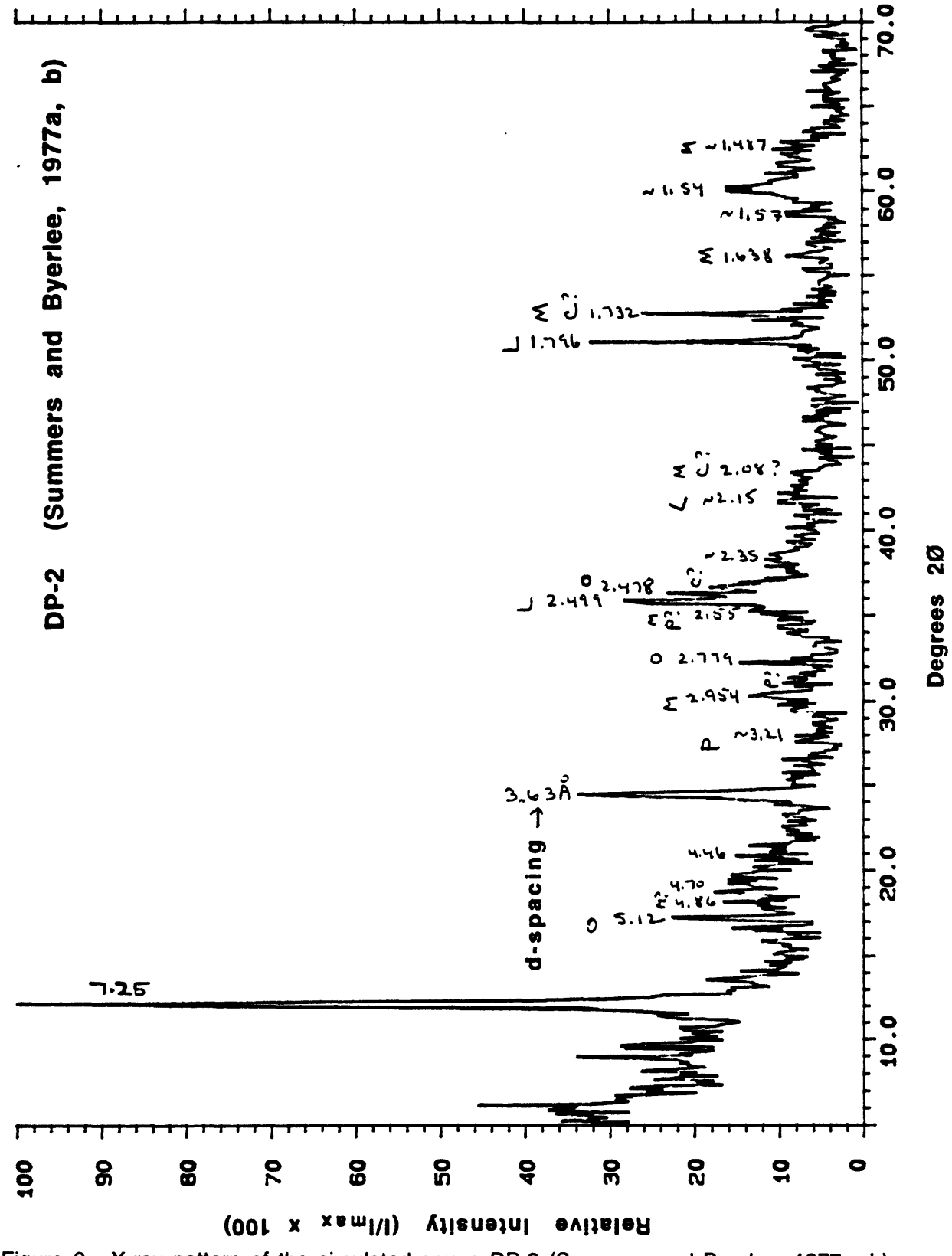

Figure 9. X-ray pattern of the simulated gouge DP-2 (Summers and Byerlee, 1977a, b), collected in Del Puerto canyon, California. There are peaks attributable not only to lizardite 1*T* but also to olivine (O), magnetite (M), and possibly pyroxene (P) and clinochrysotile (C), consistent with the mineral assemblage in Table 1.

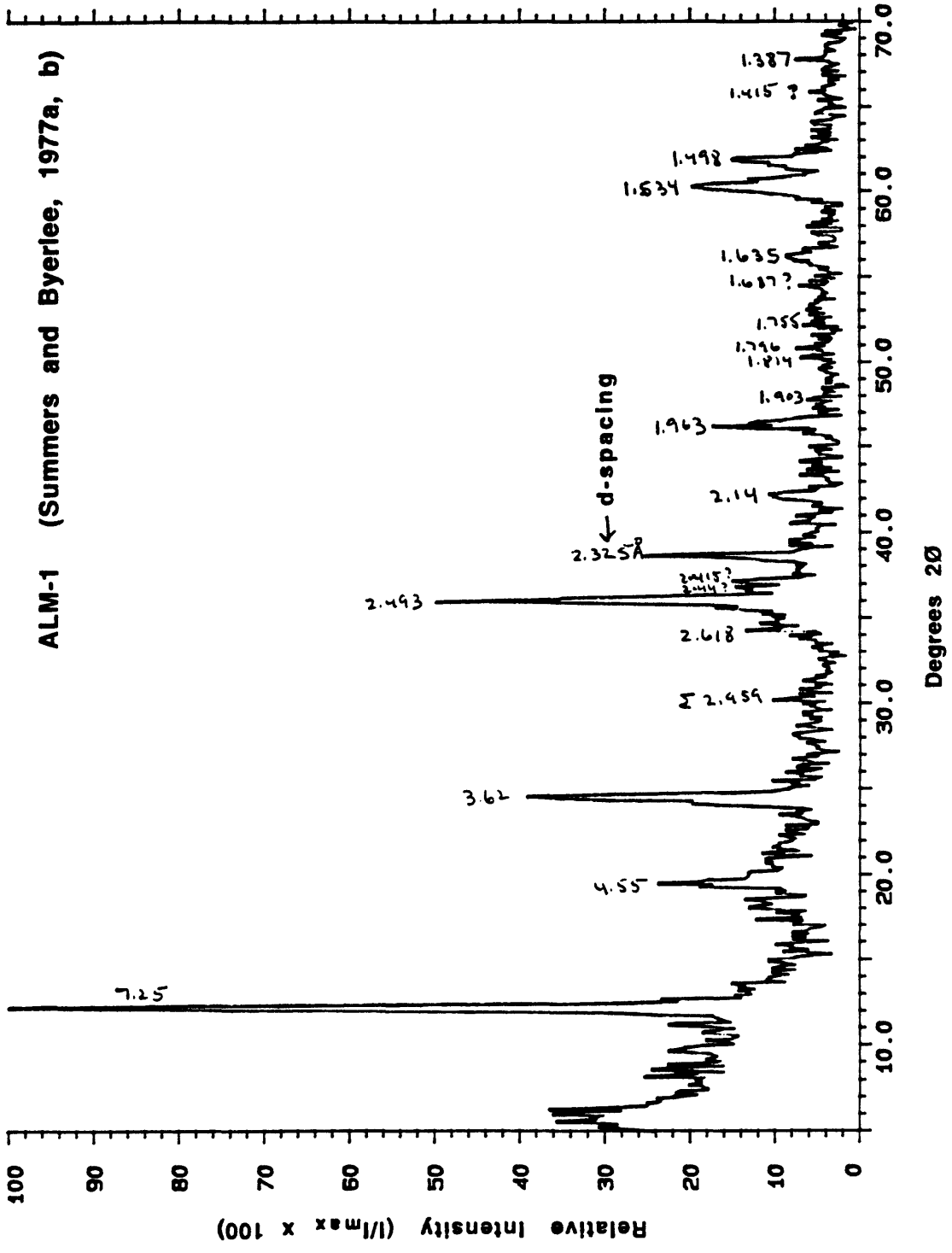

Figure 10. X-ray diffraction pattern of the simulated gouge ALM-1 (Summers and Byerlee, 1977a, b), from New Almaden, California. This sample was originally identified as antigorite, but serpentine minerals with this crystal structure have since been re-identified as lizardite 6*T* (Hall et al., 1976). The small peak at 2.15 Å may indicate the additional presence of lizardite 1*T*. M = Magnetite. Lizardite 6*T* and orthochrysotile have similar X-ray patterns, but orthochrysotile has a strong peak at 2.44 Å that lizardite 6*T* lacks, whereas lizardite 6*T* has a better-defined peak at 2.14 Å, along with small peaks at ≈1.81 and 1.38 Å.

crystal structure was worked out by Hall et al. (1976). Small magnetite (M) peaks can be seen in Figure 10, and magnetite is relatively abundant in the examined thin section (Table 1).

Halloysite — Halloysite is a clay mineral, not a serpentine mineral, but its frictional properties were of interest to this investigation, because halloysite commonly takes on a tubular form similar to chrysotile. Summers and Byerlee (1977a, b) determined that halloysite is as strong as the clay minerals illite and kaolinite, which suggests that the tubular form of itself cannot be the cause of the low strength of chrysotile. The sample used by Summers and Byerlee (1977a, b) was retrieved and X-rayed, because the name halloysite has been applied to two mineral varieties. Halloysite can take on interlayer water in a similar fashion to montmorillonite, and the hydrated and expanded form, which has a ≈10 Å layer spacing, is generally referred to as halloysite. The structure lacking interlayer water has a ≈7 Å layer thickness and is commonly called metahalloysite, but it has also been termed halloysite (7 Å) (e.g., Giese, 1988). The X-ray pattern of the material used by Summers and Byerlee (Fig. 11) corresponds to the non-expanded variety, metahalloysite or halloysite (7 Å).

Morrow et al. (1982) measured the room-temperature strength of two natural serpentinite gouge samples, one from the Hayward fault (D St. Hayward) and one from near the San Andreas fault (Golden Gate bridge). They describe both samples as being 100% serpentine minerals, of unspecified variety. The Hayward fault gouge was somewhat stronger than the Golden Gate Bridge sample. The original gouge materials were examined by a combination of X-ray diffraction, stereomicroscope, and scanning electron microscope (SEM) techniques. The gouges used in two of the friction experiments were also X-rayed, for comparison with the starting materials.

Golden Gate Bridge — This gouge, which was provided by R. Nason, consists of elongate, grayish-green fragments of serpentinite up to a centimeter or so in length that are set in a fine-grained, paler green matrix. Partial alignment of the fragments imparts a modest fabric

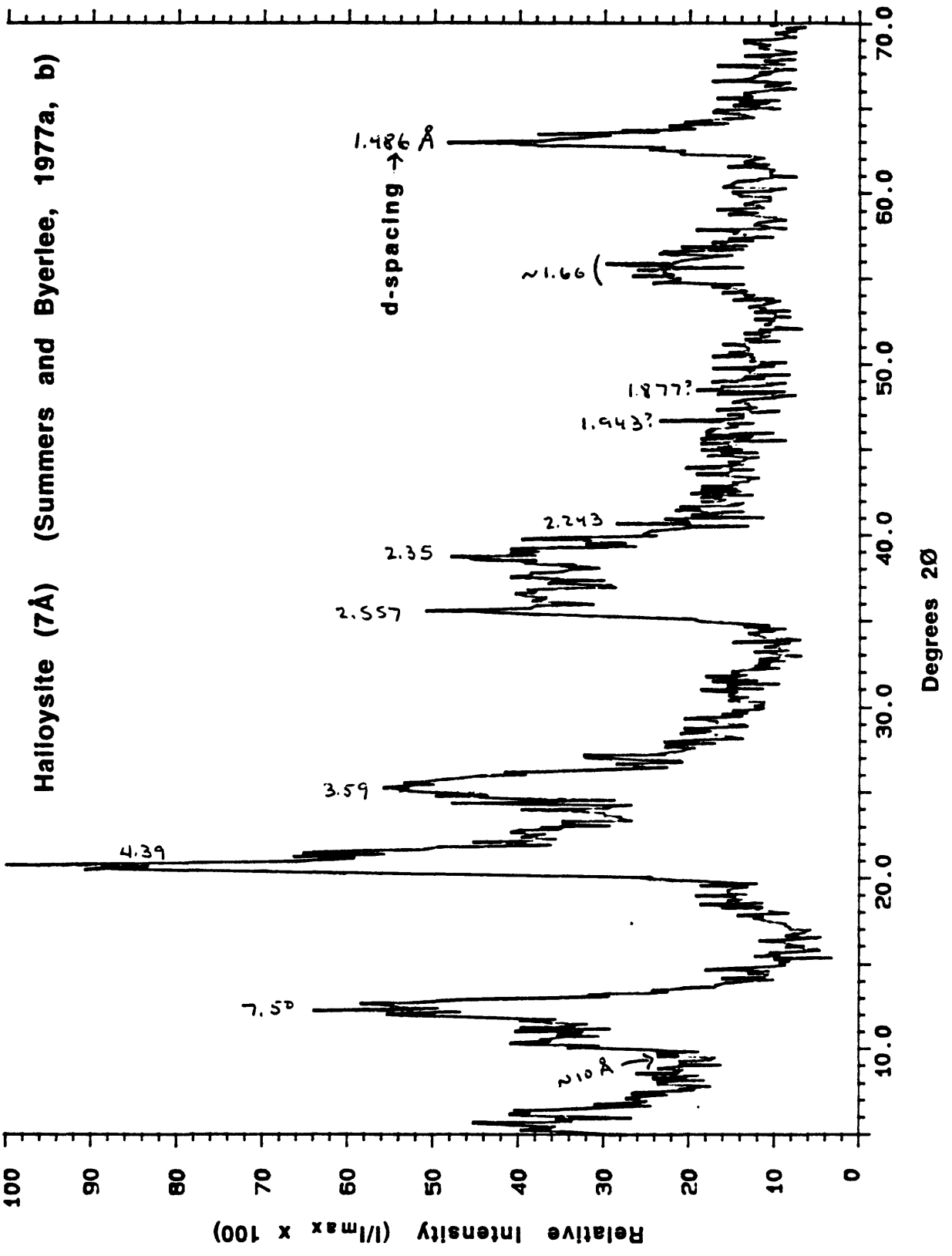

Figure 11. X-ray diffraction pattern of halloysite, tested by Summers and Byerlee (1977a, b). The name halloysite can refer to a ≈7 Å layer-thickness clay mineral or its ≈10 Å expanded form. The X-ray pattern corresponds to the non-expanded clay, halloysite (7Å).

to the gouge. Bulk X-ray diffraction analysis (Fig. 12) suggests the presence of both lizardite 1*T* and clinochrysotile (L > C), with accessory magnetite and possible traces of spinel.

D. St. Hayward — The hand specimen consists of two distinct parts, a serpentinite-rich gouge with a pebbly soil draped over parts of it. The serpentine-rich material is a fine-grained, waxy, grayish green gouge with reddish-brown iron stains on the surface. Clots of white fibers protrude from the sample, and scattered magnetite grains are visible under the stereomicroscope and SEM. Void spaces in the gouge are lined with a chalky white mineral that fizzes upon treatment with HCl and thus is probably calcite. The attached soil is a dull brown silt or clay that contains numerous small pebbles of grayish and pinkish quartz. The X-ray diffraction pattern of the sieved gouge used in the experiments (Fig. 13) contains peaks consistent with the assemblage clinochrysotile + quartz + calcite + magnetite, indicating that the serpentinite gouge and the soil were mixed together for use in the laboratory experiments.

Experimental Methods and Correction Procedures

The prepared serpentinite samples were hand ground sufficiently to pass through an 88-μm sieve, to produce simulated gouges. For the friction experiments, a 1-mm thick layer of gouge was placed along a 30° sawcut in a cylinder of antigoritic serpentinite (Fig. 14), obtained from some of the same blocks as the antigorite-rich gouge. Serpentinite cylinders were used to avoid the possibility of metasomatic reactions with the gouge. The sawcut surfaces were roughened with #60 SiC prior to sample assembly. A borehole for pore fluid entry was drilled all the way through the upper piece of the cylinder (Fig. 14), to ensure that the gouge did not become isolated from the pore-fluid system. The borehole was packed with quartz beads, which minimized the extrusion of gouge into the borehole but allowed free flow of fluid. The serpentinite samples, along with titanium carbide and alumina spacers, were placed in annealed copper jackets (Fig. 14), to separate them from the confining pressure medium. A limited

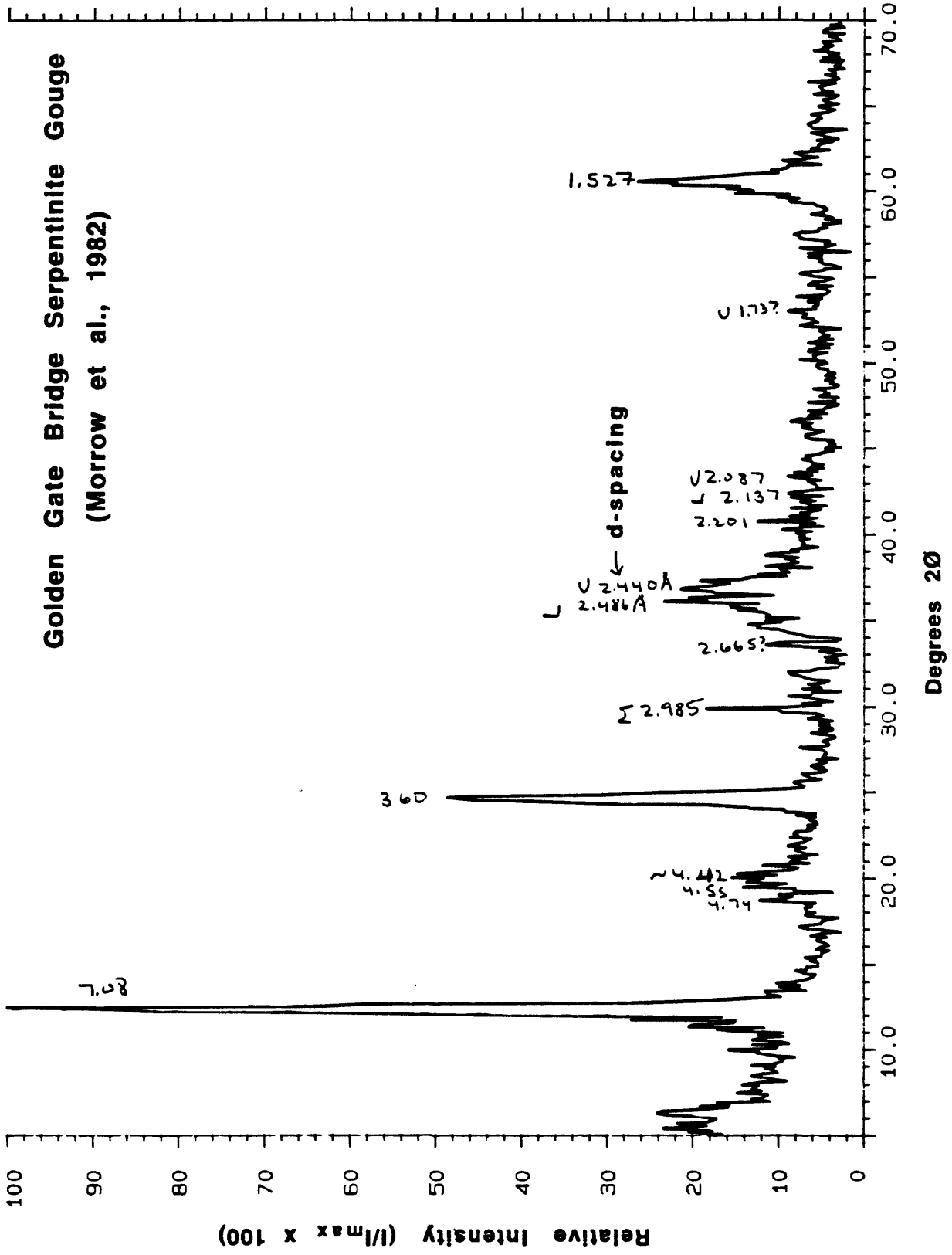

Figure 12. X-ray diffraction pattern of the "Golden Gate bridge" serpentinite gouge (Morrow et al, 1982). The gouge appears to be a mixture of lizardite 1*T* (L) with slightly subsidiary clinochrysotile (C). M = Magnetite.

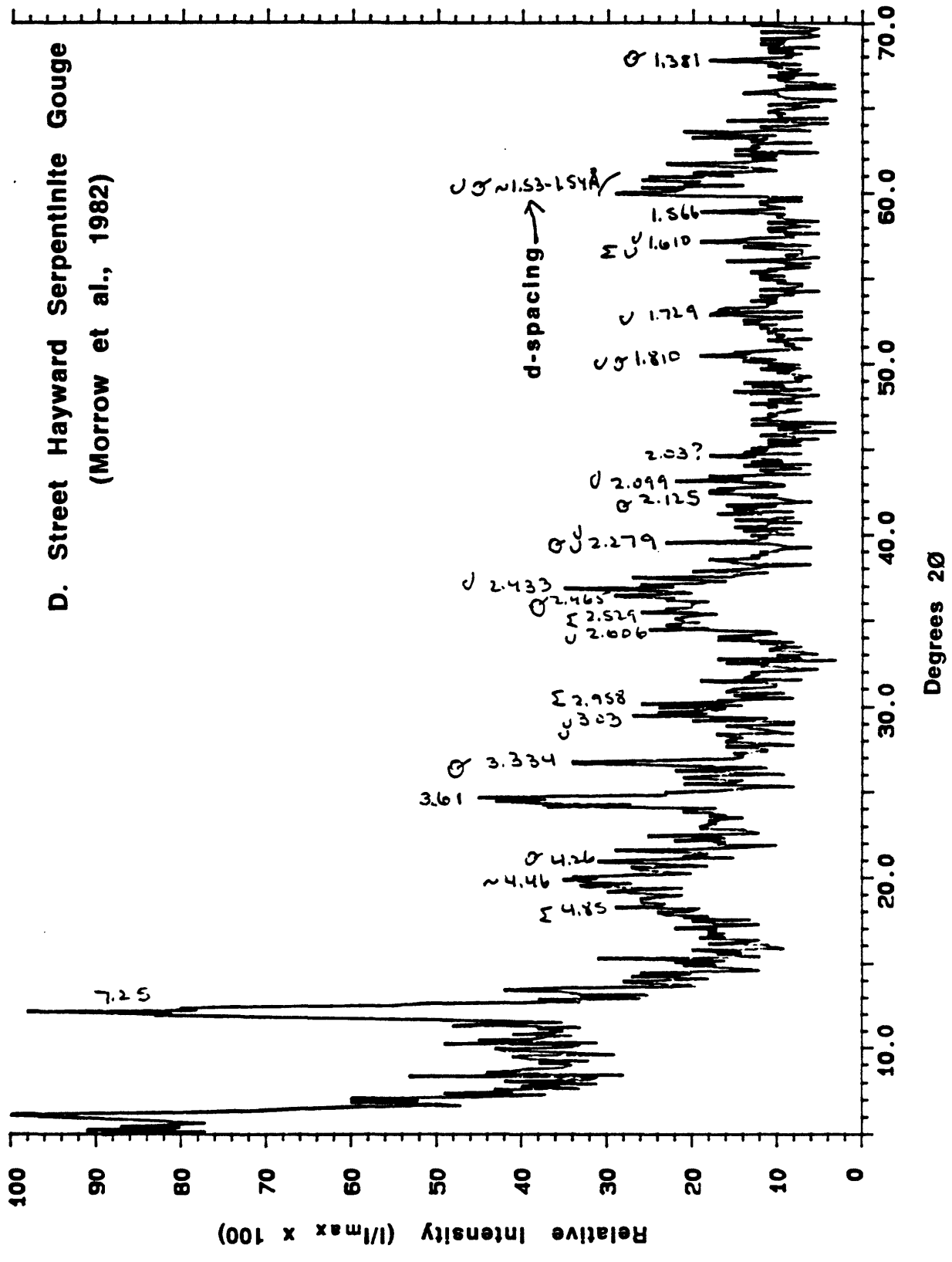

Figure 13. Diffraction pattern of the sieved sample prepared from the "D St. Hayward" serpentinite gouge (Morrow et al., 1982). The complex pattern appears to show the assemblage clinochrysotile (C) + quartz (Q) + calcite (Cc) + magnetite (M); the same minerals are present in the original gouge material.

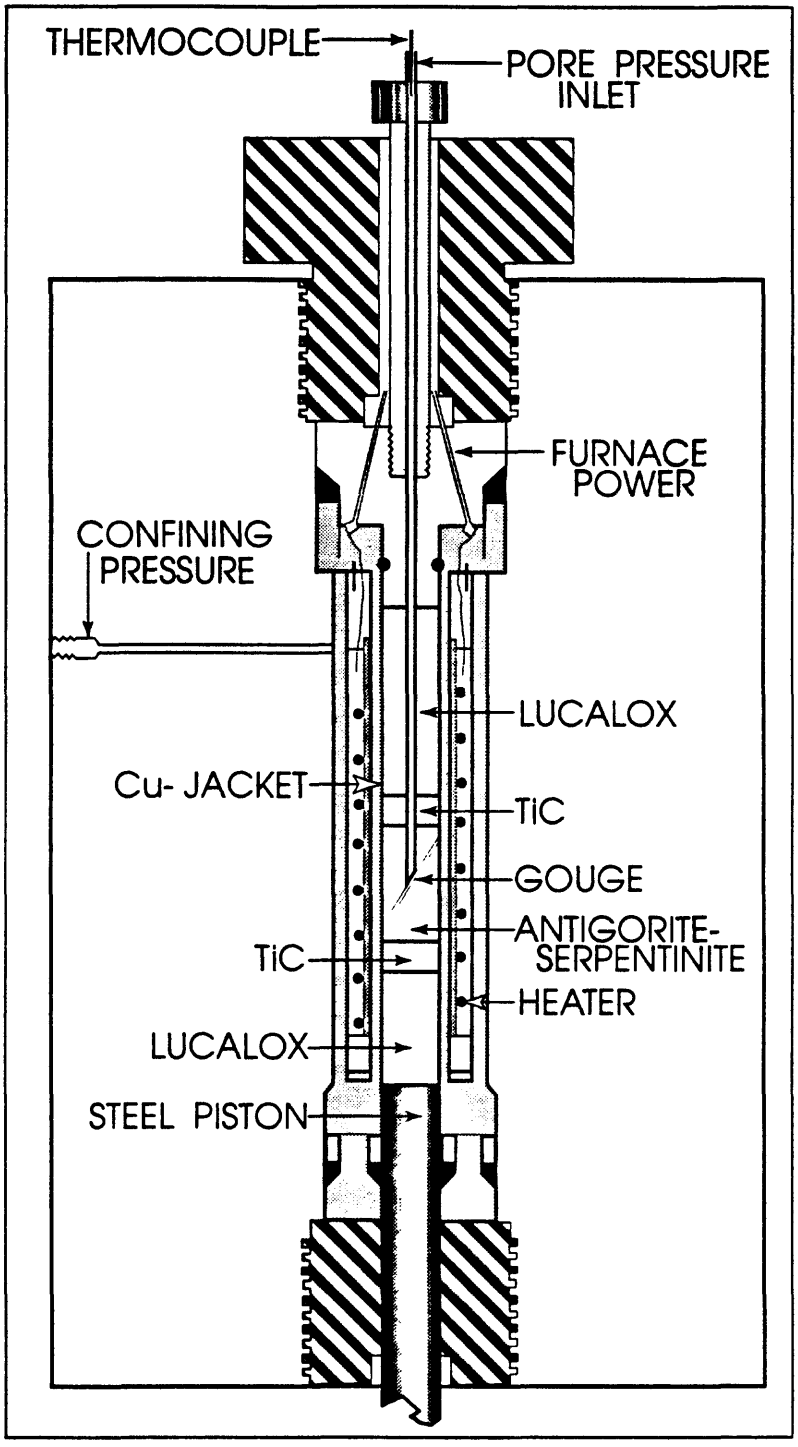

Figure 14. Experimental apparatus used for friction experiments at elevated temperatures.

number of runs used polyurethane or viton jackets, to provide independent measures of copper jacket strength corrections.

Confining pressure was applied first to the sample, followed by the pore pressure, with deionized water as the pore fluid. Confining pressure was measured to within 0.02 MPa, at an accuracy of ±0.3 MPa. Pore pressure was also measured to a precision of 0.02 MPa and ±0.2 MPa accuracy. After the pressures had equilibrated, the temperature was raised to the desired value. Temperature was monitored by a thermocouple inserted through the pore-pressure inlet. The samples were positioned in the furnace such that the temperature maximum — as then determined — was located near one end, with temperature decreasing by 2% across the length of the samples. After these experiments were completed, however, we discovered that the position of the peak temperature along the length of the furnace varies with the pressure of the argon gas that was used as the confining-pressure medium. For the range of confining pressures applied in this study, the actual temperatures along the samples were ≈3% lower than we thought. Corrected temperatures are used throughout this report.

All experiments were run at a constant normal stress, which was maintained by means of computer-controlled adjustments to the confining pressure. Axial stress was measured to a precision of 0.1 MPa and an accuracy of 1.0–1.5 MPa, and displacement measurements were made to a precision of 0.1 μm and an accuracy of approximately 5.0 μm. The machine stiffness is equivalent to 495 MPa/mm shear stress for a 19.1-mm-diameter sample. Corrections for changes in contact area along the sliding surface were made according to the calculations presented by Scott et al. (1994). The absolute value of seal friction was zeroed out before a given sliding test commenced. Because seal friction is a function of confining pressure, an additional correction was applied during the experiment, to account for the continuing adjustments to confining pressure to maintain a constant normal stress. The overall correction to confining pressure for the seal friction is about 1% of the value of confining pressure.

Corrections for the strength of the copper jackets (annealed, 0.38-mm wall thickness) were determined from a series of test experiments. Because copper becomes progressively softer with increasing temperature, a separate correction factor was obtained for each temperature tested in the serpentinite experiments. Three experiments were run at 25, 97, and 194 °C using the copper jackets but substituting a 1-mm-thick sheet of teflon for the gouge layer and steel end pieces for the antigorite cylinder (Fig. 15a). Teflon should be stable for the length of the experiments at all temperatures tested. Linear equations were fit to the portions of each curve between 0.5 and 4.0 mm axial displacement, where Z is the amount of axial shortening in millimeters (Fig. 15a). While not strictly correct, the teflon is asssumed to show no strain-hardening effects; the strain-hardening term in each equation is attributed entirely to the copper jacket. The room-temperature offset value (at Z = 0) was determined by comparison to experiments conducted in polyurethane jackets of 3.18-mm wall thickness. The strength correction for polyurethane was determined by means of a steel/teflon experiment of the type described above (Fig. 15b). The ≈1.57 MPa term in the linear fit to the shear-stress data (Fig. 15b) is assumed to represent the yield stress of teflon, making the room-temperature correction (in MPa) for the polyurethane jacket as follows:

$$\tau_{jacket}\ [MPa] = 1.09\ Z\ [mm] \qquad (1)$$

Three room-temperature chrysotile-gouge experiments were conducted using polyurethane jackets. The measured shear stresses, corrected for the strength of the polyurethane jackets [equation (1)], are plotted in Figure 15c, along with the equivalent room-temperature data for copper-jacketed chrysotile gouge, without jacket corrections. Average trend lines fit to each group of experiments (dashed lines in Fig. 15c) are offset by ≈10.2 MPa at 0 displacement. This offset exceeds the room-temperature value in Figure 15a by ≈1.6 MPa. Since all experiments shown in Figure 15c were at identical pressures and used the same gouge, they should all reflect the same gouge strength. We therefore concluded that our

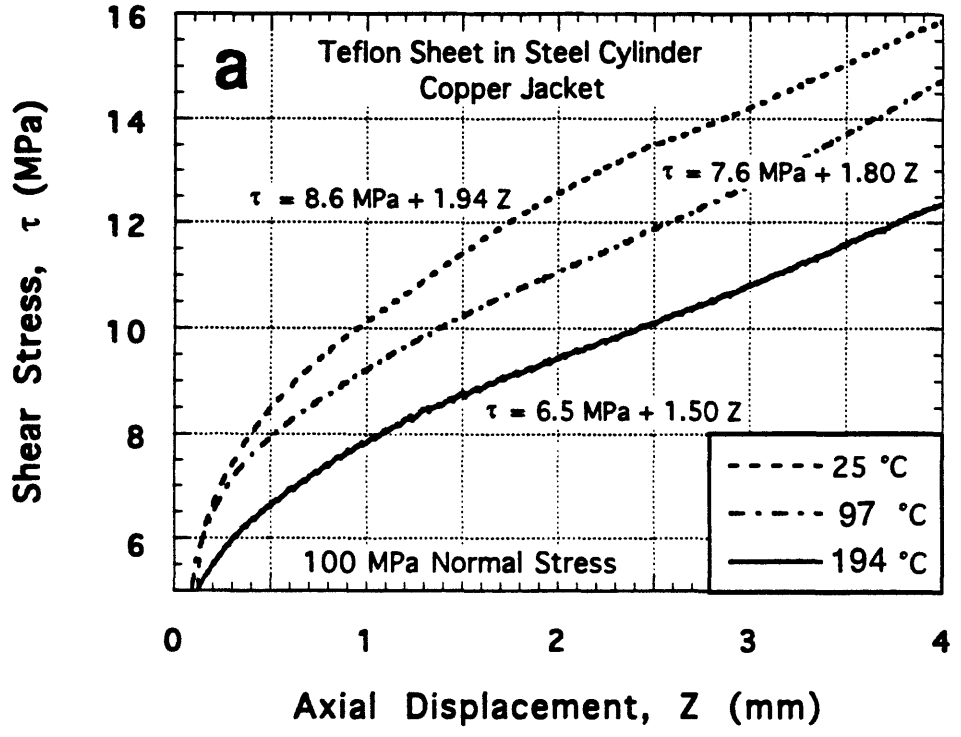

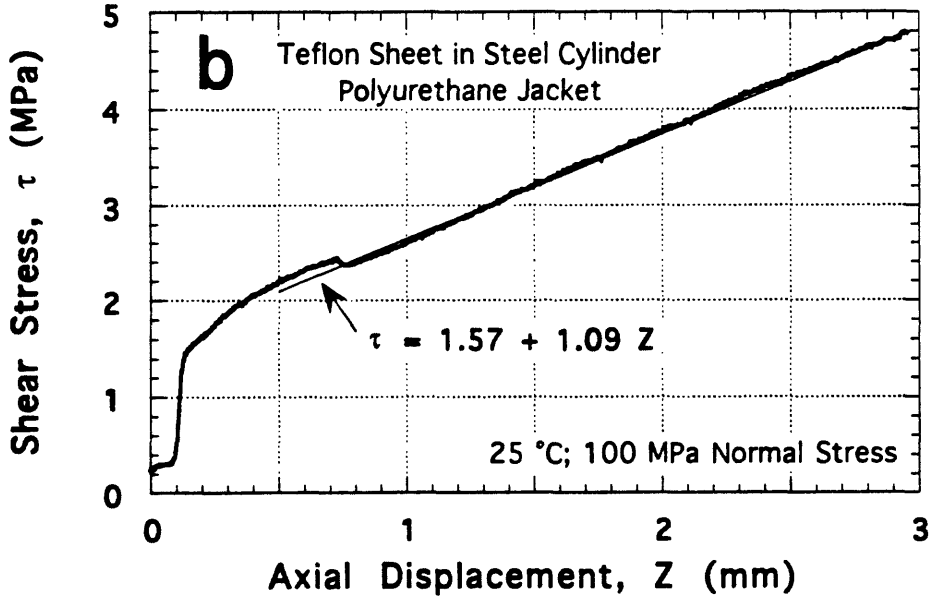

Figure 15. Experiments conducted to determine jacket corrections. a) Friction experiments on samples consisting of a 1.02-mm-thick teflon sheet between steel end pieces, housed in annealed copper jackets of 0.38-mm wall thickness. Experiments conducted at 100 MPa normal stress. Linear fits to the data were made over the axial-displacement range 0.5-4.0 mm. b) Plot of shear stress versus axial displacement for a teflon/steel sample housed in a

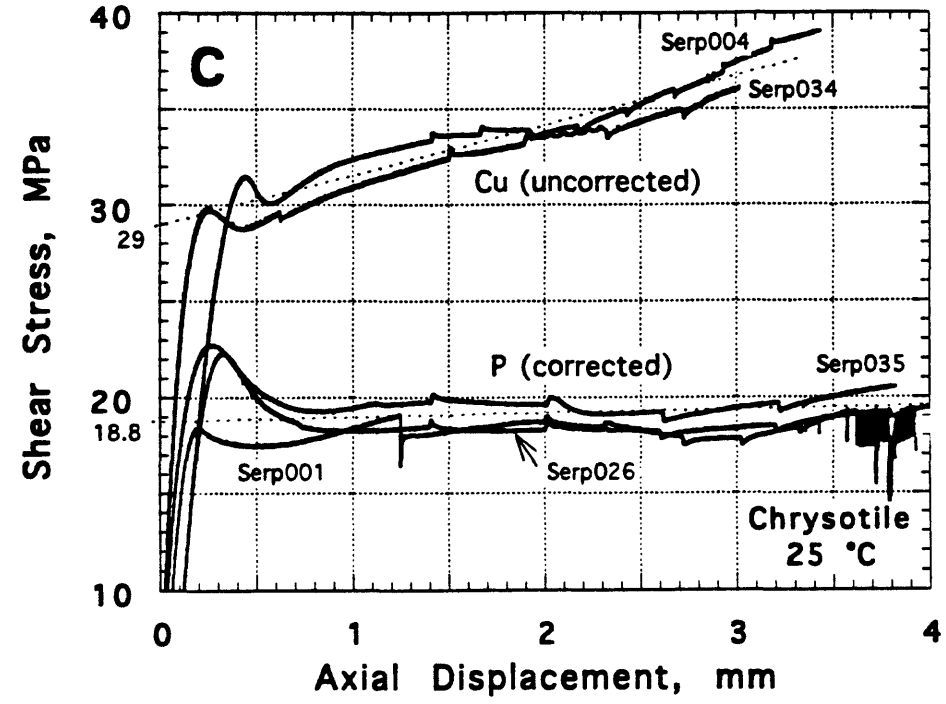

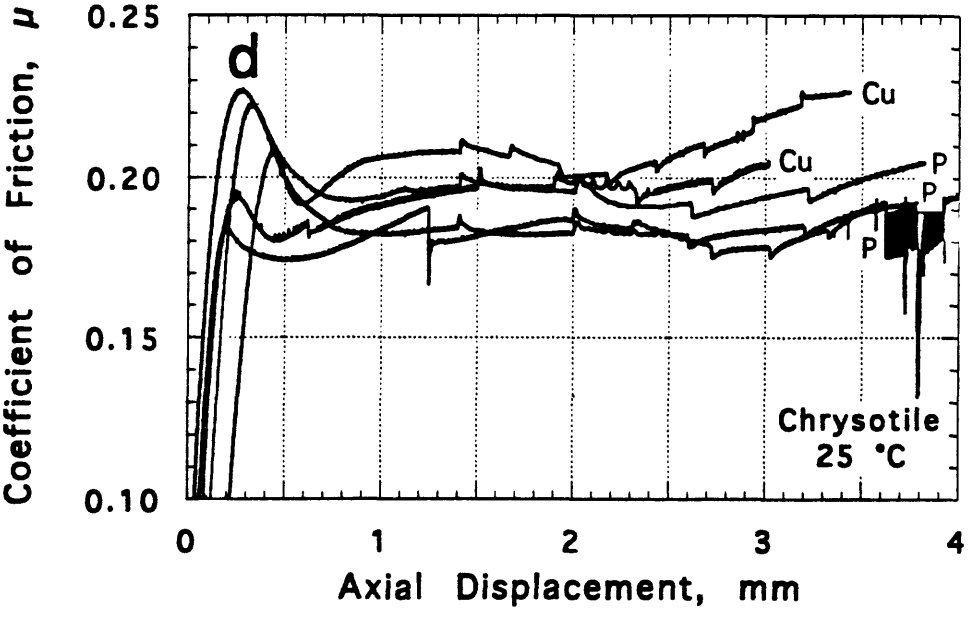

Figure 15, continued.

polyurethane jacket of 3.18-mm wall thickness. Normal stress = 100 MPa. c) Measured shear strengths from room-temperature chrysotile-gouge experiments in polyurethane (P) and copper (Cu) jackets. A jacket correction was applied only to the data from polyurethane experiments. Dashed lines are average shear stresses for the two groups of experiments, extrapolated to 0 displacement. d) Coefficient of friction of chrysotile gouge at 25 °C; jacket corrections applied to all samples.

estimates of the yield strength of the copper jackets as shown in Figure 15a should be increased by 1.6 MPa. Consequently, the copper jacket cortrections used in this study are:

$$(25\ °C) \qquad \tau_{jacket} = 10.2\ MPa + 1.94\ Z\ [mm] \qquad (2)$$

$$(97\ °C) \qquad \tau_{jacket} = 9.2\ MPa + 1.80\ Z\ [mm] \qquad (3)$$

$$(194\ °C) \qquad \tau_{jacket} = 8.1\ MPa + 1.50\ Z\ [mm] \qquad (4)$$

Figure 15d compares the same experiments as in Figure 15c, this time with the room-temperature correction of equation (2) applied to the two copper-jacketed samples. The copper-jacketed samples plot towards the high end of the range of μ, but it should be noted that the velocity sequence varies from sample to sample (Table 4). We estimate that the correction matches the jacket strength to ±2 MPa (±0.02 variation in μ at 100 MPa effective normal stress). The 97 °C correction factor of equation (3) was also applied to one experiment conducted at 107 °C.

A few additional experiments were conducted at 194 and 281 °C using unannealed, silver-plated copper jackets of 0.5-mm wall thickness. (Silver was added because it is less reactive than copper, although no evidence of reaction between the copper and the serpentinite samples was found). Jacket corrections were made in the same manner as described above, to yield:

$$(194\ °C) \qquad \tau_{jacket} = 11.1\ MPa + 1.50\ Z \qquad (5)$$

$$(281\ °C) \qquad \tau_{jacket} = 8.6\ MPa + 0.3\ Z \qquad (6)$$

As seen from the initial loading in Figure 15c-d, elastic shortening of the sample column results in a small apparent displacement approximated by:

$$Z_{elastic} = 0.00714\ mm/MPa \times \tau \qquad (7)$$

Axial displacements used in computing jacket strength corrections included this adjustment. Combining all sources of error, a reported value of frictional shear strength is estimated to be accurate to within 10%. Relative changes in friction will have much better accuracy, because velocity steps were made within a single experiment.

Finally, as a test of pore-fluid communication, at the end of two 194 °C experiments, pore pressure and normal stress were increased together by about 5 MPa from starting values of 10 MPa (pore pressure) and 110 MPa (normal stress), at a constant velocity of 0.2 μm/s. In both cases, almost no change in shear strength was measured, as expected for a sample in good hydraulic communication with the external pore pressure system. If the fault had been hydraulically isolated from the pore pressure system, the increase in normal stress would have resulted in a 5% increase in shear strength.

Results

The results of all the friction experiments, summarized in Table 4, are plotted in Figures 16–22, in which the coefficient of friction, μ = shear stress/(normal stress – pore pressure). Experiment numbers are included in the figures, for correlation with Table 4 and the velocity data in Table 5. Most of the experiments were run at a pore pressure of 10 MPa and a normal stress of 110 MPa, to yield an effective normal stress of 100 MPa. For comparative purposes, a few additional experiments were conducted at other combinations of pore pressure and normal stress, particularly on chrysotile (Figs. 19e, 21e) but also on antigorite (Fig. 16c, d). The velocities indicated in the figures are axial velocities; nominal slip rates along the inclined sawcut (Fig. 14) would be 15.5% higher. Comparative behavior of the different serpentinite gouges was principally determined over the velocity range 0.1–10.0 μm/s. In addition, one lizardite (Fig. 17c) and several chrysotile (Fig. 21) experiments were run at velocities as low as 0.001 μm/s, which corresponds to a slip rate along the inclined sawcut surface of about 36.4 mm/yr. The average slip rate of the San Andreas fault in central California is 33–38 mm/yr (Thatcher, 1990).

All of the experiments are characterized by stable slip, and the friction behavior follows similar overall trends, whatever the serpentinite gouge tested. The coefficient of friction

Table 4. Experiments Conducted

(Except as noted, samples are 19.1-mm diameter and housed in 0.38-mm-thick annealed-Cu jackets)

Exp. #	Gouge	Temp. (°C)	Norm. Str. (MPa)	Pore Pr. (MPa)	Velocity Range (μm/s)	Comments
Serp001	Chrysotile	25	100	0(wet)	0.1–10	25.4-mm diam. spl; polyurethane jacket
Serp002	Chrysotile	194	110	10	0.1–10	
Serp003	Chrysotile	97	110	10	0.1–10	
Serp004	Chrysotile	25	110	10	0.1-10	
Serp005	Antigorite	194	110	10	1–10	
Serp006	Antigorite	25	110	10	1–10	
Serp007	Antigorite	25	110	10	0.1–1	
Serp008	Antigorite	25	60	10	1–10	
Serp009	Antigorite	25	60	10	0.1–1	
Serp010	Antigorite	194	110	10	0.1–1	
Serp011	Antigorite	194	110	10	0.1–1	
Serp012	Antigorite	97	110	10	0.1–1	
Serp013	Antigorite	97	110	10	1–10	
Serp014	Antigorite	194	110	10	0.1–1	
Serp015	NI-1 (L>C)	25	110	10	1–10	
Serp016	Orthochrysotile	25	110	10	1–10	

Table 4, continued.

Exp. #	Gouge	Temp. (°C)	Norm. Str. (MPa)	Pore Pr. (MPa)	Velocity Range (μm/s)	Comments
Serp017	NI-2 (L>C)	25	110	10	0.1–1	
Serp018	Chrysotile	194	110	10	1–10	
Serp019	Chrysotile	194	110	10	0.1–1	
Serp020	Chrysotile	97	110	10	1–10	
Serp021	Lizardite	25	110	10	0.1–1	
Serp022	T91NI6	25	110	10	1–10	
Serp023	T91NI6	97	110	10	1–10	
Serp024	T91NI6	194	110	10	1–10	
Serp025	T91NI6	194	110	10	0.1–1	
Serp026	Chrysotile	25	110	10	0.001–10	25.4-mm diam. spl.; polyurethane jacket
Serp027	T91NI6	194	110	10	0.1–1	
Serp028	T91NI6	97	110	10	0.1–1	
Serp029	Lizardite	97	110	10	1–10	
Serp030	Lizardite	194	110	10	1–10	
Serp031	Lizardite	25	110	10	0.001–10	25.4-mm diam. spl.; polyurethane jacket
Serp032	Lizardite	97	110	10	0.1–1	
Serp033	Lizardite	194	110	10	0.1–1	

Table 4, continued.

Exp. #	Gouge	Temp. (°C)	Norm. Str. (MPa)	Pore Pr. (MPa)	Velocity Range (μm/s)	Comments
Serp034	Chrysotile	25	110	10	1–10	
Serp035	Chrysotile	25	110	10	1–10	Polyurethane jacket
Serp036	Chrysotile	97	110	10	0.001–1	
Serp037	Chrysotile	194	110	10	0.001–1	
Serp038	Chrysotile	194	110	10	0.001–1	
Serp039	Chrysotile	194	110	10	0.001–0.01	
Serp040	Chrysotile	107	76.5	30	0.001–1	
Serp043	Chrysotile	281	229.5	90	0.001–0.1	Unannealed, 0.51-mm thick Cu jacket
Serp044	Chrysotile	194	153	60	0.001–0.32	Unannealed, 0.51-mm thick Cu jacket
Serp045	Chrysotile	25	100/110	dry/10	0.2	Dry/wet experiment
Serp046	Lizardite	25	110	10	1–10	

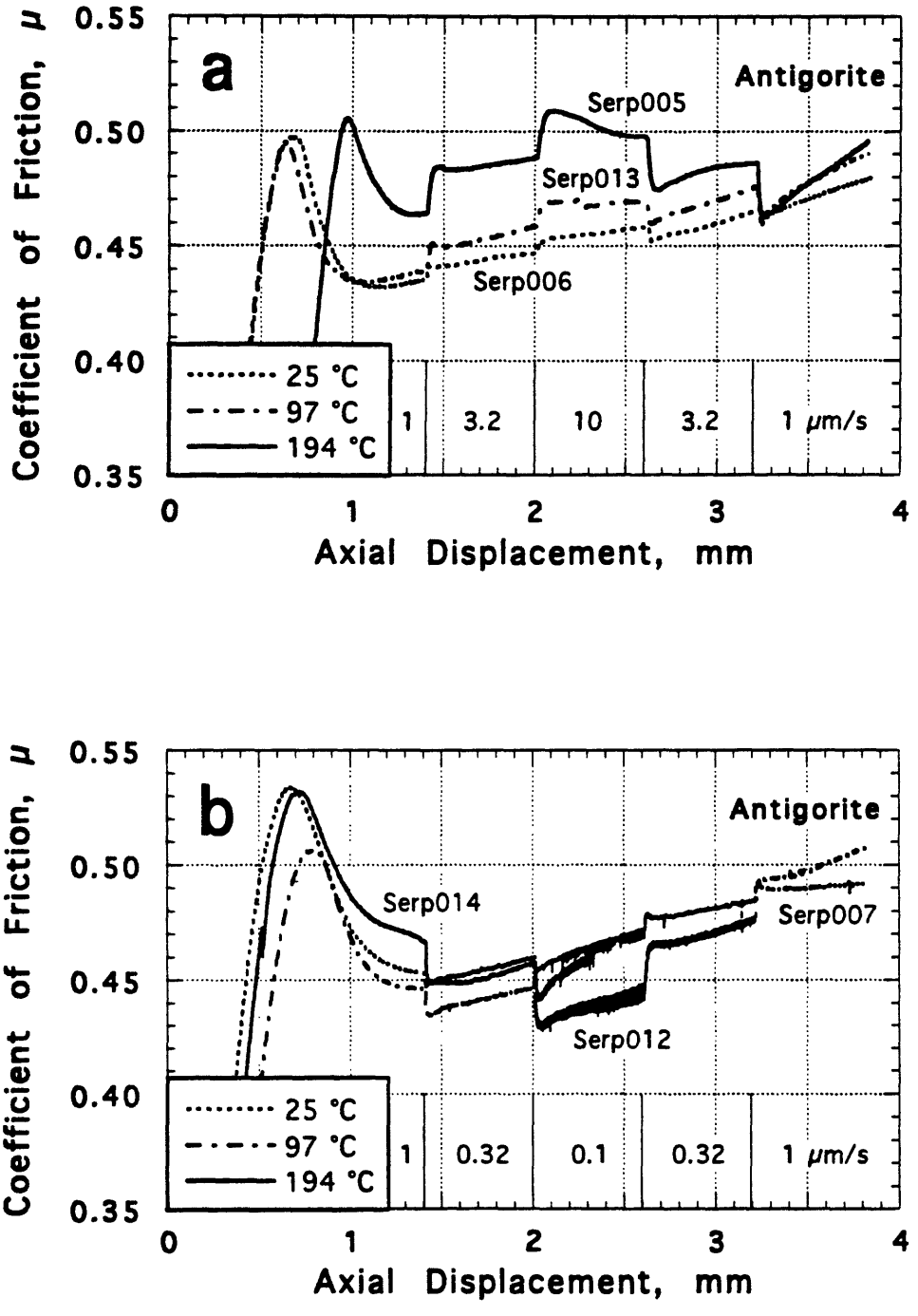

Figure 16. Coefficient of friction, μ, of the antigorite-rich gouge (New Idria) at temperatures to 194 °C, as a function of displacement and sliding rate: a) and c) 1–10 μm/s; b) and d) 0.1–1.0 μm/s axial velocities. Experiments Serp008 in c) and Serp009 in d) were run at 10 MPa pore pressure and 60 MPa normal stress (50 MPa effective normal stress); the others were run at 10 MPa pore pressure and 110 MPa normal stress (100 MPa effective normal stress).

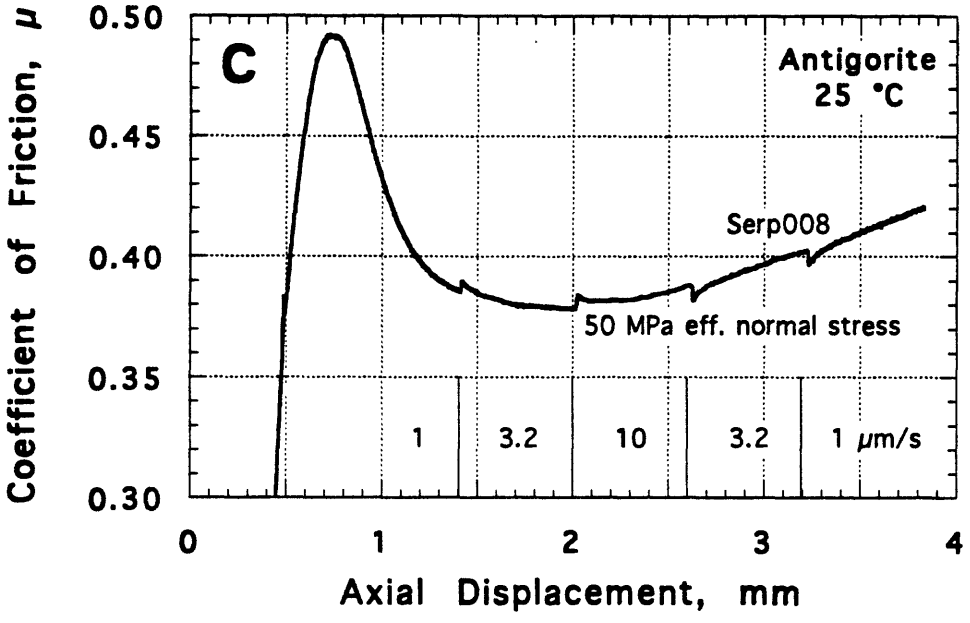

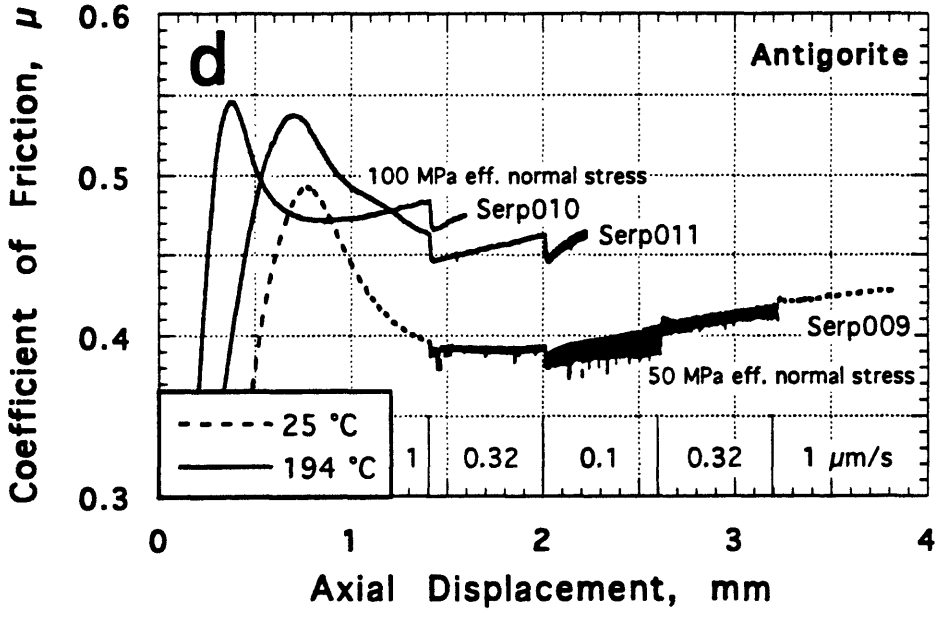

Figure 16, continued.

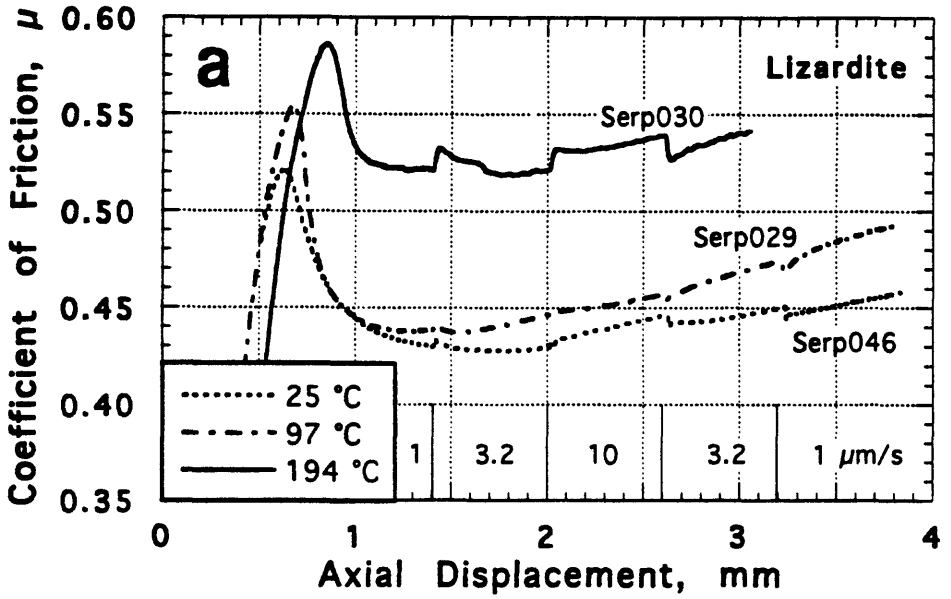

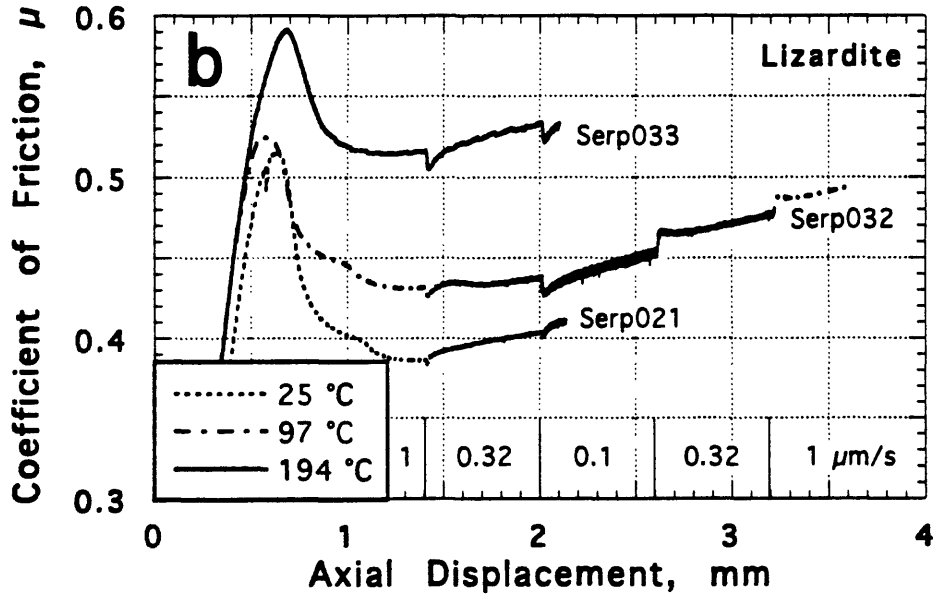

Figure 17. Coefficient of friction of the lizardite gouge from Oregon in the temperature range 25–194 °C, at 100 MPa effective normal stress (110 MPa normal stress and 10 MPa pore pressure). Experiments in a) and b) used 19.1-mm diameter serpentinite cylinders housed in copper jackets; the experiment in c) was conducted with a 25.4-mm diameter serpentinite cylinder and a polyurethane jacket.

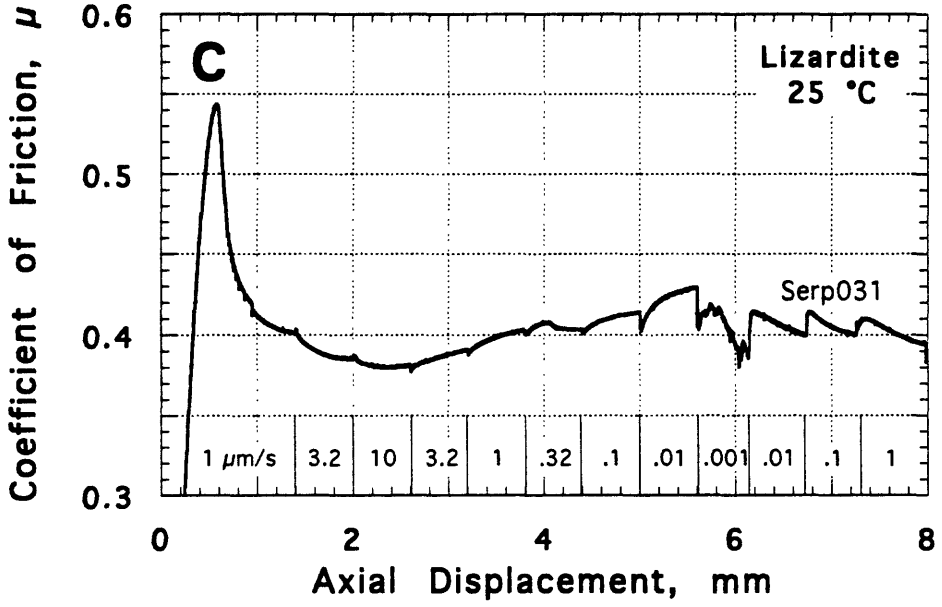

Figure 17, continued.

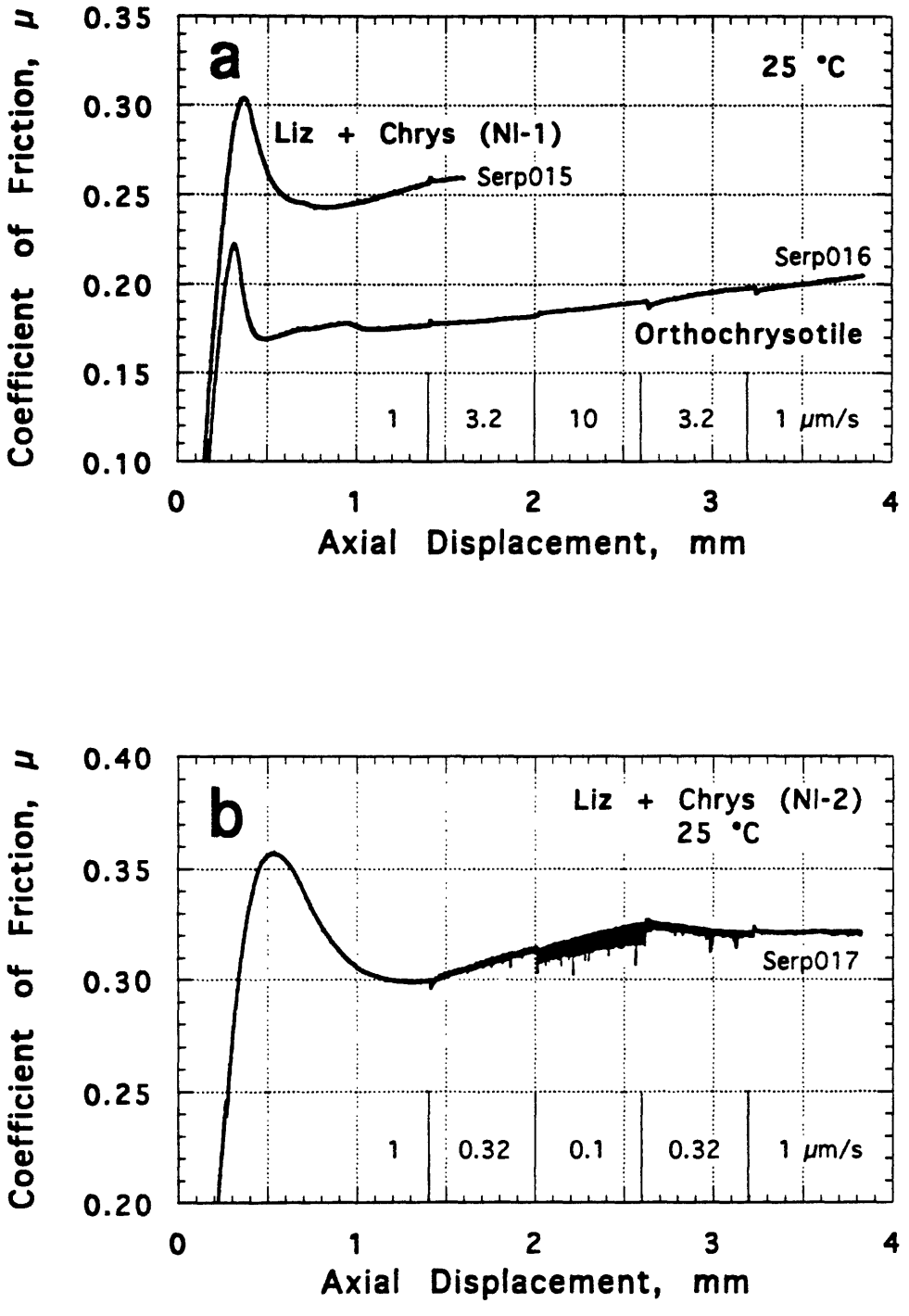

Figure 18. Room-temperature friction data for assorted serpentinite gouges: a) orthochrysotile and mixed sample NI-1 (New Idria), with lizardite 1*T* > clinochrysotile; b) bulk lizardite-rich sample NI-2 (New Idria), also with lizardite 1*T* > clinochrysotile. Effective normal stress = 100 MPa (110 MPa normal stress and 10 MPa pore pressure).

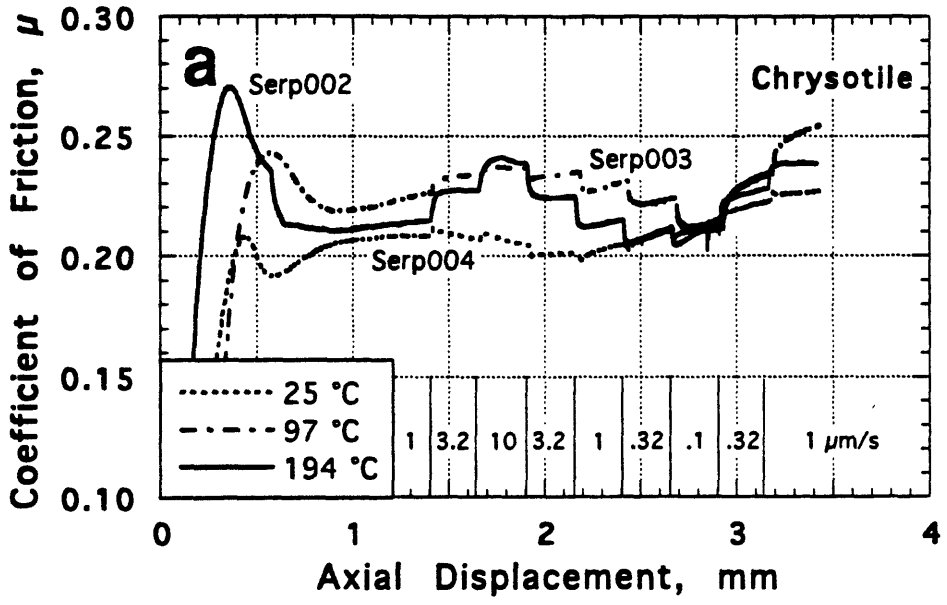

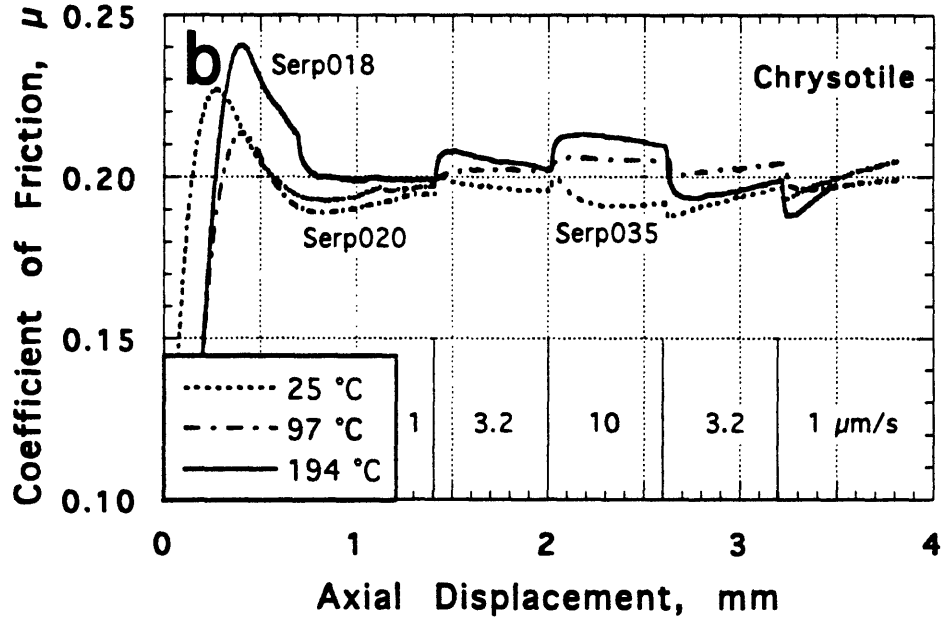

Figure 19. Strengths to 194 °C of our clinochrysotile gouge (New Idria), at a) 0.1–10 μm/s, b) and c) 1–10 μm/s, d) 0.32–1.0 μm/s, and e) 0.1–10.0 μm/s axial velocities. The experiment in e) was conducted on a gouge sample that was assembled wet, but that had no externally applied pore pressure; those in a) – d) were conducted at 10 MPa pore pressure and 110 MPa normal stress (100 MPa effective normal stress).

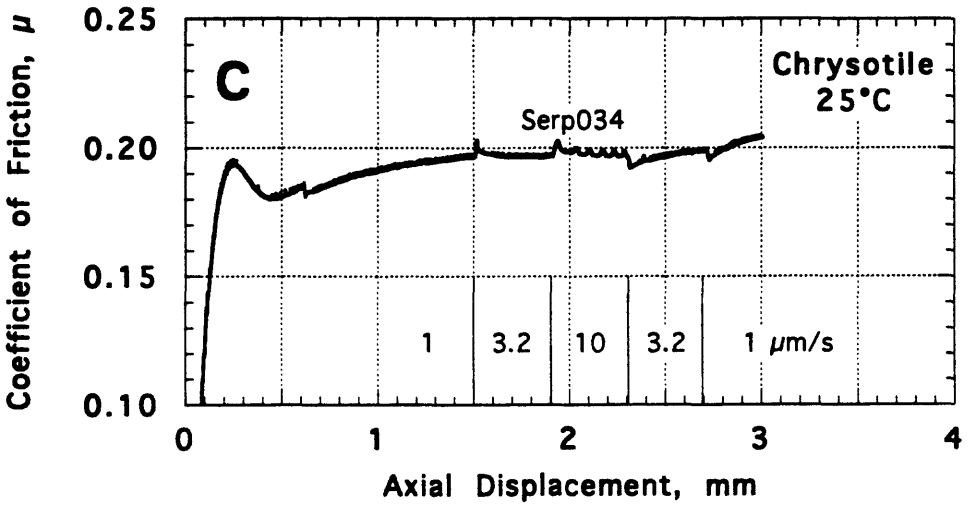

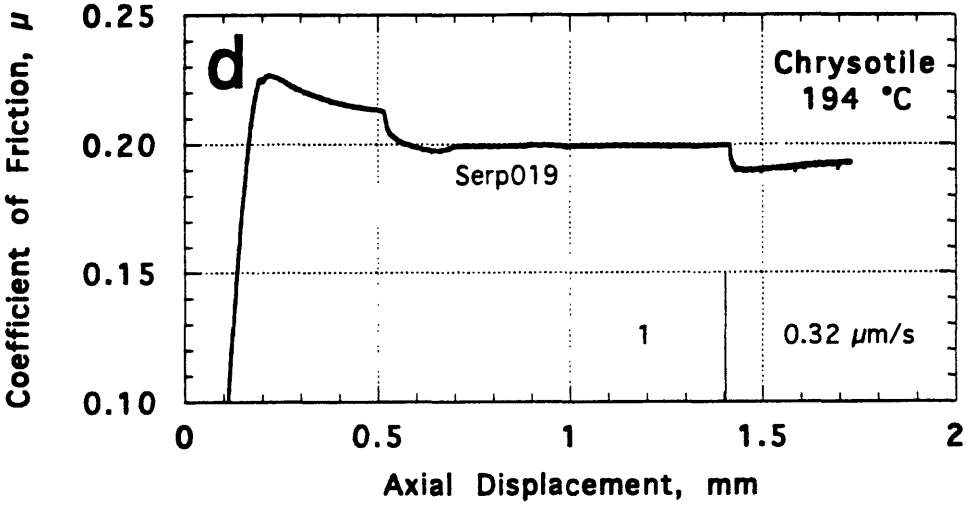

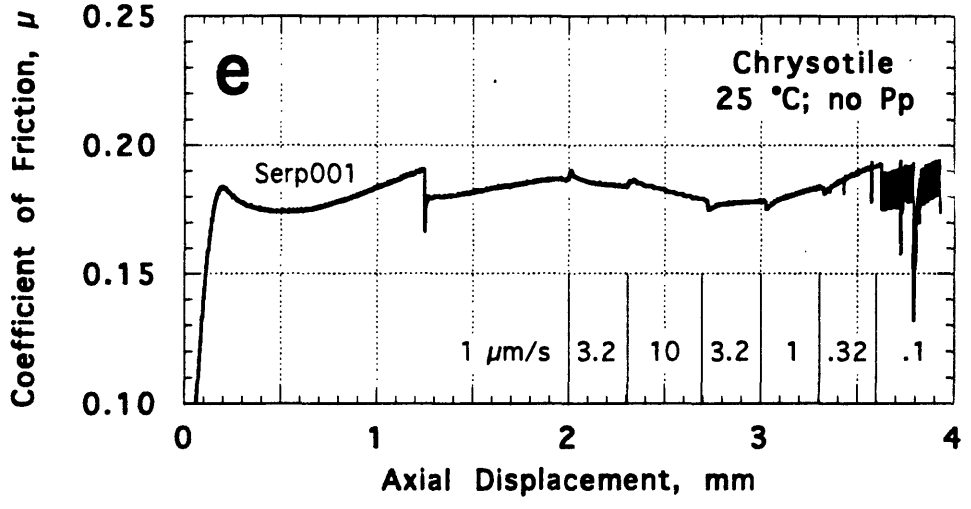

Figure 19, continued.

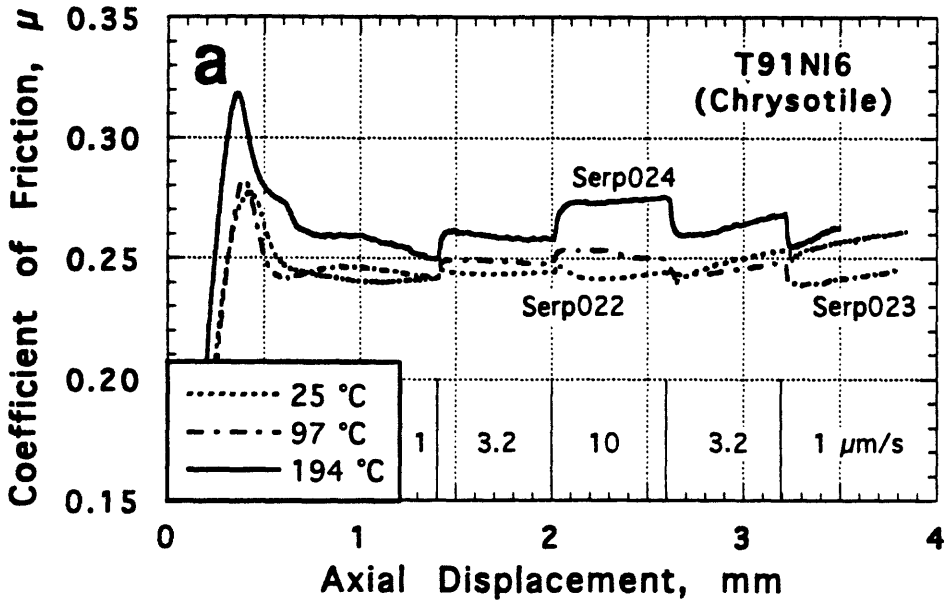

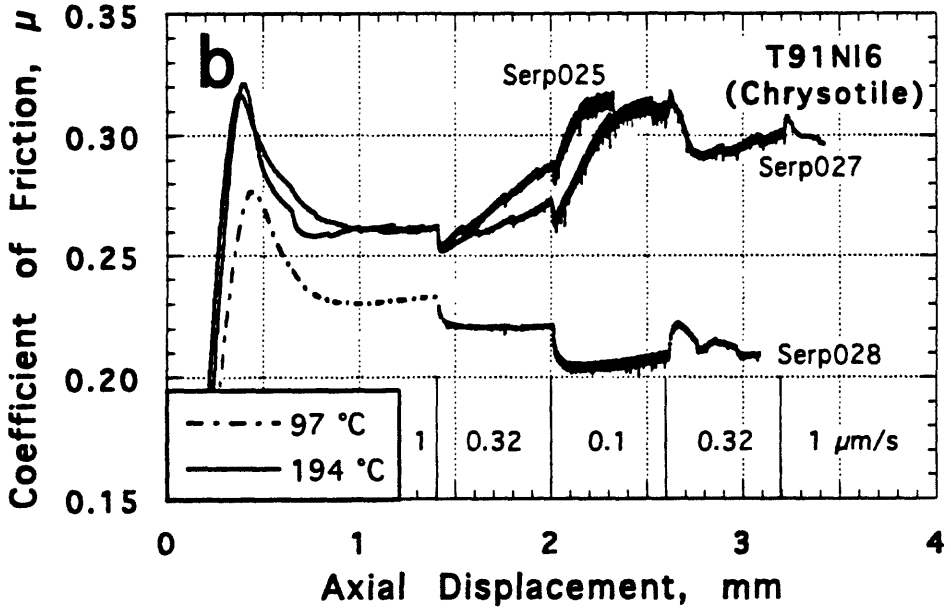

Figure 20. Coefficient of friction of clinochrysotile sample T91NI6, at temperatures to 194 °C; a) 1–10 μm/s, b) 0.1–1.0 μm/s axial velocity. Pore pressure was 10 MPa and normal stress was 110 MPa in all experiments.

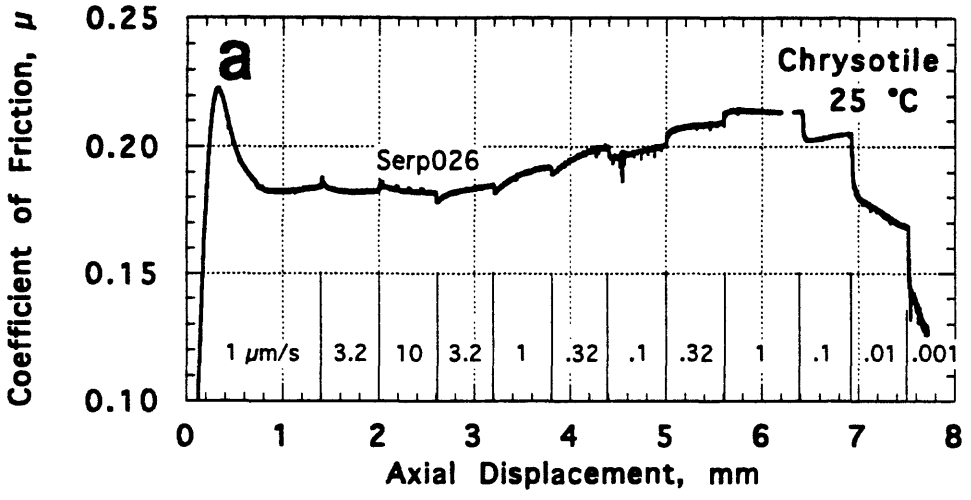

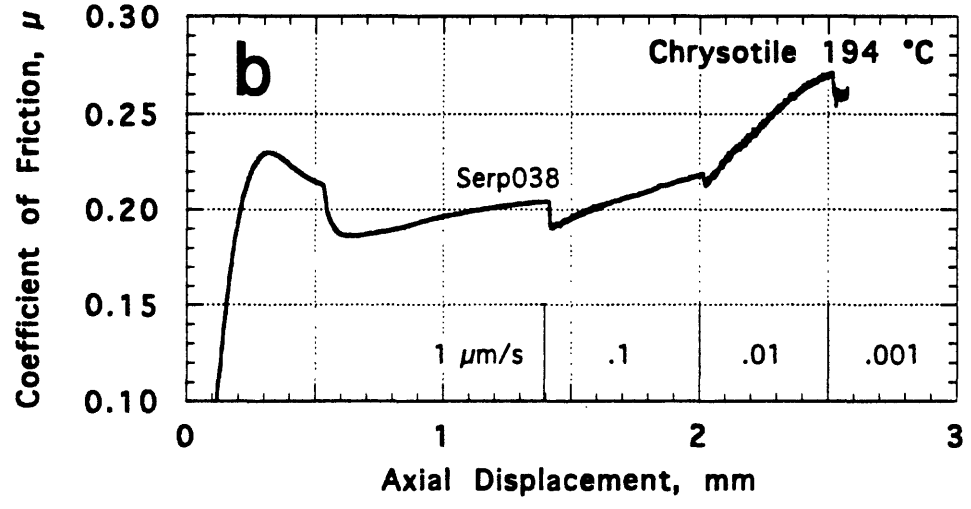

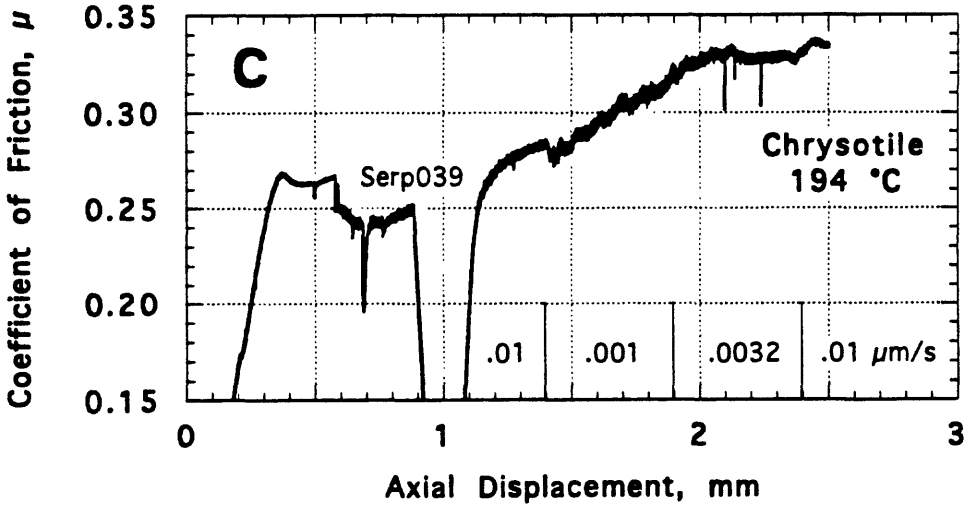

Figure 21. Coefficient of friction of our clinochrysotile gouge (New Idria) at axial velocities to

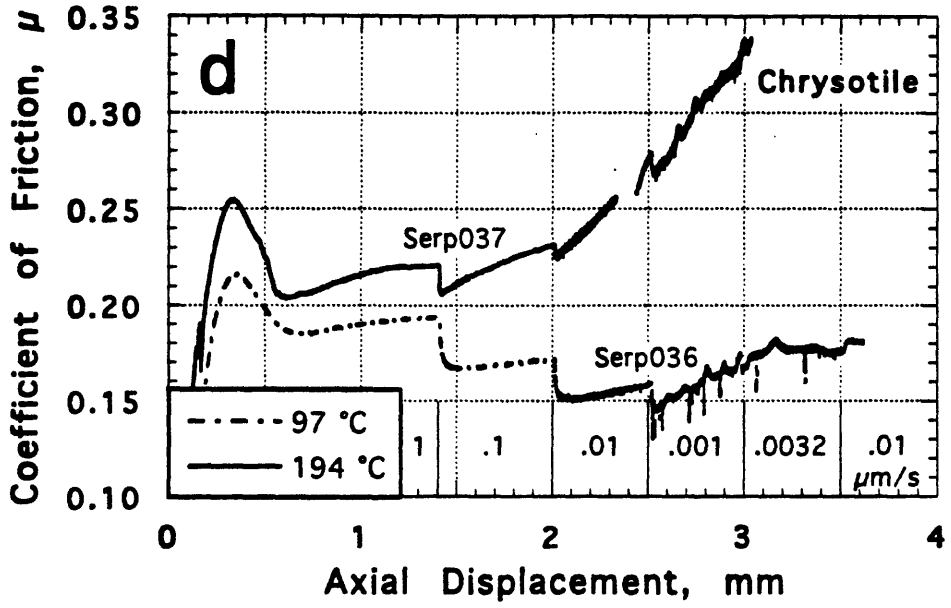

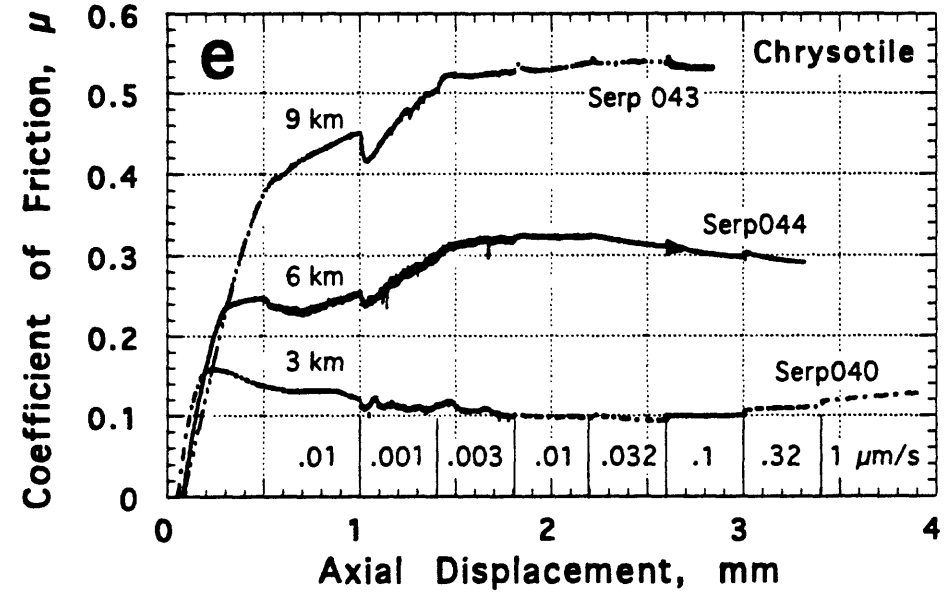

Figure 21, continued.

as low as 0.001 μm/s. a) – d) Pore pressure of 10 MPa and normal stress of 110 MPa; e) experiments simulating depths of burial of 3, 6, and 9 km in a fault zone; 3 km = 107 °C, 46.5 MPa effective normal stress (76.5 MPa normal stress and 30 MPa pore pressure); 6 km = 194 °C, 93 MPa effective normal stress (153 MPa normal stress and 60 MPa pore pressure); 9 km = 281 °C, 139.5 MPa effective normal stress (229.5 MPa normal stress and 90 MPa pore pressure). The sample used in experiment Serp026 in a) was 25.4 mm in diameter and housed in a polyurethane jacket.

increases initially to a peak value at 0.5–1 mm displacement for antigorite and lizardite (Figs. 16, 17) and 0.3–0.5 mm for our chrysotile sample and for T91NI6 (Figs. 19, 20). The coefficient of friction then decreases by as much as 0.1, after which it levels off or gradually increases again as a result of strain hardening. The final value of μ in some experiments reaches or even exceeds the early peak value. The principal exceptions to these general trends are chrysotile experiments whose first velocity interval was 0.01 μm/s (Figs. 20c, e); these experiments lack the early peak in μ during that interval that is shown by the many experiments at 1 μm/s initial velocity.

The antigorite- and lizardite-rich gouges have coefficients of friction in the range 0.4–0.6 (Figs. 16-17), whereas under comparable conditions the two chrysotile gouges are only about one-half as strong, at $\mu \approx 0.2$–0.3 (Figs. 19, 20). The room-temperature results for sample T91NI6 are consistent with those obtained for that gouge by Reinen et al. (1994), indicating that reported strengths from the two laboratories are directly comparable. The gouge T91NI6 is also consistently stronger than our chrysotile sample; their gouge may contain lizardite or antigorite in amounts too small to appear in bulk X-ray diffraction patterns. Lizardite gouge strength clearly increases with temperature (Fig. 17), whereas the curves at 25–194 °C for the antigorite (Fig. 16b) and chrysotile (Fig. 19a, b) gouges overlap to a considerable degree. The room-temperature experiments conducted on samples containing lizardite + chrysotile (NI-1 and NI-2) (Fig. 18) yield values of μ intermediate between the chrysotile and lizardite gouges. The gouge labelled NI-2 is the bulk lizardite-rich sample from New Idria, and NI-1 is the separated material that was slightly enriched in chrysotile. Comparing results at 1 μm/s velocity, NI-2 has a slightly larger coefficient of friction than NI-1, consistent with its slightly higher lizardite content. The room-temperature coefficient of friction of orthochrysotile (Fig. 18a) is at the same low levels as for clinochrysotile (Fig. 19), indicating that different polytypes of a given serpentine mineral have the same strength.

Velocity effects are treated quantitatively in the next section, but in general terms velocity effects are hardly noticeable for antigorite and lizardite at room temperature but relatively pronounced at 194 °C. Chrysotile weakens as velocity decreases from 10 to 0.1 μm/s (Fig. 19a). Further decreasing the velocity from 1.0 to 0.001 μm/s at 25 (Fig. 21a) and 97 °C (Fig. 21d), leads to successively smaller increments of strength decrease, to a minimum of $\mu \approx 0.15$. At 194 °C, chrysotile strength is almost independent of velocity change at the slowest rates, and the samples are significantly stronger, with $\mu \approx 0.35$ when the jackets failed (Fig. 21c, d). Much of the increase at 194 °C is attributable to a marked, time-dependent strengthening of the gouge during the 0.001-μm/s velocity interval.

Because the unusually low strength of chrysotile could have significant implications for fault-zone behavior, additional low-velocity experiments were run on chrysotile samples at the temperature-pressure conditions corresponding roughly to depths of about 3, 6, and 9 km in the San Andreas fault (Fig. 21e). Conditions at depth were calculated assuming a hydrostatic pore-pressure gradient, a surface temperature of 20 °C, a geothermal gradient of ≈30 °C/km (Lachenbruch and Sass, 1973) (29 °C/km in effect, because of the problems with the temperature profile of the furnace), a serpentinite density of 2.55 gm/cm^3 (Deer et al., 1962; Coleman, 1971), and a normal stress equal to the lithostatic pressure at all depths. With respect to the latter assumption, Mount and Suppe (1987) and Zoback et al. (1987) have shown that over most of its length, the maximum principal stress on the San Andreas fault is almost normal to the fault, making the normal stress approximately equal to the maximum stress. In-situ stresses near the San Andreas fault have been measured at a few places, principally in southern California (e.g., McGarr et al., 1982; Hickman et al., 1988; Stock and Healy, 1988; Zoback and Healy, 1992). The deepest measurements — to 3.5 km — were reported by Zoback and Healy (1992), who found that the maximum horizontal stress is approximately equal to or slightly greater than the vertical (lithostatic) stress, and it increases with depth at a rate similar to that of the vertical stress. Thus, the normal stress can

be considered to approximate the lithostatic stress, although stress conditions will certainly vary somewhat along the length of the fault. Temperature-stress profiles will also differ on other serpentinite-bearing faults.

During the experiment simulating conditions at 3-km depth (Fig. 21e), the coefficient of friction dropped to a minimum value of ≈0.10. The conditions of the 6-km (194 °C) experiment are nearly the same as those of the 194 °C experiments in Figure 21b-d, and the results are also similar. The 9-km (281 °C) sample has $\mu > 0.5$, which is close to estimates of μ for the lizardite and antigorite gouges at that temperature, extrapolated from our data at lower temperatures. Pronounced strength increases occurred during the 0.001 μm/s step of the 6- and 9-km experiments (Fig. 21e), which was placed early in the velocity sequence, and the strengths remained high during subsequent velocity intervals.

One final experiment (Fig. 22) investigates the cause of the unusually low frictional strength of chrysotile, which is comparable to that of the swelling clays montmorillonite and vermiculite (Summers and Byerlee, 1977a, b; Logan and Rauenzahn, 1987; Morrow et al., 1992). The interlayer water of swelling clays is postulated to provide a "pseudo-pore pressure" (Summers and Byerlee, 1977a), such that these clays are subjected to a higher fluid pressure than that imposed by free water in the pore spaces. Chrysotile is not a swelling clay, but it can have anomalously high adsorbed water contents (e.g., Table 2). Adsorption of water causes swelling of fiber bundles; at 100% relative humidity at 25 °C, 2.5 weight percent H_2O can be adsorbed onto chrysotile, leading to a 6.7% increase in volume (Deer et al., 1962). We tested the possibility that adsorbed water is responsible for the reduced strength of chrysotile. The water adsorbed onto chrysotile can be removed without damage to the crystal structure by heating to 175-200 °C (Deer et al., 1962). Accordingly, a prepared chrysotile sample was held in a drying oven at 180 °C, under vacuum, for about 120 hours. The sample was cooled while still under evacuation and then transferred directly from the oven to the triaxial apparatus. The strength of the dried chrysotile sample was measured at room temperature, a

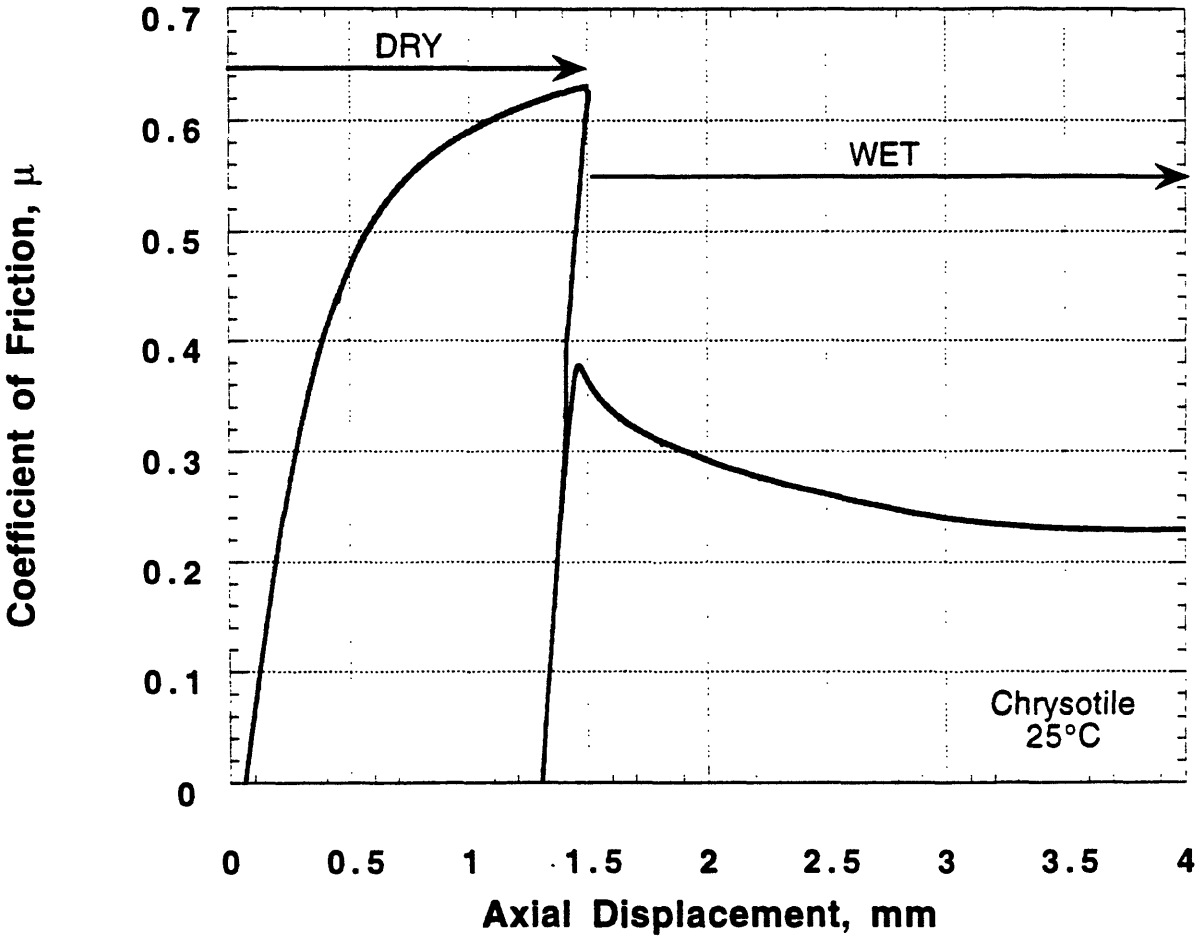

Figure 22. Strength of oven-dried versus wet chrysotile gouge at 25 °C, 100 MPa effective normal stress, and 0.2 μm/s velocity. The strength of the oven-dried sample was measured to 1.5-mm displacement, then the load was partly removed and 10 MPa fluid pressure was applied to the sample. Displacement was resumed after 15 minutes equilibration time.

constant velocity of 0.2 μm/s, and a constant normal stress of 100 MPa (Fig. 22). After 1.5 mm axial displacement, the shear stress was partly reduced, and water was introduced to the gouge layer to a pressure of 10 MPa. The sample was allowed to sit for 15 minutes, and then the strength test was resumed at the same velocity as before and at a constant normal stress of 110 MPa, to maintain the 100 MPa effective normal stress of the dry run.

The oven-dried chrysotile sample is three times as strong as the wet sample (Fig. 22), and its strength was still increasing at the 1.5-mm termination of the dry run. The dry chrysotile sample has strength similar to relatively pure antigorite serpentinites (e.g., Raleigh and Paterson, 1965; Dengo and Logan, 1981; Reinen et al., 1994). The coefficient of friction of the wet sample initially rose to nearly 0.4 but then decreased as the chrysotile equilibrated with the fluid. By the end of the experiment, μ had stabilized at about 0.23, identical to the other room-temperature strengths measured for that gouge (Fig. 19). These results demonstrate that the water adsorbed onto the chrysotile fibers has a similar effect on strength as the interlayer water of montmorillonite and vermiculite (Summers and Byerlee, 1977a).

Velocity Dependence of Shear Strength

The strength plots (Figs. 16–22) suggest varying velocity dependence of gouge strength. The sliding-rate sensitivity of shear strength is represented by the change in the steady-state coefficient of friction, $\Delta\mu_{ss}$, resulting from an e-fold change in sliding rate: $\Delta\mu_{ss}/\Delta\ln V$. Corrections for the absolute value and the pressure dependence of seal friction were applied to the original strength data; however, seal friction is also a function of velocity. The velocity dependence of seal friction was verified at the beginning of each experiment, by means of a velocity step that was made before the piston reached the sample. A nominal correction $\Delta\mu_{seal}/\Delta\ln V = 0.0009$ has been subtracted from all values reported in Table 5.

Table 5. Determinations of Velocity Dependence of Strength

Exp. #	Gouge	Temp (°C)	logV (μm/s)	Lockner Δμss/ΔlnV [= (a-b)] (x0.001)	Lockner error Δμ/ΔlnV (x0.001)	Moore Δμss/ΔlnV [= (a-b)] (x0.001)	Moore error Δμ/ΔlnV (x0.001)	Average Δμss/ΔlnV [= (a-b)] (X0.001)	Average error Δμ/ΔlnV (x0.001)	a (x0.001)	b (x0.001)	dc (μm)
Serp001	Chrys	25	0.25	-1.6	0.7	-2.0	0.3	-1.8	0.9	2.5	4.3	86
			0.75	-1.6	0.7	0.2	0.3	-0.7	1.6	1.8	2.5	65
			0.75	0.2	0.7	0.3	0.3	0.2	0.7	2.5	2.3	43
			0.25	-0.9	0.7	-0.4	0.3	-0.6	1.0	1.8	2.4	43
			-0.25	-1.9	0.7	-2.3	0.3	-2.1	0.9	1.2	3.3	86
			-0.75			2.8	0.7	2.8	0.7	-	-	-
Serp002	Chrys	194	0.25	9.0	1.0	8.6	0.7	8.8	1.2	8.8	0	-
			0.75	10.4	1.0	8.6	1.4	9.5	2.3	9.5	0	-
			0.75	11.3	1.0	12.8	0.7	12.0	1.7	12.0	0	-
			0.25	9.4	1.0	9.7	0.7	9.5	1.1	9.5	0	-
			-0.25	6.4	1.0	6.1	1.4	6.3	1.6	6.3	0	-
			-0.75	3.8	1.0	3.9	1.4	3.8	1.5	3.8	0	-
			-0.75	4.0	1.0	4.4	1.4	4.2	1.6	4.2	0	-
			-0.25	6.4	1.0	6.0	1.4	6.2	1.6	6.2	0	-
Serp003	Chrys	97	0.25	3.6	0.5	3.5	0.8	3.5	0.8	3.5	0	-
			0.75	0.4	0.5	1.0	0.7	0.7	1.0	1.8	1.1	72
			0.75	1.7	0.5	1.0	0.8	1.4	1.2	3.2	1.8	-
			0.25	4.6	0.5	3.8	1.4	4.2	1.8	7.3	3.1	-
			-0.25	8.8	1.3	7.1	0.7	7.9	2.2	7.9	0	-
			-0.75	11.9	1.3	11.6	1.4	11.8	1.6	11.8	0	-
			-0.75	10.1	1.3	8.9	1.4	9.5	2.0	9.5	0	-
			-0.25	8.5	1.3	8.0	1.4	8.3	1.7	8.3	0	-
Serp004	Chrys	25	0.25	-0.2	0.7	-0.1	0.4	-0.1	0.8	2.5	2.6	36
			0.75	0.5	0.7	0.3	0.4	0.4	0.8	2.5	2.1	72
			0.75	0.5	0.7	1.6	0.4	1.1	1.3	3.2	2.1	36
			0.25	-1.9	0.7	-0.3	0.4	-1.1	2.0	2.5	3.6	36

Table 5, continued.

Exp. #	Gouge	Temp (°C)	logV (μm/s)	Lockner Δμss/ΔlnV [= (a-b)] (x0.001)	Lockner error Δμ/ΔlnV (x0.001)	Moore Δμss/ΔlnV [= (a-b)] (x0.001)	Moore error Δμ/ΔlnV (x0.001)	Average Δμss/ΔlnV [= (a-b)] (X0.001)	Average error Δμ/ΔlnV (x0.001)	a (x0.001)	b (x0.001)	dc (μm)
			-0.25	-0.9	0.7	-1.3	0.4	-1.1	0.9	1.8	2.9	36
			-0.75	0.9	0.7	1.0	0.4	0.9	0.7	2.5	1.6	18
			-0.75	0.9	0.7	1.6	0.4	1.2	1.0	2.5	1.3	0
			-0.25	-0.5	0.7	0.1	0.4	-0.2	1.0	2.5	2.7	36
Serp005	Antig	194	0.25	13.4	2.1	14.2	1.4	13.8	2.5	16.5	2.7	101
			0.75	2.6	2.1	3.5	0.4	3.1	2.6	16.9	13.8	404
			0.75	10.9	2.1	11.8	1.4	11.4	2.6	19.6	8.2	303
			0.25	2.3	4.2	-3.6	4.1	-0.7	7.2	19.6	20.3	-
Serp006	Antig	25	0.25	0.7	1.0	2.6	1.0	1.6	2.0	4.6	3.0	43
			0.75	1.9	1.0	2.5	1.2	2.2	1.5	3.9	1.7	-
			0.75	2.3	1.0	3.0	1.2	2.6	1.6	5.3	2.7	43
			0.25	1.2	1.0	0.6	0.3	0.9	1.3	6.0	5.1	86
Serp007	Antig	25	-0.25	0.2	0.7	-1.0	0.4	-0.4	1.3	4.6	5.0	173
			-0.75	1.9	0.7	1.9	1.4	1.9	1.4	5.3	3.4	130
			-0.75	0.2	0.7	1.9	1.5	1.0	2.4	6.7	5.7	86
			-0.25	0.5	0.7	0.5	0.4	0.5	0.7	6.0	5.5	130
Serp008	Antig	25	0.25	0.2	1.0	-0.1	0.8	0.0	1.2	3.2	3.2	86
			0.75	-0.2	1.0	0.8	0.7	0.3	1.5	3.9	3.6	86
			0.75	0.2	1.0	0.6	0.3	0.4	1.2	4.6	4.2	86
			0.25	0.5	1.0	0.4	0.5	0.5	1.0	4.6	4.1	86
Serp009	Antig	25	-0.25	0.4	1.0	-2.0	1.2	-0.8	2.4	-	-	-
			-0.75	0.7	1.6	4.1	1.5	2.4	3.3	6.0	3.6	86
			-0.75	-0.9	1.0	4.1	2.1	1.6	4.6	6.0	4.4	86
			-0.25	0.7	1.0	2.1	1.7	1.4	2.4	4.6	3.2	86
Serp010	Antig	194	-0.25	13.7	1.8	11.6	1.2	12.7	2.8	15.5	2.8	71
Serp011	Antig	194	-0.25	5.4	2.1	4.5	3.4	4.9	3.8	14.9	10.0	195
			-0.75	4.7	2.1	5.4	1.5	5.0	2.4	14.2	9.2	151
Serp012	Antig	97	-0.25	5.4	2.8	5.0	1.8	5.2	3.0	10.1	4.9	130

Table 5, continued.

Exp. #	Gouge	Temp (°C)	logV (μm/s)	Lockner Δμss/ΔlnV [= (a-b)] (x0.001)	Lockner error Δμ/ΔlnV (x0.001)	Moore Δμss/ΔlnV [= (a-b)] (x0.001)	Moore error Δμ/ΔlnV (x0.001)	Average Δμss/ΔlnV [= (a-b)] (X0.001)	Average error Δμ/ΔlnV (x0.001)	a (x0.001)	b (x0.001)	dc (μm)
			-0.75	12.3	2.1	11.2	1.5	11.8	2.6	15.5	3.7	86
			-0.75	11.3	1.7	13.5	3.0	12.4	4.1	17.6	5.2	130
			-0.25	10.9	1.7	10.2	1.5	10.6	2.0	14.2	3.6	130
Serp013	Antig	97	0.25	4.7	1.4	5.3	1.1	5.0	1.7	9.4	4.4	86
			0.75	5.0	2.8	1.7	2.5	3.4	4.4	8.0	4.6	130
			0.75	4.3	1.4	6.0	1.1	5.2	2.3	8.0	2.8	86
			0.25	4.0	1.4	0.3	0.5	2.2	3.2	10.8	8.6	130-390
Serp014	Antig	194	-0.25	11.3	2.1	10.5	2.9	10.9	3.3	14.2	3.3	-
			-0.75	8.2	1.7	9.3	2.1	8.7	2.7	14.2	5.5	65
Serp015	Liz NI	25	0.25	-0.8	0.7	0.1	0.3	-0.4	1.1			
Serp016	CSM och	25	0.25	-0.9	0.7	-0.4	0.3	-0.7	0.9			
			0.75	-0.2	0.7	-0.3	0.3	-0.2	0.7			
			0.75	-0.9	0.7	-0.3	0.3	-0.6	1.0			
			0.25	-0.2	0.7	0.4	0.3	0.1	0.8			
Serp017	Liz NI	25	-0.25	-3.3	1.7	-2.9	1.0	-3.1	1.9			
			-0.75	1.6	1.7	1.6	2.1	1.6	2.1			
			-0.75	-4.3	3.5	-2.0	3.4	-3.2	5.6			
			-0.25	-0.2	1.0	0.2	0.5	0.0	1.2			
Serp018	Chrys	194	0.25	5.4	1.7	3.9	0.8	4.6	2.5	7.3	2.7	-
			0.75	9.9	2.1	9.3	1.6	9.6	2.4	9.6	0	-
			0.75	11.6	2.1	9.3	2.3	10.5	3.5	14.2	3.7	-
			0.25	7.8	2.1	3.7	3.1	5.8	5.2	9.4	3.6	-
Serp019	Chrys	194	-0.25	8.2	1.4	6.2	0.9	7.2	2.0	7.3	0.1	-
Serp020	Chrys	97	0.25	4.0	1.4	4.1	1.0	4.0	1.4	4.0	0	-
			0.75	1.9	1.4	2.5	0.6	2.2	1.7	2.2	0	-
			0.75	2.6	1.4	2.1	0.7	2.4	1.6	2.4	0	-
			0.25	6.4	1.4	6.0	0.4	6.2	1.6	6.2	0	-
Serp021	Liz Ore	25	-0.25	-7.8	1.4	-6.6	1.0	-7.2	2.0	1.2	8.4	86

Table 5, continued.

Exp. #	Gouge	Temp (°C)	logV (µm/s)	Lockner Δµss/ΔlnV [= (a-b)] (x0.001)	Lockner error Δµ/ΔlnV (x0.001)	Moore Δµss/ΔlnV [= (a-b)] (x0.001)	Moore error Δµ/ΔlnV (x0.001)	Average Δµss/ΔlnV [= (a-b)] (X0.001)	Average error Δµ/ΔlnV (x0.001)	a (x0.001)	b (x0.001)	dc (µm)
			-0.75	-5.4	1.4	-4.7	1.0	-5.0	1.8	1.8	6.8	65
Serp022	T91NI6	25	0.25	0.2	1.0	-0.2	0.2	0.0	1.2	2.5	2.5	130
			0.75	-4.3	2.1	-5.0	0.6	-4.7	2.3	1.8	6.5	130
			0.75	-1.9	1.0	-2.3	0.3	-2.1	1.2	3.9	6.0	173
			0.25	-0.9	1.0	-0.3	0.2	-0.6	1.3	3.2	3.8	86
Serp023	T91NI6	97	0.25	6.1	1.4	6.0	0.8	6.0	1.5	6.0	0	-
			0.75	4.0	2.8	3.5	1.3	3.8	3.0	3.8	0	-
			0.75	3.6	1.4	4.5	0.5	4.1	1.9	4.1	0	-
			0.25	8.9	2.1	7.6	1.0	8.2	2.8	8.2	0	-
Serp024	T91NI6	194	0.25	9.2	1.7	8.2	1.7	8.7	2.2	10.1	1.4	-
			0.75	11.3	1.7	12.7	1.4	12.0	2.4	12.1	0.1	-
			0.75	14.1	1.7	12.2	1.6	13.1	2.7	13.2	0.1	173
			0.25	11.6	1.7	8.1	2.4	9.9	4.2	12.2	2.3	130
Serp025	T91NI6	194	-0.25	4.0	1.7	-0.3	3.4	1.8	5.5	7.3	5.5	65
			-0.75	-14.1	2.8	-14.9	1.4	-14.5	3.2	4.6	19.1	130
Serp026	Chrys	25	0.25	-4.3	1.0	-3.0	1.0	-3.6	1.7	2.5	6.1	173
			0.75	-1.6	1.0	-2.3	1.0	-2.0	1.4	1.8	3.8	173
			0.75	-0.1	1.0	-0.2	0.8	-0.1	1.0	1.8	1.9	86
			0.25	-4.0	1.0	-2.6	0.7	-3.3	1.7	1.8	5.1	173
			-0.25	-4.0	1.0	-3.8	1.0	-3.9	1.1	1.2	5.1	173
			-0.75	3.0	1.0	3.0	0.8	3.0	1.0	3.2	0.2	0
			-0.75	4.1	1.0	3.1	1.2	3.6	1.7	3.9	0.3	0
			-0.25	1.7	1.0	1.1	1.4	1.4	1.7	2.5	1.1	86
			-0.50	3.8	0.7	4.3	0.6	4.1	1.0	4.3	0.2	0
			-1.50	16.3		12.6	2.1	14.4		-	-	-
			-2.50	16.3		15.6	4.8	15.9		-	-	-
Serp027	T91NI6	194	-0.25	5.4	1.7	3.1	0.8	4.2	2.9	8.0	3.8	130
			-0.75	-21.7	3.5	-16.4	6.2	-19.1	8.9	7.3	26.4	173

Table 5, continued.

Exp. #	Gouge	Temp (°C)	logV (µm/s)	Lockner Δµss/ΔlnV [= (a-b)] (x0.001)	Lockner error Δµ/ΔlnV (x0.001)	Moore Δµss/ΔlnV [= (a-b)] (x0.001)	Moore error Δµ/ΔlnV (x0.001)	Average Δµss/ΔlnV [= (a-b)] (X0.001)	Average error Δµ/ΔlnV (x0.001)	a (x0.001)	b (x0.001)	dc (µm)
			-0.75	-21.0	3.5	-17.5	4.1	-19.3	7.9	4.6	23.9	86-130
Serp028	T91NI6	97	-0.25	11.3	1.4	10.8	1.4	11.0	1.7	11.0	0	-
			-0.75	16.2	2.1	14.1	2.1	15.1	3.2	15.1	0	-
Serp029	Liz Ore	97	0.25	-3.3	0.7	-3.6	1.4	-3.4	1.6	2.5	5.9	86
			0.75	-3.6	0.7	-3.9	0.7	-3.8	0.9	0.2	4.0	173
			0.75	-2.3	0.7	-1.3	0.7	-1.8	1.2	1.8	3.6	86
			0.25	-2.3	0.7	-2.6	0.7	-2.4	0.9	3.2	5.6	130
Serp030	Liz Ore	194	0.25	-0.9	3.1	-0.8	3.1	-0.8	3.2	9.4	10.2	108
			0.75	4.7	1.0	5.4	0.7	5.0	1.3	8.7	3.7	108
			0.75	7.1	1.0	6.4	1.0	6.8	1.4	10.8	4.0	108
Serp031	Liz Ore	25	0.25	-8.9	1.4	-9.4	2.7	-9.1	3.0	1.2	10.3	236
			0.75	-4.0	1.0	-4.3	1.4	-4.2	1.5	1.2	5.4	157
			0.75	-3.3	1.0	-2.4	1.0	-2.8	1.5	2.5	5.3	79
			0.25	-4.3	1.0	-3.0	0.7	-3.7	1.6	1.8	5.5	157
			-0.25	-2.6	3.5	-1.6	0.7	-2.1	4.0	1.2	3.3	79
			-0.75	-4.7	1.4	-3.3	1.2	-4.0	2.1	1.2	5.2	118
			-1.50	-3.3	0.5	-3.8	0.7	-3.6	0.9	3.9	7.5	157
			-2.50	6.1	1.0	4.1	1.7	5.1	2.7	10.1	5.0	-
Serp032	Liz Ore	97	-0.25	-0.9	1.7	-0.9	1.7	-0.9	1.7	3.9	4.8	-
			-0.75	0.2	1.0	0.9	2.1	0.5	2.5	9.4	8.9	130
			-0.75	4.3	1.0	5.3	2.7	4.8	3.2	5.5	0.7	130
			-0.25	3.6	1.0	4.6	1.4	4.1	1.7	8.0	3.9	86
Serp033	Liz Ore	194	-0.25	-0.9	0.7	-2.0	0.3	-1.4	1.2	9.4	10.8	86
			-0.75	3.0	2.1	2.7	1.0	2.8	2.3	9.4	6.6	-
Serp034	Chrys	25	0.25	-1.9	0.8	-1.6	0.7	-1.8	0.9	4.6	6.4	72
			0.75	-1.6	0.8	-0.3	0.7	-1.0	1.4	5.3	6.3	72
			0.75	-1.9	0.8	0.9	0.7	-0.5	2.2	3.9	4.4	54
			0.25	-4.0	1.0	-2.0	0.7	-3.0	2.0	2.5	5.5	36

Table 5, continued.

Exp. #	Gouge	Temp (°C)	logV (μm/s)	Lockner Δμss/ΔlnV [= (a-b)] (x0.001)	Lockner error Δμ/ΔlnV (x0.001)	Moore Δμss/ΔlnV [= (a-b)] (x0.001)	Moore error Δμ/ΔlnV (x0.001)	Average Δμss/ΔlnV [= (a-b)] (X0.001)	Average error Δμ/ΔlnV (x0.001)	a (x0.001)	b (x0.001)	dc (μm)
Serp035	Chrys	25	0.25	-1.4	1.0	-2.0	1.0	-1.7	1.3	2.5	4.2	173
			0.75	-4.4	1.3	-4.3	1.0	-4.4	1.3	2.5	6.9	130
			0.75	-0.1	1.0	0.6	1.0	0.3	1.4	3.2	2.9	130
			0.25	-2.4	1.0	-1.8	1.0	-2.1	1.3	2.5	4.6	130-303
Serp036	Chrys	97	-0.50	11.3	0.6	11.0	0.5	11.2	0.7	11.2	0	-
			-1.50	6.3	0.6	8.1	0.7	7.2	1.6	7.2	0	-
			-2.50	0.1	0.6	0.5	1.0	0.3	1.2	4.9	4.6	229
			-2.75	3.7	1.3	1.6	1.4	2.7	2.5	3.2	0.5	-
			-2.25	2.5	1.3	0.9	1.7	1.7	2.5	3.2	1.5	-
Serp037	Chrys	194	-0.50	0.7	1.3	1.0	0.5	0.8	1.4	6.0	5.2	150-200
			-1.50	0.1	1.3	-1.6	0.8	-0.8	2.2	1.9	2.7	100-200
			-2.50	2.0	2.7	-1.6	0.7	0.2	4.5	-	-	-
			-2.75	-0.6	3.6	0.9	1.8	0.2	4.4	-	-	-
Serp038	Chrys	194	-0.50			1.6	1.0	1.6	1.0	5.3	3.7	143
			-1.50			-3.1	1.4	-3.1	1.4	1.9	5.0	71-214
Serp039	Chrys	194	-2.50			-0.9	1.2	-0.9	1.2	2.9	3.8	-
			-2.75			-0.3	1.4	-0.3	1.4	5.3	5.6	-
			-2.25			1.7	2.5	1.7	2.5	1.8	0.1	-
Serp040	Chrys	107	-2.50			1.7	2.7	1.7	2.7			
			-2.75			2.6	2.7	2.6	2.7			
			-2.25			0.9	1.4	0.9	1.4			
			-1.75			-2.3	1.0	-2.3	1.0			
			-1.25			1.2	1.5	1.2	1.5			
			-0.75			4.0	1.0	4.0	1.0			
			-0.25			4.8	1.0	4.8	1.0			
Serp043	Chrys	281	-2.50			-4.8	1.9	-4.8	1.9			
			-2.75			2.7	2.7	2.7	2.7			
			-2.25			-4.2	1.4	-4.2	1.4			

Table 5, continued.

Exp. #	Gouge	Temp (°C)	logV (µm/s)	Lockner Δµss/ΔlnV [= (a-b)] (x0.001)	Lockner error Δµ/ΔlnV (x0.001)	Moore Δµss/ΔlnV [= (a-b)] (x0.001)	Moore error Δµ/ΔlnV (x0.001)	Average Δµss/ΔlnV [= (a-b)] (X0.001)	Average error Δµ/ΔlnV (x0.001)	a (x0.001)	b (x0.001)	dc (µm)
			-1.75			-4.4	1.4	-4.4	1.4			
			-1.25			-6.1	3.4	-6.1	3.4			
Serp044	Chrys	194	-2.50			-0.2	0.7	-0.2	0.7			
			-2.75			1.5	1.1	1.5	1.1			
			-2.25			1.6	0.7	1.6	0.7			
			-1.75			-1.8	1.0	-1.8	1.0			
			-1.25			-2.3	1.0	-2.3	1.0			
			-0.75			1.7	1.0	1.7	1.0			
Serp046	Liz Ore	25	0.25			0.0	0.9	0.0	0.9	2.5	2.5	86
			0.75			2.2	0.7	2.2	0.7	2.5	0.3	64
			0.75			5.5	0.8	5.5	0.8	-	-	86
			0.25			3.5	0.7	3.5	0.7	4.6	1.1	21

As described previously, many of the strength plots show an overall trend of increasing μ with displacement and time, and much of the uncertainty in determinations of $\Delta\mu_{ss}/\Delta\ln V$ arises from difficulties in separating velocity-dependent effects from these irreversible strain- and time-dependent effects. To account for these uncertainties, an error estimate was assigned to each measurement of $\Delta\mu_{ss}$. In addition, because the choice of $\Delta\mu_{ss}$ can be a subjective process, separate sets of calculations were made by two of the authors (Table 5). The individual data sets are very similar overall, with differences in $\Delta\mu_{ss}/\Delta\ln V$ nearly always <0.002. We averaged the two sets of results and assigned error estimates that maximize the range of error of the individual data points as depicted in Figure 23. The average values of $\Delta\mu_{ss}/\Delta\ln V$ from Table 5 are plotted at the midpoints of the velocity steps, in terms of axial shortening rates, on a log scale in Figures 24–27.

The room-temperature results for our chrysotile gouge and the T91NI6 chrysotile sample are essentially identical (Fig. 24), and they duplicate the velocity effects reported by Reinen et al. (1994) for T91NI6. At room temperature, chrysotile gouge is slightly velocity weakening at velocities ≥1.0 μm/s, that is, μ decreases with increasing velocity . In contrast, at velocities ≤0.32 μm/s, chrysotile is strongly velocity strengthening (μ increases with increasing velocity). Raising temperature leads to marked changes in velocity behavior. The trend of the 97 °C data resembles a bell-shaped curve of velocity-strengthening behavior that peaks between 0.1 and 0.32 μm/s velocity and levels off at 0 change in μ. By comparison, the 25 and 194 °C results could be interpreted as showing the right and left halves of the bell-shaped curve, respectively, so that the peak migrates towards higher velocities with increasing temperature. Additional experiments at both higher and lower velocities are required to test this interpretation. The sole exceptions to the otherwise consistent results for chrysotile are the large negative values of $\Delta\mu_{ss}/\Delta\ln V$ for T91NI6 at 194 °C and a velocity step between 0.1 and 0.32 μm/s. The three aberrant data points were obtained from two separate experiments.

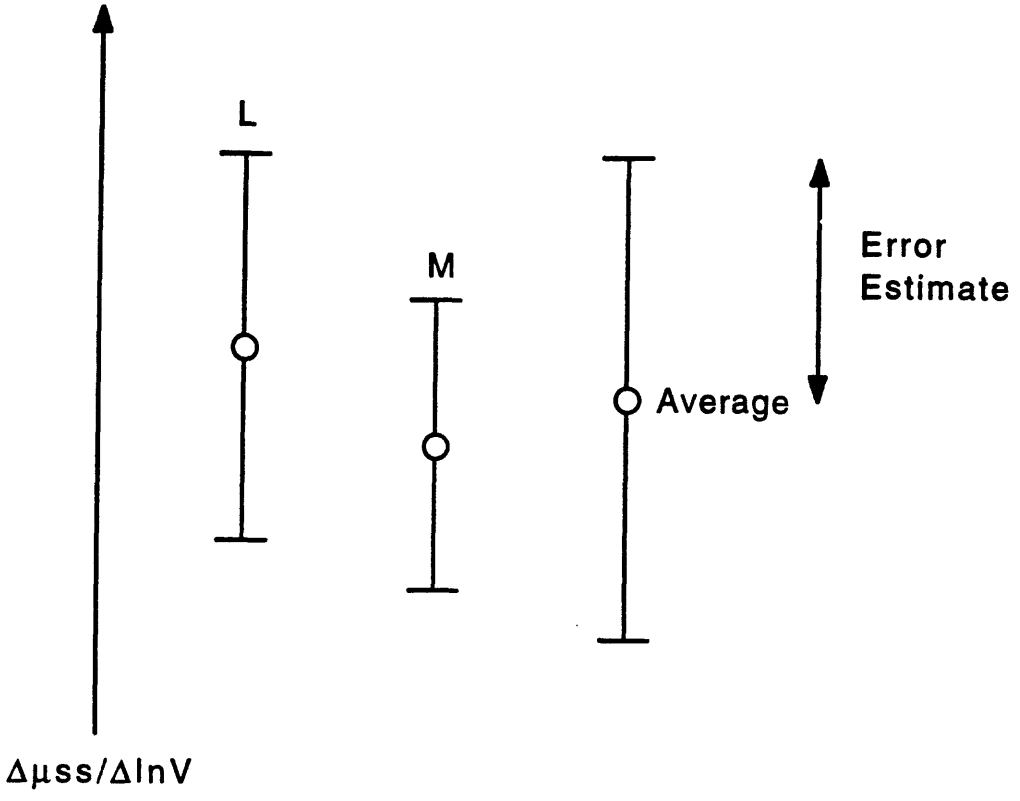

Figure 23. Method of estimating error of averaged values of $\Delta\mu_{ss}/\Delta\ln V$. The error was maximized to include the entire range covered by the individual measurements.

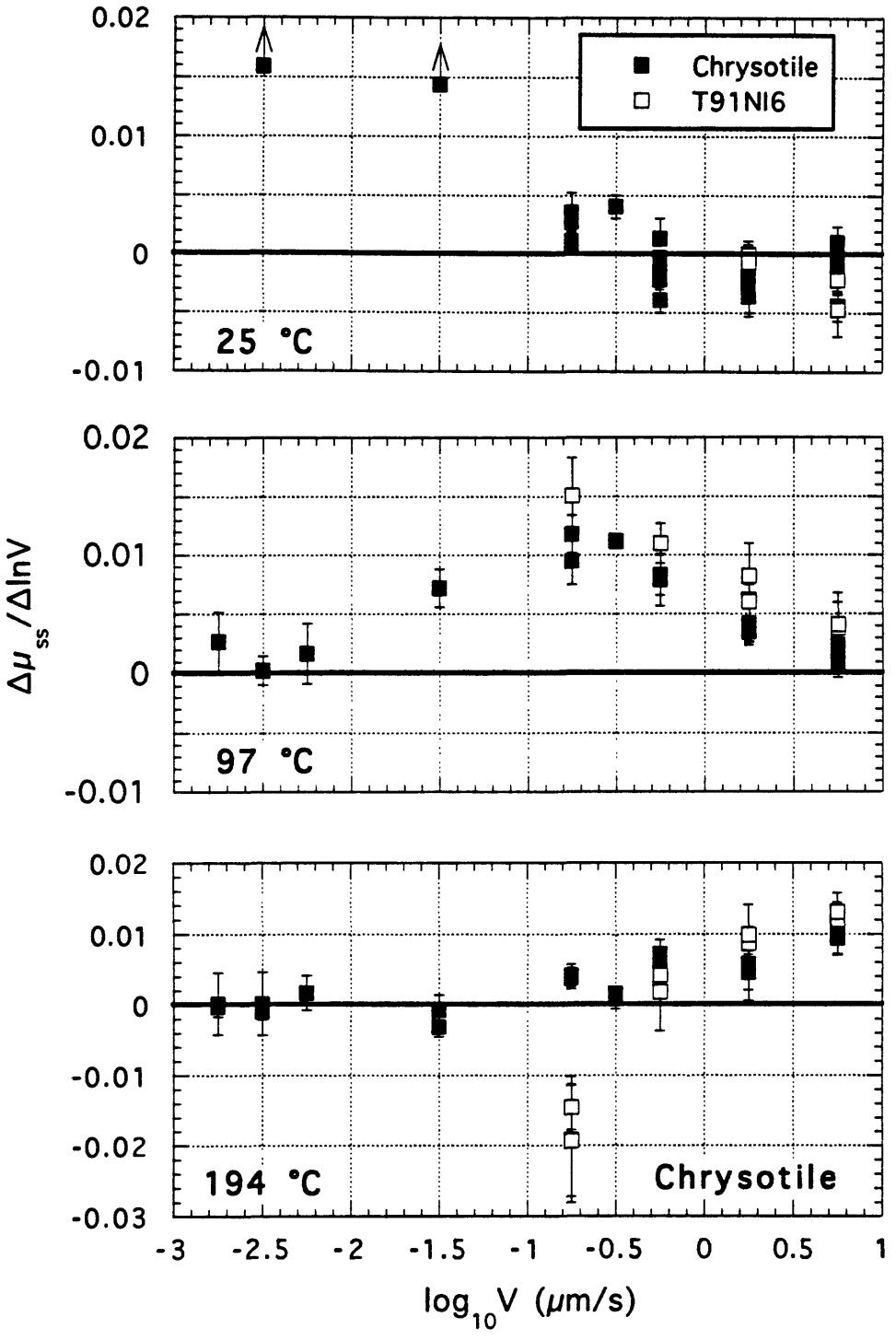

Figure 24. Steady-state velocity dependence of μ for the two clinochrysotile gouges at different temperatures; effective normal stress = 100 MPa. The normalized changes in μ in Figures 24-27 are plotted at the mean of the logs of the axial velocities before and after a velocity step.

Velocity-dependence data for the 3-, 6-, and 9-km-simulation experiments on chrysotile (Fig. 25) follow similar trends to those in Figure 24. The 194 °C results in the two figures are nearly identical, as expected given the close similarity of the experimental conditions. The peak of velocity-strengthening behavior at 107 °C appears to be displaced to higher velocities relative to the 97 °C curve for chrysotile. This shift may be attributable to the 10 °C increase in temperature, because the direction of change is consistent with the temperature trends in Figure 24. The 107 °C experiment was also conducted at a relatively low effective normal stress of 46.5 MPa; however, changes in normal stress between 0 and 100 MPa may have little effect on the velocity behavior of serpentinite (Reinen et al., 1991). Almost all of the 281 °C results are in the velocity-weakening field, and they constitute the most strongly negative values obtained for chrysotile. The results in Figure 25 suggest a shift towards velocity-weakening behavior at higher temperature ± effective-stress conditions.

In general, the velocity data for antigorite (Fig. 26) are similar to those for chrysotile (Fig. 24) over the limited velocity range tested. The 97 °C results, in particular, are nearly identical for the two serpentinite gouges. The 25 °C antigorite data are shifted to slightly more positive values compared to both the chrysotile results and to the velocity data for antigorite at 50 and 100 MPa normal stress reported by Reinen et al. (1991). At the faster velocities at 25 °C, the antigorite-rich gouge is slightly more velocity strengthening at 100 MPa than at 50 MPa effective normal stress, but the data overlap at the lower velocities. Despite the wide scatter of the data at 194 °C, they suggest the possible presence of a velocity-strengthening peak between 1.0 and 3.2 μm/s velocity. Interpreting the velocity behavior of lizardite (Fig. 27) is also difficult, but lizardite may follow the same general trends as chrysotile, although shifted towards more velocity-weakening behavior. Of the three serpentinite gouge types, the lizardite gouge yielded the largest proportion of negative values of $\Delta\mu_{ss}/\Delta\ln V$. Also plotted in Figure 27 are room-temperature values of $\Delta\mu_{ss}/\Delta\ln V$ for the mixed gouges of lizardite and chrysotile, NI-1 and NI-2. Although lizardite is the more abundant serpentine variety in both

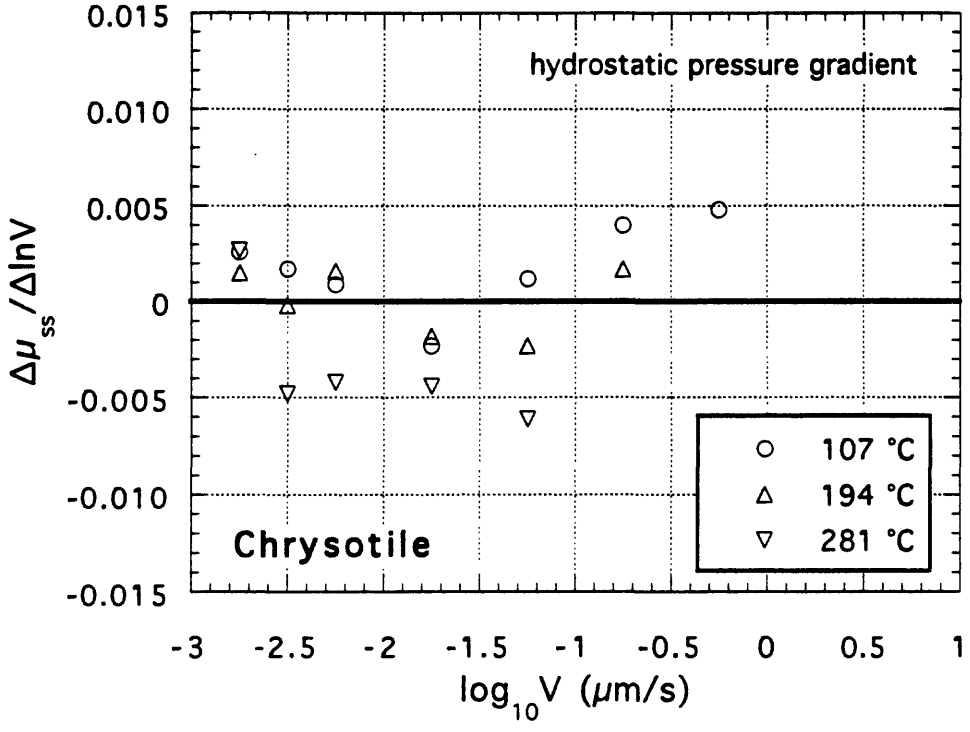

Figure 25. Steady-state velocity dependence of μ for our clinochrysotile gouge, from experiments simulating different depths in a fault (Fig. 21e). 3-km simulation — 107 °C, 46.5 MPa effective normal stress; 6 km — 194 °C, 93 MPa effective normal stress; 9 km — 281 °C, 139.5 MPa effective normal stress.

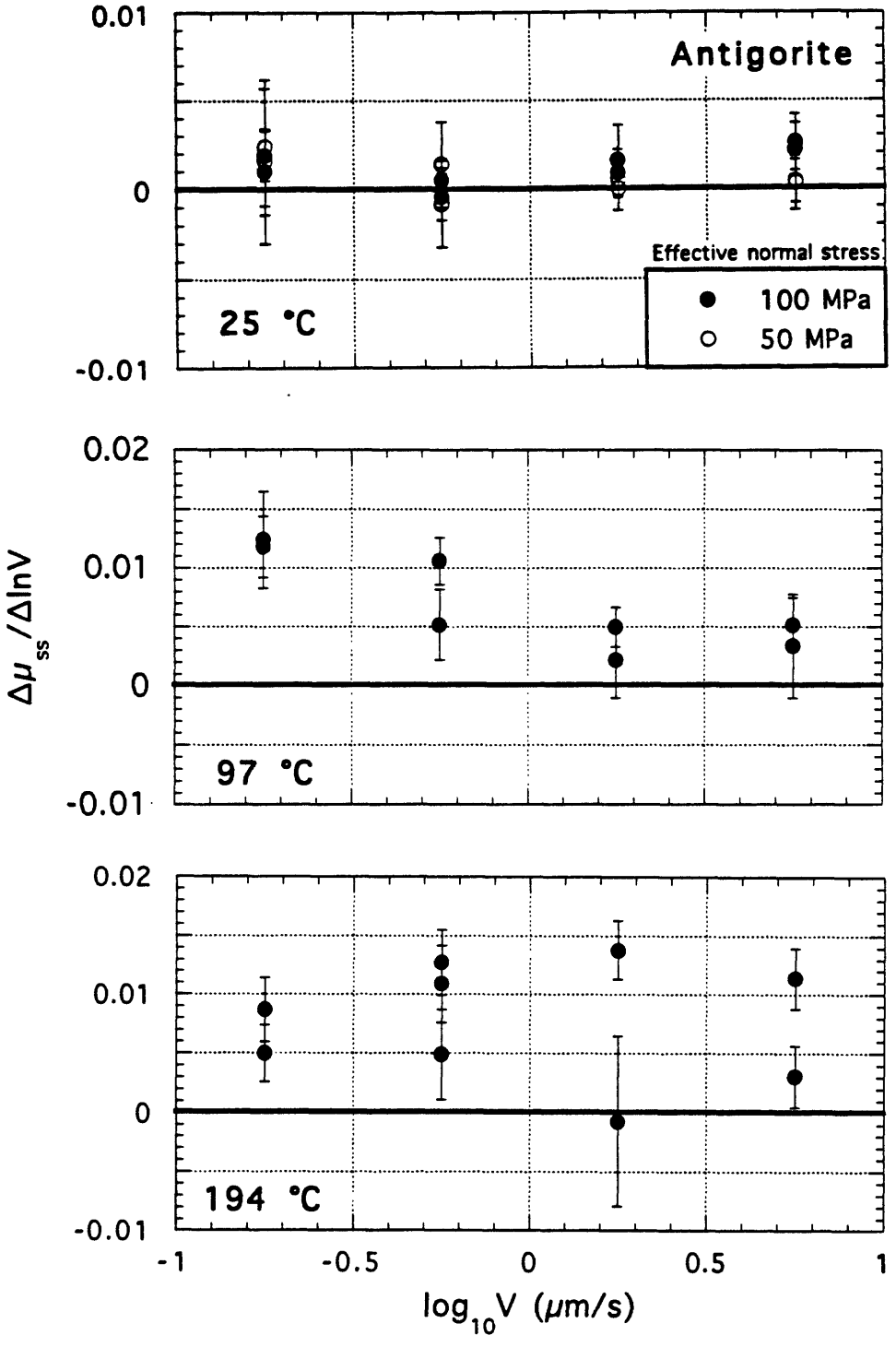

Figure 26. Velocity dependence at different temperatures of the coefficient of friction of the antigorite-rich gouge (New Idria). Some room-temperature data are for 50 MPa effective normal stress; the rest are for 100 MPa.

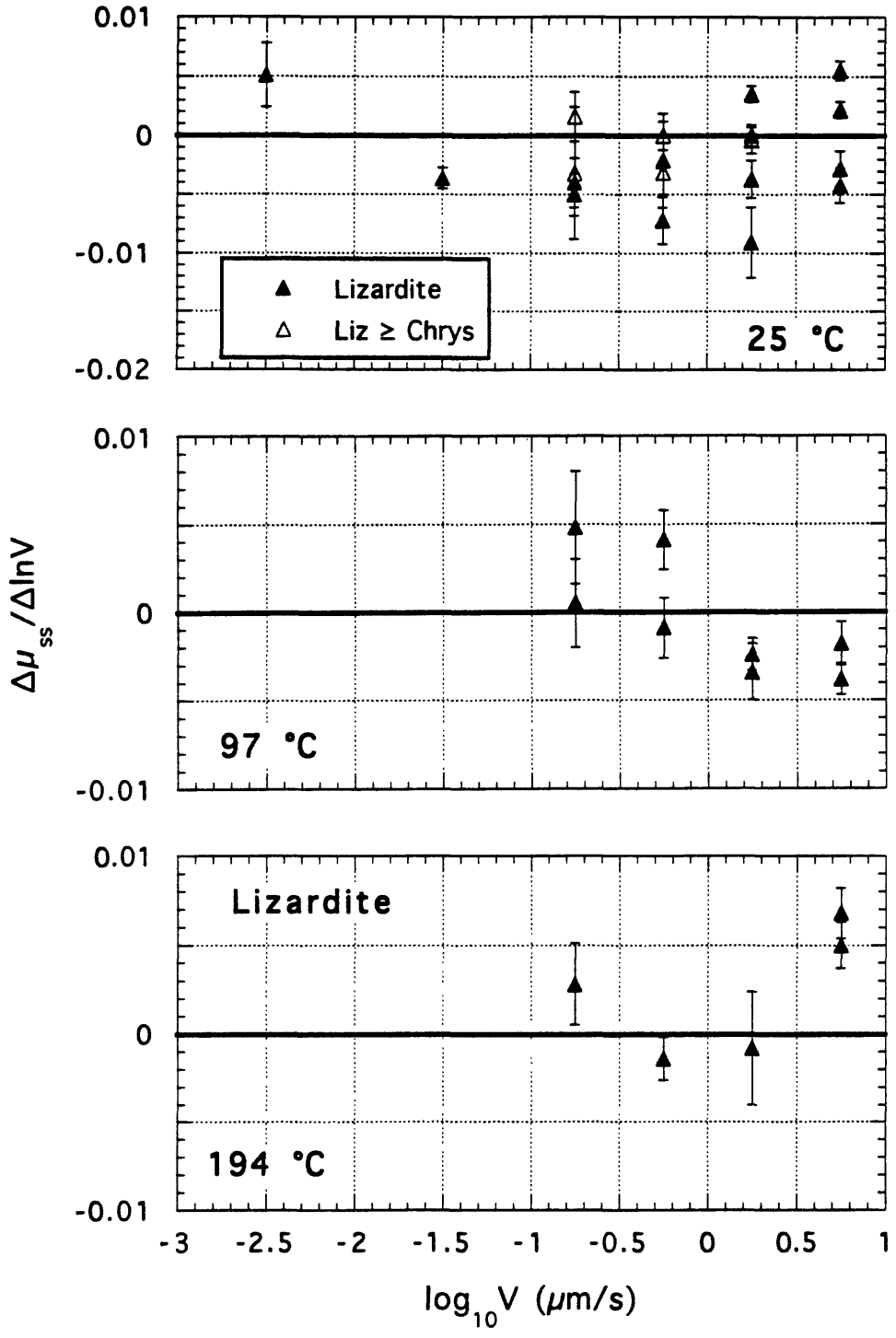

Figure 27. Variation in steady-state coefficient of friction with changing axial velocity for lizardite gouge (Oregon) at 25, 97, and 194 °C. Also included are room-temperature results for the mixed gouges NI-1 and NI-2 from New Idria containing lizardite > chrysotile (Fig. 18). Effective normal stress = 100 MPa in all experiments.

gouges, their velocity dependence may correspond somewhat more closely to the chrysotile gouge (Fig. 24), particularly at the lowest velocity step tested (0.1 to 0.32 μm/s).

The net change in μ with changing velocity is the product of two competing, time-dependent effects:

$$\Delta\mu_{ss}/\Delta\ln V = (a - b)$$

where *a* is the immediate response to the velocity step and *b* is the amount of subsequent decay to the steady-state value of μ (e.g., Rice and Gu, 1983; Logan and Rauenzahn, 1987). We measured *a*, where possible, for most of the experiments. Values of *a* were measured directly from the original strength plots, and not modeled to take machine stiffness and other factors into account. Values of *b* were then obtained by subtracting *a* from the average values of $\Delta\mu_{ss}/\Delta\ln V$ in Table 5. The unmodeled determinations of *a* and *b* reported here are likely to be lower than corresponding values obtained from modeled data (B. Kilgore, personal communication, 1996). Despite some scatter, *b* appears to be relatively constant at a given temperature for a particular gouge (Figs. 28–30). The average value of *b* is ≈0.004-0.005 for both lizardite and antigorite at 25 and 97 °C; *b* is slightly larger at 194 °C, averaging ≈0.007 for lizardite and ≈0.010 for antigorite. Values of *b* for chrysotile are all <0.007 and typically <0.003, with most of the largest values obtained at 25 °C and many determinations of $b = 0$ at 97 and 194 °C. In contrast, the three data points for T91NI6 at 194 °C that have marked negative values of $\Delta\mu_{ss}/\Delta\ln V$ also have the largest values of *b* in the entire data set. Because *b* is roughly independent of velocity in the range measured, the values of *a* for all three serpentinite gouges mimic the trends in Figures 24, 26, and 27, offset by the appropriate estimate of *b*. Where possible, we also determined values of d_c (Table 5), which is the characteristic sliding distance to reach steady state following a velocity step (Dieterich, 1978, 1979). Most estimates of d_c were less than ≈200 μm (Fig. 31); the largest values, ≈300 and ≈400 μm, were measured on the antigorite gouge at 194 °C for the velocity step between 3.2 and 10 μm/s. There are no obvious correlations between d_c and either temperature or velocity. The measured range in d_c

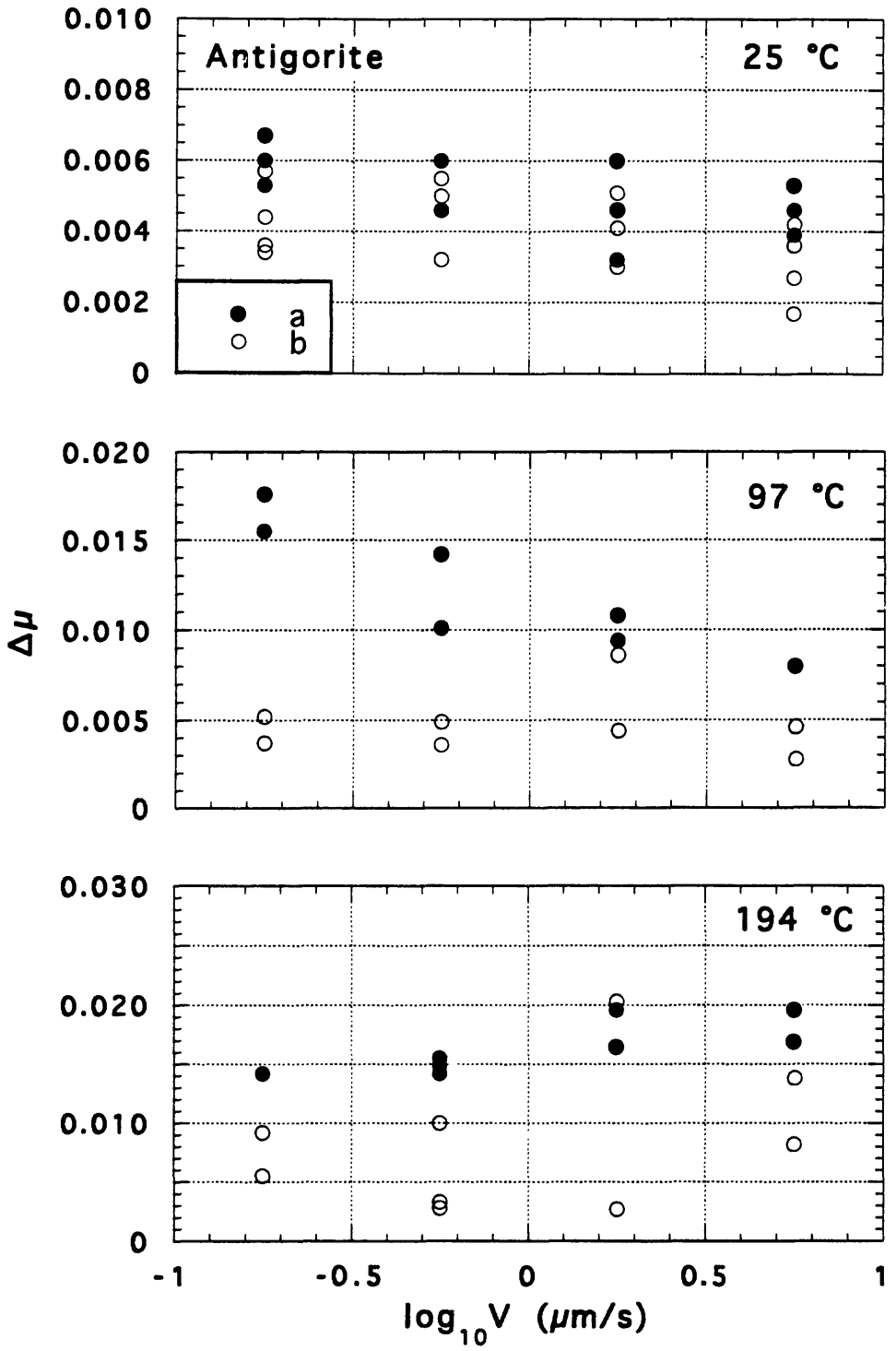

Figure 28. Variation in the parameters *a* and *b* [$(a\text{-}b) = \Delta\mu_{ss}/\Delta\ln V$] for the antigorite-gouge experiments (Fig. 26). Values of *a* in Figures 28–30 were measured directly from the plots of μ versus axial displacement (unmodeled); values of *b* were calculated by difference.

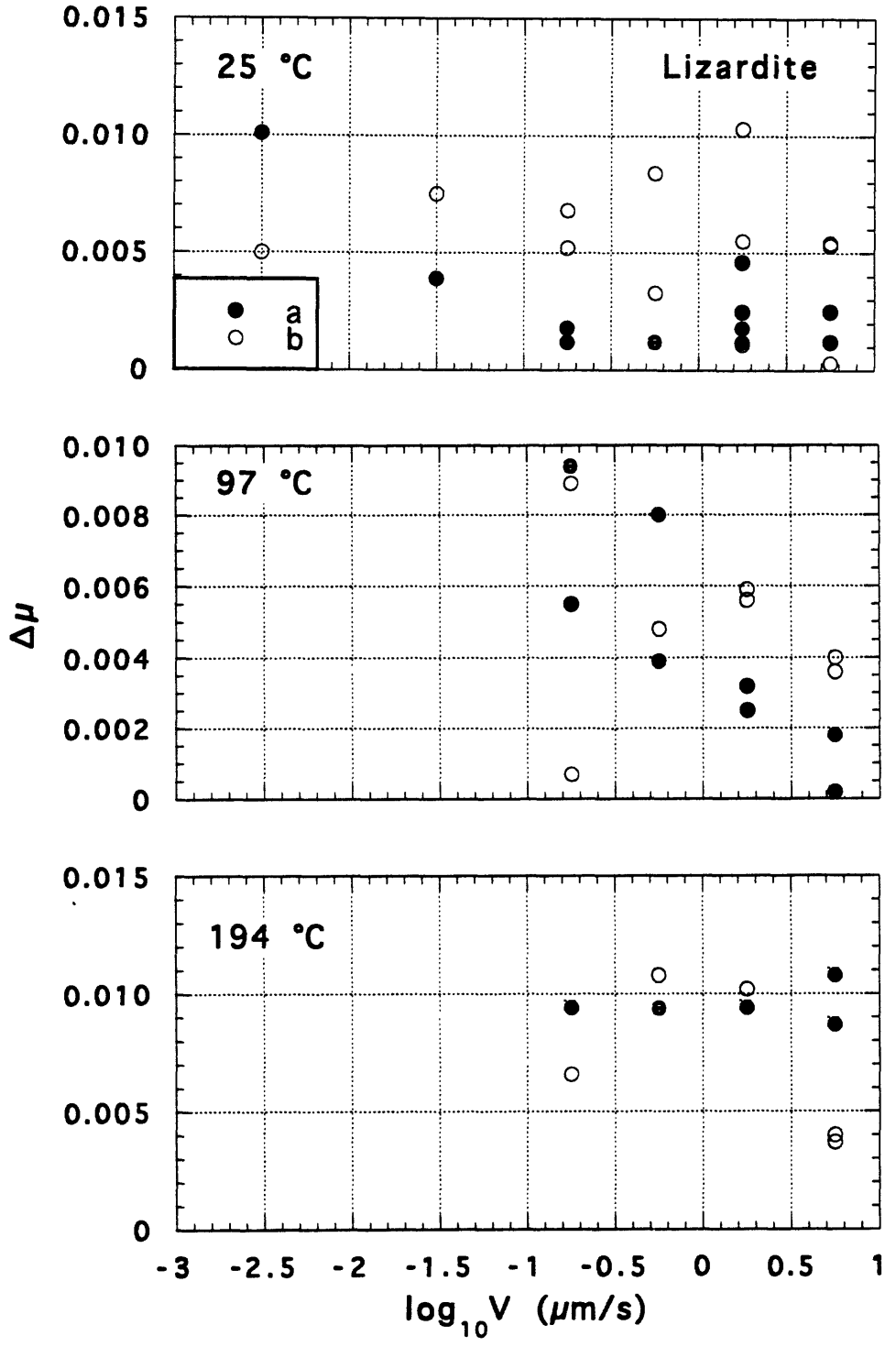

Figure 29. Estimates of *a* and *b* for the lizardite (Oregon) experiments (Fig. 27).

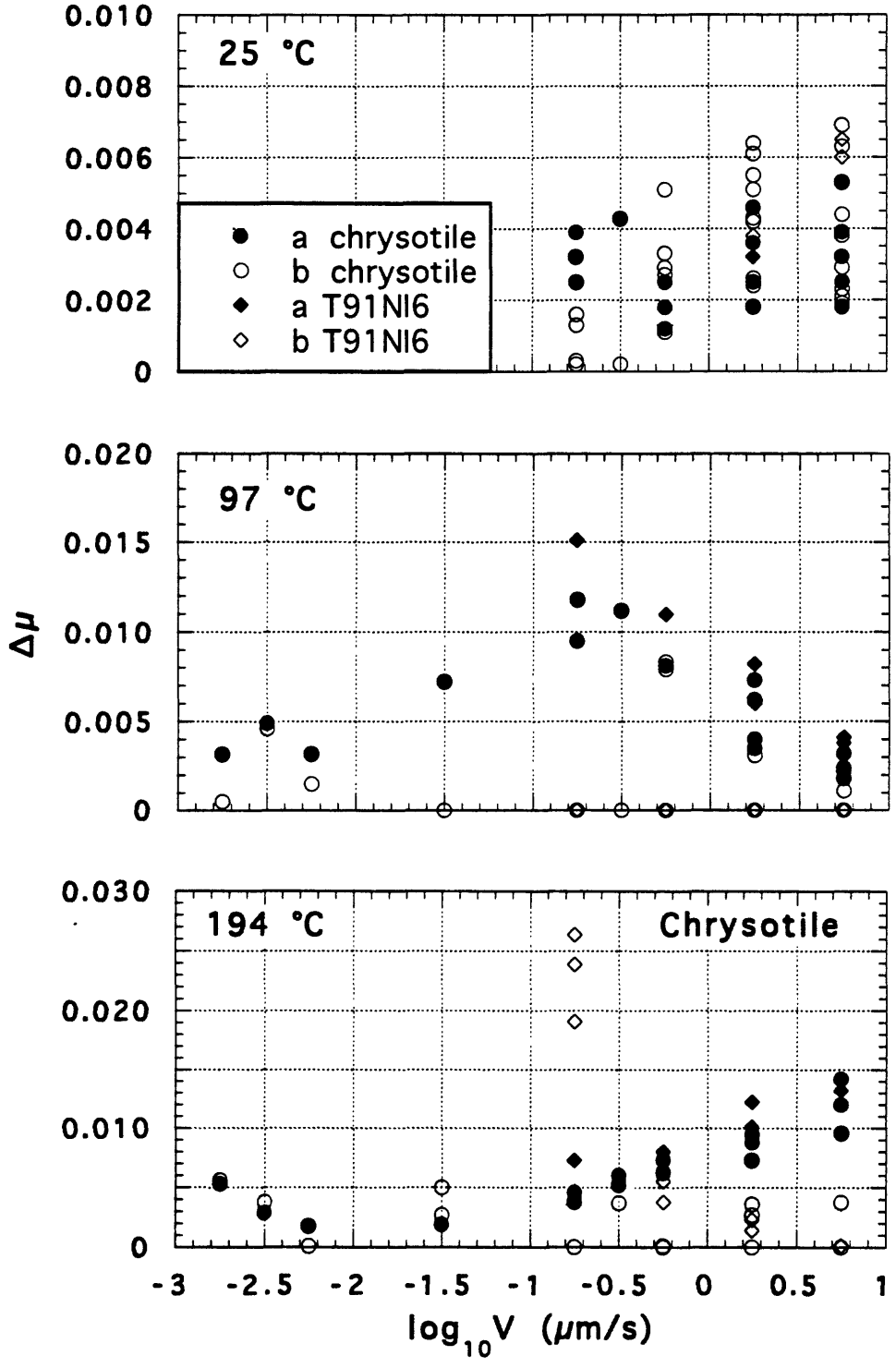

Figure 30. Estimates of *a* and *b* for the two clinochrysotile gouges (Fig. 24).

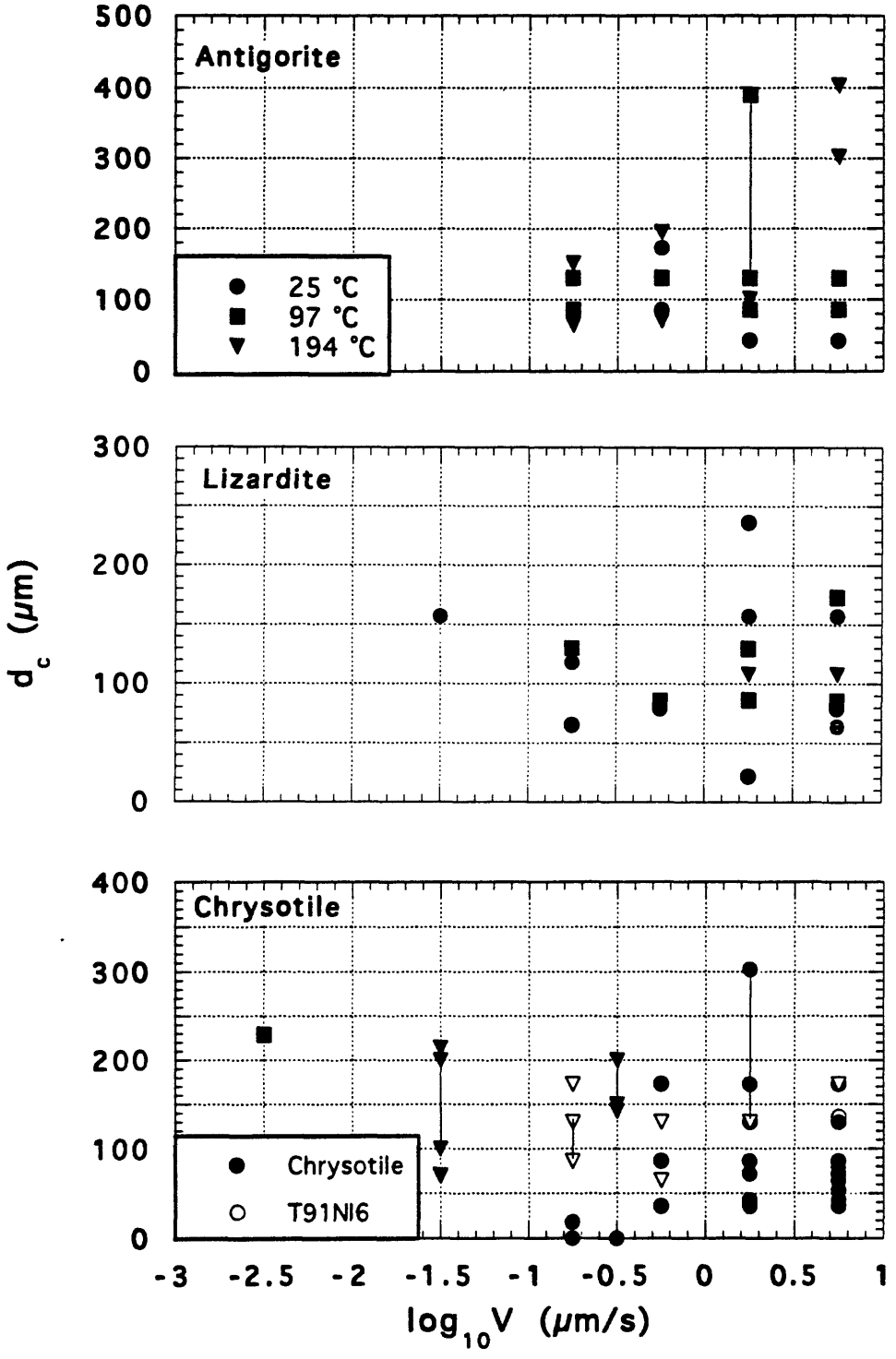

Figure 31. Values of d_c for antigorite, lizardite, and the two chrysotile gouges, measured directly from the plots of μ versus axial displacement. In all three plots, circles = 25 °C data, squares = 97 °C, and inverted triangles = 194 °C; in the chrysotile plot filled symbols = our chrysotile sample, open symbols = T91NI6. Vertical lines connect the limiting values of ranges of d_c reported in Table 5.

for the serpentinite gouges is consistent with previous measurements (e.g., Logan and Rauenzahn, 1987).

Discussion: Comparison to Other Studies

The frictional strengths of various types of serpentinite have been measured in a number of previous studies, principally at room temperature. Some of those studies provide no information on the mineralogy of the samples (e.g., Horn and Deere, 1962; Rummel et al., 1978), which makes the results of limited use, given the great variability in serpentine-mineral strengths. Fortunately, Raleigh and Paterson (1965), Dengo and Logan (1981), Rutter and Brodie (1988), and Reinen et al. (1991, 1994) include sample descriptions of varying detail. Raleigh and Paterson (1965) reported friction data for an antigorite-rich serpentinite that also contained 5–10% olivine, 10% magnetite, and 2% magnesite, and for a partly serpentinized peridotite composed of 40% serpentine minerals, mostly lizardite, and 60% olivine + enstatite. Dengo and Logan (1981) determined the room-temperature strengths of two groups of serpentinite samples from the Motagua fault zone, Guatemala. One group contained roughly 70% serpentine in the general proportions 3/4 lizardite to 1/4 antigorite, with traces of chrysotile concentrated in veins. The remaining minerals consisted of 11% relict enstatite and 19% oxides. The other group contained about 84% serpentine, predominantly antigorite, less than 5% relict enstatite, and 11% oxide + carbonate minerals.

Rutter and Brodie (1988) investigated the behavior of a lizardite-rich serpentinite from Jenner, California. The rock originally contained 60–70% olivine and 15–20% each orthopyroxene and clinopyroxene. Nearly all the olivine was replaced by lizardite + magnetite, whereas much of the clinopyroxene and orthopyroxene remained. Reinen et al. (1991, 1994) tested two antigorite-rich serpentinites. One sample was determined by point count to contain approximately 90% antigorite, 5% magnetite, and 5% magnesite, the latter mineral being

concentrated in veins. The mineral content of the second sample, obtained from a quarry in Vermont, was not determined, but it was considered to be similar to the first, and it should also be comparable to the Vermont antigorite of Table 2 and Figure 7.

Room-temperature friction data for the serpentinites described above and those of Summers and Byerlee (1977a, b) and Morrow et al. (1982) are plotted in Figure 32, for comparison with our room-temperature results. The quartz-rich serpentinite-bearing gouge of Morrow et al. (1982) (Fig. 13) was omitted, because the quartz has a substantial effect on the strength of that sample. The results are somewhat variable, given the great variation in experimental apparatus and conditions among the different studies; nevertheless, they can be grouped according to the principal serpentine mineral(s) present. Overall, antigoritic serpentinite has a room-temperature coefficient of friction in the range 0.6–0.9 and lizardite-rich serpentinite has μ = 0.45–0.80. These ranges overlap to a considerable degree, but when results from a single laboratory are compared, antigorite-rich serpentinites are consistently stronger than lizardite-rich ones. Our antigorite-rich gouge is rather weaker than the other antigorite serpentinites plotted in Figure 32, probably because some chrysotile remains in the sample. The wide range of lizardite strengths reflects varying degrees of preservation of relict minerals. For example, the relatively strong lizardite-bearing samples of Summers and Byerlee (1977a, b) (L2 in Fig. 32) and Raleigh and Paterson (1965) contain several percent pyroxene ± olivine. The average value of μ for our lizardite-rich gouge plots among the lizardite samples that lack relict minerals. All the mixed gouges of lizardite + chrysotile have coefficients of friction intermediate between chrysotile and lizardite.

In general, the strength of both lizardite- and antigorite-rich serpentinites decreases with increasing effective pressure, although our room-temperature antigorite results appear to show the reverse trend. Raleigh and Paterson (1965) attributed this effect to increased ductility of serpentinite at high pressures. Because chrysotile strength is controlled by its adsorbed water content, increasing pressure could lead to an increase rather than a decrease in

Figure 32. Comparison of our averaged strength data for serpentinite gouges (labelled A, L, L>C, and C in Figure) with previous room-temperature friction experiments on serpentinite. Abbreviations in Legend — (D/L) Dengo and Logan (1981): A = 84% serpentine, mostly antigorite, 10% oxides, 6% magnesite + dolomite; L = 70% serpentine, mostly lizardite, 11% enstatite, 19% oxides. (R/P) Raleigh and Paterson (1965): A = antigorite-rich serpentinite, with 5-10% olivine, 10% magnetite, 2% magnesite; L = partly serpentinized peridotite, with 40% serpentine, mostly lizardite, 60% olivine + enstatite. (S/B) Summers and Byerlee (1977b): L1 (their sample ALM-1) = Lizardite 6*T*, magnetite and possibly some lizardite 1*T* (Table 1; Fig. 10); L2 (their sample DP-2) = Lizardite 1*T*, with olivine, magnetite, pyroxene, and clinochrysotile (Table 1; Fig. 9). (R) Reinen et al. (1994): A = 90% serpentine, mostly antigorite, 5% magnetite, 5% magnesite; C = clinochrysotile (Fig. 2). The chrysotile data of Reinen et al. (1994) are plotted at 21 MPa confining pressure, although portions of some experiments were run at higher confining pressures; they also added an unspecified amount of water to the sample surfaces. (R/B) Rutter and Brodie (1988): L = 70% serpentine, mostly lizardite, 30% clinopyroxene and orthopyroxene. (M) Morrow et al. (1982): L>C (Golden Gate Bridge) = lizardite 1*T* and lesser amounts of clinochrysotile and magnetite (Fig. 12).

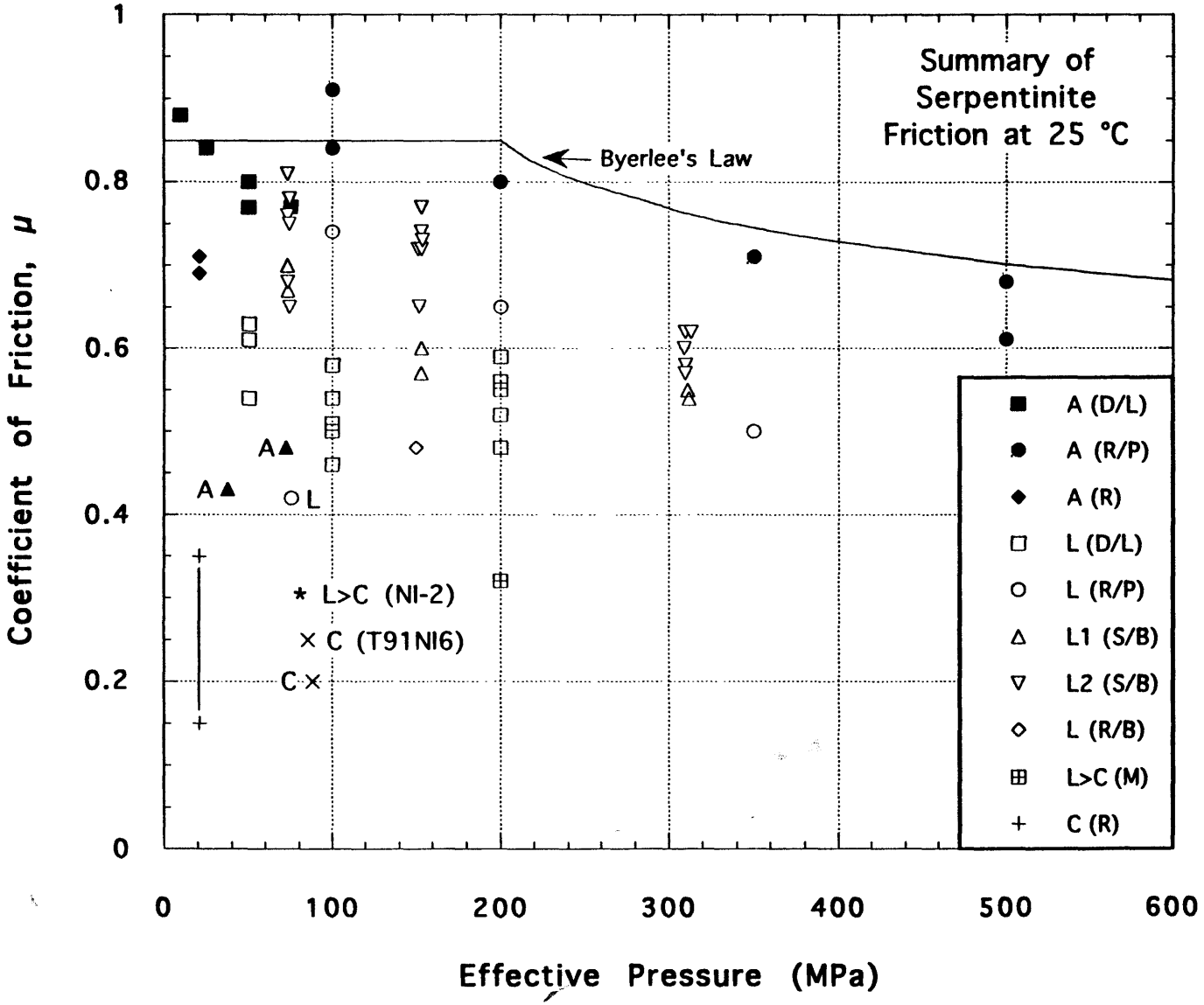
Summary of Serpentinite Friction at 25 °C
Byerlee's Law
Coefficient of Friction, μ
Effective Pressure (MPa)
0
0.2
0.4
0.6
0.8
1
0
100
200
300
400
500
600
A (D/L)
A (R/P)
A (R)
L (D/L)
L (R/P)
L1 (S/B)
L2 (S/B)
L (R/B)
L>C (M)
C (R)
* L>C (NI-2)
× C (T91NI6)

μ, as the adsorbed water is squeezed out of the fiber bundles of chrysotile. The very low values of μ obtained during the 107 °C chrysotile experiment (Fig. 21e) may be a function of the relatively low effective normal stress (48.5 MPa) of that experiment. If chrysotile is the major cause of the reduced strength of our antigorite-rich gouge, it might also control the pressure-dependence of strength for that gouge.

The lizardite 6*T* sample studied by Summers and Byerlee (1977a, b) (L1 in Fig. 32) has μ in the range of the other lizardite-rich samples, which are all likely to be lizardite 1*T*. Similarly, orthochrysotile and clinochrysotile have essentially the same strength (Figs. 18a, 19). That different polytypes of a given mineral have similar strengths is consistent with crystallographic considerations. The differences in the stacking order of the polytypes of lizardite and chrysotile should have little effect on strength, because O–H bonds of similar strength will form between the layers of different polytypes. The very low orthochrysotile strength further suggests that orthochrysotile adsorbs substantial amounts of water. These results are of some significance to fault zones, because Banfield et al. (1995) demonstrated that deformation can induce changes in the polytype of lizardite, as a result of shearing along the basal plane.

Few studies have been conducted on heated serpentinite samples. Raleigh and Paterson (1965) measured serpentinite strength at temperatures to 700 °C, but most of their experiments were conducted in closed systems, in which water released during dehydration reactions at temperatures aboved 300–500 °C substantially decreased the effective pressure (by unknown amounts) and consequently the strength. In contrast, one vented, heated sample remained relatively strong. Rutter and Brodie (1988) determined that the strength of a lizardite-rich serpentinite was higher at 300 °C than 20 °C, under controlled conditions of fluid pressure. Similarly, Moore et al. (1983, 1986) reported a strength increase between 200 and 400 °C for a natural serpentinite gouge containing roughly equal amounts of lizardite and chrysotile. These few data suggest that lizardite- and antigorite-bearing serpentinites

should maintain or increase their strength upon heating, consistent with the results of our experiments. Moore et al. (1986) attributed the increasing strength of lizardite-rich serpentinite gouge with temperature increase (at temperatures below the transformation of serpentine to olivine) to progressive lithification of the gouge. Lithification processes may also be operative, to a lesser degree, in the lower-temperature gouge experiments of this study.

Reinen et al. (1993) postulated that increasing temperature might possibly lower the strength of chrysotile. Our results for chrysotile suggest that at appropriate conditions of effective stress and velocity the coefficient of friction of chrysotile may be at a minimum at temperatures around 100 °C. However, chrysotile strength approaches that of the other serpentine minerals at pressure-temperature conditions near its upper limit of stability (Fig. 21b–e). The marked strength increases of chrysotile probably reflect in large part the progressive loss of adsorbed water with increasing temperature and pressure. Because chrysotile strength increases with increasing depth of burial, a chrysotile-filled fault zone will not be significantly weaker over its depth range than faults filled with other gouge materials. The possible implications to models of the San Andreas fault zone are discussed by Moore et al. (in press, and in preparation).

Conclusions

(1) The basic layered structure of all serpentine minerals is essentially the same, making their X-ray diffraction patterns very similar overall. Nevertheless, variations in the spacing and intensity of several X-ray reflections make it possible to distinguish among the most important serpentine minerals lizardite 1*T*, antigorite, and clinochrysotile. Other polytypes of chrysotile and lizardite can also be identified with some confidence. Lizardite 1*T* and clinochrysotile commonly occur together in low-temperature serpentinites, and their X-

ray patterns are sufficiently different that both can be identified if they each comprise ≥10 volume percent of the sample.

(2) Copper provides a stable, impermeable jacketing material for experiments at elevated temperatures. However, copper is relatively strong at low temperatures, and for a weak material such as chrysotile, the copper-jacket strength may be comparable to the shear strength of the chrysotile gouge layer. A series of test experiments, centered around a comparison of copper- and polyurethane-jacket strengths, led to the determination of a correction factor for jacket strength at each temperature tested in this investigation. In addition, the corrected room-temperature friction data for one chrysotile sample duplicate the results obtained for that same sample from rotary-shear experiments.

(3) Our room-temperature strength measurements of the three major serpentine varieties corroborate previous reports that lizardite and antigorite gouge are both relatively strong materials and at least twice as strong as chrysotile gouge. The low coefficient of friction of chrysotile is caused by its high adsorbed water content; when the adsorbed water is removed, chrysotile is as strong as the other serpentine varieties. The coefficient of friction of all three serpentinite gouges increases at least slightly with increasing temperature. Our metasomatically altered antigorite gouge has reduced strength compared to pure antigorite, but the altered gouge is as strong as lizardite- and illite-rich gouges. The coefficient of friction of chrysotile goes through a minimum of about 0.1 at temperatures near 100°C but increases substantially with further heating, such that chrysotile is essentially as strong as lizardite and antigorite at temperatures approaching 300°C. This trend suggests that chrysotile gradually loses its adsorbed-water content with increasing depth of burial, at least under the condition of a hydrostatic fluid-pressure gradient. The effects on chrysotile strength of raising fluid pressure above hydrostatic levels will be considered in a subsequent study.

(4) The velocity dependence of heated chrysotile gouge differs significantly from its room-temperature behavior. The data for chrysotile may be explained by a band of velocity-

strengthening behavior that migrates to higher velocities with increasing temperature; outside this band μ is nearly independent of velocity. The velocity dependence of heated antigorite and lizardite gouges may follow trends similar to that of chrysotile, but the smaller velocity range tested for these minerals precludes a definite correlation.

References

Bailey, S. W., 1988, X-ray diffraction identification of the polytypes of mica, serpentine, and chlorite, Clays and Clay Minerals, 36, 193-213.

Bailey, S. W., and Banfield, J. F., 1995, Derivation and identification of nonstandard serpentine polytypes, American Mineralogist, 80, 1104-1115.

Banfield, J. F., Bailey, S. W., Barker, W. W., and Smith, R. C., II, 1995, Complex polytypism: Relationships between serpentine structural characteristics and deformation, American Mineralogist, 80, 1116-1131.

Coleman, R. G., 1971, Petrologic and geophysical nature of serpentinites, Geological Society of America Bulletin, 82, 897-918.

Coleman, R. G., and Keith, T. E., 1971, A chemical study of serpentinization — Burro Mountain, California, Journal of Petrology, 12, 311-328.

Deer, W. A., Howie, R. A., and Zussman, J., 1962, Rock-forming Minerals, Vol. 3, Sheet Silicates, John Wiley and Sons, New York, pp. 170-190.

Dengo, C. A., and Logan, J. M., 1981, Implications of the mechanical and frictional behavior of serpentinite to seismogenic faulting, Journal of Geophysical Research, 86, 10771-10782.

Dieterich, J. H., 1978, Time-dependent friction and the mechanics of stick-slip, Pure and Applied Geophysics, 116, 103–120.

Dieterich, J. H., 1979, Modeling of rock friction 1. Experimental reaults and constitutive equations, Journal of Geophysical Research, 84, 2161-2168.

Dungan, M. A., 1979, A microprobe study of antigorite and some serpentine pseudomorphs, Canadian Mineralogist, 17, 771-784.

Evans, B. W., Johannes, W., Oterdoom, H., and Trommsdorff, V., 1976, Stability of chrysotile and antigorite in the serpentine multisystem, Schweizerische mineralogische und petrographische Mitteillungen, 56, 79-93.

Faust, G. T., and Fahey, J. J., 1962, The serpentine group minerals, U. S. Geological Survey Professional Paper 384-A, 91 pp.

Giese, R. F., Jr., 1988, Kaolin Minerals: Structures and Stabilities, in Hydrous Phyllosilicates (exclusive of micas), Bailey, S. W., ed., Reviews in Mineralogy, 19, 29–66.

Hall, S. H., Guggenheim, S., Moore, P., and Bailey, S. W., 1976, The structure of Unst-type 6-layer serpentines, Canadian Mineralogist, 14, 314-321.

Hickman, S. H., Zoback, M. D., and Healy, J. H., 1988, Continuation of a deep borehole stress measurement profile near the San Andreas fault 1. Hydraulic fracturing stress measurements at Hi Vista, Mojave Desert, California, Journal of Geophysical Research, 93, 15183-15195.

Horn, H. M., and Deere, D. U., 1962, Frictional characteristics of minerals, Geotechnique, 12, 319-335.

Jahns, R. H., 1967, Serpentinites of the Roxbury district, Vermont, in Ultramafic and Related Rocks, Wyllie, P. J., ed., Robert E. Krieger Publishing Co., Huntington, N. Y., 137-160.

Lachenbruch, A. H., and Sass, J. H., 1973, Thermo-mechanical aspects of the San Andreas fault system, in Proceedings of the Conference on the Tectonic Problems of the San Andreas Fault System, Kovach, R. L., and Nur, A., eds., Stanford University Publications in the Geological Sciences, 13, 192–205.

Logan, J. M., and Rauenzahn, K. A., 1987, Frictional dependence of gouge mixtures of quartz and montmorillonite on velocity, composition and fabric, Tectonophysics, 144, 87–108.

McGarr, A., Zoback, M. D., and Hanks, T. C., 1982, Implications of an elastic analysis of in situ stress measurements near the San Andreas fault, Journal of Geophysical Research, 87, 7797-7806.

Moore, D. E., Lockner, D. A., Ma Shengli, Summers, R., and Byerlee, J. D., Strengths of serpentinite gouges at elevated temperatures, submitted to Journal of Geophysical Research.

Moore, D. E., Lockner, D. A., Summers, R., Ma Shengli, and Byerlee, J. D., 1996, Strength of chrysotile-serpentinite gouge under hydrothermal conditions: Can it explain a weak San Andreas fault?, Geology, 24, 1041-1044.

Moore, D. E., Summers, R., and Byerlee, J. D., 1983, Strengths of clay and non-clay fault gouges at elevated temperatures and pressures, Proceedings 24th U. S. Symposium on Rock Mechanics, 489-500.

Moore, D. E., Summers, R., and Byerlee, J. D., 1986, The effects of sliding velocity on the frictional and physical properties of heated fault gouge, Pure and Applied Geophysics, 124, 31-52.

Morrow, C., Radney, B., and Byerlee, J., 1992, Frictional strength and the effective pressure law of montmorillonite and illite clays, in Fault Mechanics and Transport Properties of Rocks, Evans, B., and Wong, T.-F., eds., Academic Press, San Diego, California, 69–88.

Morrow, C. A., Shi, L. Q., and Byerlee, J. D., 1982, Strain hardening and strength of clay-rich fault gouges, Journal of Geophysical Research, 87, 6771-6780.

Mount, V. S., and Suppe, J., 1987, State of stress near the San Andreas fault: Implications for wrench tectonics, Geology, 15, 1143–1146.

Mumpton, F. A., and Thompson, C. S., 1975, Mineralogy and origin of the Coalinga asbestos deposit, Clays and Clay Minerals, 23, 131-143.

O'Hanley, D. S., 1996, Serpentinites, Records of Tectonic and Petrological History, Oxford University Press, Oxford, 277 pp.

O'Hanley, D. S., Chernosky, J. V., Jr., and Wicks, F. W., 1989, The stability of lizardite and chrysotile, Canadian Mineralogist, 27, 483-493.

O'Hanley, D. S., and Wicks, F. J., 1995, Conditions of formation of lizardite, chrysotile and antigorite, Cassiar, British Columbia, Canadian Mineralogist, 33, 753-773.

Page, N. J., 1968, Chemical differences among the serpentine "polymorphs", American Mineralogist, 53, 201-215.

Page, N. J., and Coleman, R. G., 1967, Serpentine mineral analyses and physical properties, U. S. Geological Survey Professional Paper 575-B, B103-B107.

Raleigh, C. B., and Paterson, M. S., 1965, Experimental deformation of serpentinite and its tectonic implications, Journal of Geophysical Research, 70, 3965-3985.

Reinen, L. A., Tullis, T. E., and Weeks, J. D., 1993, A mechanism for weak, creeping faults, Eos Transactions AGU, 74(43), 589.

Reinen, L. A., Weeks, J. D., and Tullis, T. E., 1991, The frictional behavior of serpentinite: Implications for aseismic creep on shallow crustal faults, Geophysical Research Letters, 18, 1921-1924.

Reinen, L. A., Weeks, J. D., and Tullis, T. E., 1994, The frictional behavior of lizardite and antigorite serpentinites: Experiments, constitutive models, and implications for natural faults, Pure and Applied Geophysics, 143, 317-358.

Rice, J. R., and Gu, J., 1983, Earthquake after effects and triggered seismic phenomena, Pure and Applied Geophysics, 121, 187–219.

Rummel, F., Alheid, H. J., and Frohn, C., 1978, Dilatancy and fracture induced velocity changes in rock and their relation to frictional sliding, Pure and Applied Geophysics, 116, 743-764.

Rutter, E. H., and Brodie, K. H., 1988, Experimental "syntectonic" dehydration of serpentinite under conditions of controlled pore water pressure, Journal of Geophysical Research, 93, 4907-4932.

Scott, D. R., Lockner, D. A., Byerlee, J. D., and Sammis, C. G., 1994, Triaxial testing of Lopez fault gouge at 150 MPa mean effective stress, Pure and Applied Geophysics, 142, 749–775.

Stock, J. M., and Healy, J. H., 1988, Continuation of a deep borehole stress measurement profile near the San Andreas fault 2. Hydraulic fracturing stress measurements at Black Butte, Mojave Desert, California, Journal of Geophysical Research, 93, 15196-15206.

Summers, R., and Byerlee, J., 1977a, A note on the effects of fault gouge composition on the stability of frictional sliding, International Journal of Rock Mechanics and Mining Science, 14, 155-160.

Summers, R., and Byerlee, J., 1977b, Summary of results of frictional sliding studies, at confining pressures up to 6.98 kb, in selected rock materials, U. S. Geological Survey Open-File Report 77-142, 129 pp.

Thatcher, W., 1990, Present-day crustal movements and the mechanics of cyclic deformation, in The San Andreas Fault System, California, Wallace, R. E., ed., U. S. Geological Survey Professional Paper, 1515, 189–205.

Wenner, D. B., and Taylor, H. P., Jr., 1971, Temperatures of serpentinization of ultramafic rocks based on O^{18}/O^{16} fractionation between coexisting serpentine and magnetite, Contributions to Mineralogy and Petrology, 32, 165-185.

Whittaker, E. J. W., 1957, The structure of chrysotile. V. Diffuse reflections and fibre structure, Acta Crystallographica, 16, 486-490.

Whittaker, E. J. W., and Zussman, J., 1956, The characterization of serpentine minerals by X-ray diffraction, Mineralogical Magazine, 31, 107-126.

Wicks, F. J., and O'Hanley, D. S., 1988, Serpentine Minerals: Structures and Petrology, in Hydrous Phyllosilicates (exclusive of micas), Bailey, S. W., ed., Reviews in Mineralogy, 19, 91-167.

Wicks, F. J., and Plant, A. G., 1979, Electron-microprobe and X-ray-microbeam studies of serpentine textures, Canadian Mineralogist, 17, 785-830.

Young, G. J., and Healey, F. H., 1954, The physical structure of asbestos, Journal of Physical Chemistry, 58, 881–884.

Zoback, M. D., Zoback, M. L., Mount, V. S., Suppe, J., Eaton, J. P., Healy, J. H., Oppenheimer, D., Reasenberg, P., Jones, L., Raleigh, C. B., Wong, I. G., Scotti, O., and Wentworth, C.,

1987, New evidence on the state of stress of the San Andreas fault system, Science, 238, 1105–1111.

Zoback, M. D., and Healy, J. H., 1992, In situ stress measurements to 3.5 km depth in the Cajon Pass scientific research borehole: Implications for the mechanics of crustal faulting, Journal of Geophysical Research, 97, 5039-5052, 1992.